NATIONAL CENTER FOR EARTHQUAKE
ENGINEERING RESEARCH
State University of New York at Buffalo

NONLINEAR DYNAMIC ANALYSIS OF THREE-DIMENSIONAL BASE ISOLATED STRUCTURES (3D-BASIS)

by

S. Nagarajaiah, A.M. Reinhorn and M.C. Constantinou
Department of Civil Engineering
State University of New York at Buffalo
Buffalo, New York 14260

Technical Report NCEER-89-0019

August 3, 1989

This research was conducted at the State University of New York at Buffalo and was partially supported by the National Science Foundation under Grant No. ECE 86-07591.

NOTICE

This report was prepared by State University of New York at Buffalo as a result of research sponsored by the National Center for Earthquake Engineering Research (NCEER). Neither NCEER, associates of NCEER, its sponsors, the State University of New York at Buffalo, nor any person acting on their behalf:

a. makes any warranty, express or implied, with respect to the use of any information, apparatus, method, or process disclosed in this report or that such use may not infringe upon privately owned rights; or

b. assumes any liabilities of whatsoever kind with respect to the use of, or the damage resulting from the use of, any information, apparatus, method or process disclosed in this report.

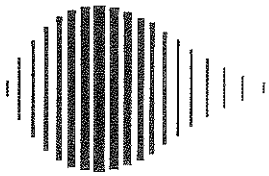

NONLINEAR DYNAMIC ANALYSIS OF THREE-DIMENSIONAL BASE ISOLATED STRUCTURES (3D-BASIS)

by

S. Nagarajaiah[1], A.M. Reinhorn[2] and M.C. Constantinou[2]

August 3, 1989

Technical Report NCEER-89-0019

NCEER Contract Number 87-2002

NSF Master Contract Number ECE 86-07591

1 Graduate Research Assistant, Dept. of Civil Engineering, State University of New York at Buffalo

2 Associate Professor, Dept. of Civil Engineering, State University of New York at Buffalo

NATIONAL CENTER FOR EARTHQUAKE ENGINEERING RESEARCH
State University of New York at Buffalo
Red Jacket Quadrangle, Buffalo, NY 14261

PREFACE

The National Center for Earthquake Engineering Research (NCEER) is devoted to the expansion and dissemination of knowledge about earthquakes, the improvement of earthquake-resistant design, and the implementation of seismic hazard mitigation procedures to minimize loss of lives and property. The emphasis is on structures and lifelines that are found in zones of moderate to high seismicity throughout the United States.

NCEER's research is being carried out in an integrated and coordinated manner following a structured program. The current research program comprises four main areas:

- Existing and New Structures
- Secondary and Protective Systems
- Lifeline Systems
- Disaster Research and Planning

This technical report pertains to Program 2, Secondary and Protective Systems, and more specifically, to protective systems. Protective Systems are devices or systems which, when incorporated into a structure, help to improve the structure's ability to withstand seismic or other environmental loads. These systems can be passive, such as base isolators or viscoelastic dampers; or active, such as active tendons or active mass dampers; or combined passive-active systems.

Passive protective systems constitute one of the important areas of research. Current research activities, as shown schematically in the figure below, include the following:

1. Compilation and evaluation of available data.
2. Development of comprehensive analytical models.
3. Development of performance criteria and standardized testing procedures.
4. Development of simplified, code-type methods for analysis and design.

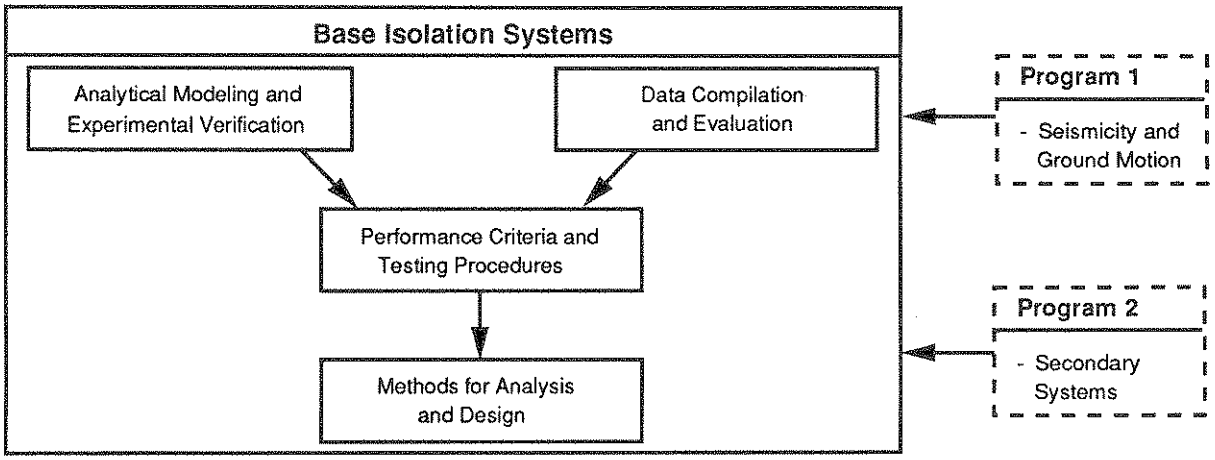

One of the activities in the area of base isolation research is the development of analytical models and computer programs for analysis of base isolated structures. This report describes the results of this effort, including a computer program, 3D-BASIS, for analysis of three-dimensional base isolated buildings. The superstructure is treated as linear. The isolation system may consist of combinations of hysteretic and frictional devices. Response quantities computed using 3D-BASIS are compared with results obtained from other existing programs and experimental results.

ABSTRACT

Base isolation for seismic protection has received considerable attention in the engineering community [1,2,3]. Natural or synthetic rubber pads, Teflon bearings sliding on stainless steel, and combinations of displacement control and energy dissipation devices are used to reduce the energy input into building structures. Reduction of energy input into the structure reduces the potential damage during severe earthquakes. Most base isolation devices experience inelastic behavior during earthquakes, thus, dissipate energy and reduce energy input into the structure. Analysis of base isolated structures subjected to ground motion involves nonlinear dynamic analysis.

Several computer models and programs have been developed for specific construction projects, the most recent being the Foothill Communities Law and Justice Center in Rancho Cucamonga, San Bernardino, California [4,5]. The model developed for this project treats the system as a combined elastic-inelastic model, however, it addresses only isolation elements with bilinear stiffness.

This report describes the development of a comprehensive analytical model and a computer program 3D-BASIS, for analysis of three-dimensional base isolated multistory buildings. Modeling various types of isolation devices with strong nonlinearities such as hysteretic and frictional devices or their combination is discussed. The superstructure, comprised of shear walls, frames and nonstructural elements, is assumed to remain elastic. Comparison of response computed using the program 3D-BASIS with various existing programs and experimental results is considered.

The hysteretic model considered in this report can reproduce bi-axial inelastic behavior of high damping rubber bearings with shear-stiffness degradation, steel dampers, viscoelastic dampers, bilinear behavior of lead-rubber bearings, and hysteretic behavior of friction interfaces effectively. The hysteretic behavior produced by this model compares well with available experimental results.

The frictional elements are modeled using a modified viscoplasticity model, with very high elastic stiffness representing near stick condition and with very low or negative post yielding stiffness representing slip condition. The computational algorithm, developed for this project, treats nonlinear terms as pseudo load and handles high and negative stiffness very effectively.

The computational model could be used for either analysis of actual systems or to develop guidelines for base isolation of building structures subjected to severe earthquakes.

ACKNOWLEDGEMENTS

This study was supported by the National Center For Earthquake Engineering Research, NCEER contract Number 87-2002, NSF Master contract Number ECE 86-07591, and other New York state and private industry sources. The support is gratefully acknowledged.

Gratitude is also expressed to Marcia Chastain for typing part of the report.

TABLE OF CONTENTS

TABLE OF CONTENTS (Cont'd)

TABLE OF CONTENTS (Cont'd)

LIST OF FIGURES

LIST OF FIGURES (Cont'd)

LIST OF FIGURES (Cont'd)

LIST OF FIGURES (Cont'd)

LIST OF FIGURES (Cont'd)

LIST OF FIGURES (Cont'd)

LIST OF FIGURES (Cont'd)

LIST OF TABLES

SECTION 1

INTRODUCTION

1.1 Base Isolation Systems

The concept of aseismic base isolation is one in which a building is uncoupled from damaging effects of ground motion by a mechanism that provides flexibility and energy absorption capacity. As such, the concept runs counter to accepted methods of aseismic design, which explains its slow rate of adoption by the professional community.

The idea of supporting the building and letting the ground move underneath is so appealing that many inventors proposed devices to achieve this result as early as the beginning of this century [1]. Almost all of the inventions remained unimplemented until the last quarter century when multilayer elastomeric bearings were developed. The concept, of a system with no horizontal restraint described above, in practice has to accommodate frequently occurring service loads such as minor earthquakes, wind and braking forces in bridge applications. Hence, a practical system usually consists of the following elements:

(a) a horizontally flexible mount which lowers the fundamental frequency of the system below the predominant ground motion frequencies and allows large horizontal displacements,

(b) additional damping to keep displacements within acceptable limits,

(c) a mechanism to provide rigidity under frequent service loads, and

(d) a fail safe system that is activated in extreme situations when the flexible mount is about to fail (a second line of defense).

Some modern isolation systems combine the first three of these elements in a single device.

Design codes require that earthquake forces be absorbed by the structural system through inelastic action which lengthens the period of the system and increases its energy dissipation capacity. This inelastic action is concentrated at beam-column connections and relies heavily on connection details or confinement and reinforcement details in concrete structures. This

action involves damage, both to the structural system and nonstructural components. The paradox with this approach is that safety is ensured by allowing damage. It is acceptable because of its economic benefits in reducing construction costs. However, earthquakes have other cost impacts such as repair and post earthquake disruption costs, earthquake insurance premiums and potential liability for losses and injuries.

The base isolation alternative reduces the forces transmitted to the structure and limits any inelastic action in a specially designed replaceable system that is placed between the building and its foundation. It provides a level of performance well beyond the normal code requirements with potential for substantial life-cycle cost reduction.

Some of the prominent base isolation systems [12] are elastomeric bearing systems, sliding systems, and sliding systems with restoring force devices.

Elastomeric bearings provide the simplest method of isolation. Like elastomeric bridge bearings, they are made by bonding sheets of rubber to thin steel plates [26]. The steel reinforcement increases the compressive stiffness. Since the inherent damping in usual rubber compounds is low, energy dissipators are used to increase damping. One such device is the lead-rubber bearing [27,28] that exhibits a behavior that is essentially bilinear hysteretic.

Sliding systems involving lead bronze-stainless steel sliding interfaces have been adopted for isolating nuclear power plants. Roller bearings have been used in Mexico City and in Japan. Sliding system in masonry buildings have been investigated [7]. Sliding systems involving Teflon-steel and other interfaces have been investigated [15,32,44]. These systems involve determination of transition between stick-slip phases and interaction between translation and rotation in generating stick-slip motion. Modeling this behavior is quite complex.

Sliding systems with restoring force involve a combination of sliding and hysteretic devices. These are used primarily for decoupling the functions of carrying the vertical load and providing horizontal stiffness. Examples of these systems are the Earthquake Barrier System [29], Alexisismon [31] and R-FBI System [30]. These systems can be modeled by a combination of hysteretic and frictional elements.

The behavior of such systems is highly nonlinear and a comprehensive model of such base isolation systems is necessary for analysis and design. This report presents the development and verification of such a model.

1.2 Objectives

The **first part** involves the development of an efficient method for analysis of the structural system, in which the superstructure remains elastic during the earthquake and in which the nonlinear behavior is restricted to the isolation system. This system consists of a combination of *linear elastic, viscous, hysteretic and frictional elements.* All these elements are located at the base of the structure. The first part also involves the development of a hysteretic model which can effectively represent hysteretic, frictional elements with velocity dependent coefficient of friction and their bi-axial behavior.

The **second part** involves validation of the bi-axial hysteretic model and verification of the computational algorithm.

1.3 Program 3D-BASIS

The analytical model developed is for both research and practical applications. Thus two options have been developed concerning the type of the superstructure and the information required for the analysis.

The two options are based on the following assumptions:

1. Superstructure remains elastic at all times.

2. Each floor has three degrees of freedom, X and Y translations and rotation about the center of mass of the floor. These degrees of freedom are attached to the center of mass of each floor.

3. There exists a rigid slab at the base level that connects all isolation elements. The three degrees of freedom at the base are attached to the center of mass of the base.

4. Since three degrees of freedom per floor are required in the three-dimensional representation of the superstructure, the number of modes required for modal reduction is always a multiple of three. The minimum number of modes required is three.

5. The isolation system is rigid in the vertical direction and torque resistance of individual pad is neglected.

In option one, stiffness and mass information of the superstructure has to be input (see APPENDIX A) in addition to the other information. In this option, the stiffness matrix and mass matrix of the superstructure are assembled in the program. The following additional assumptions are made:

1. The centers of mass of the floors and the base lie on one vertical axis and the centers of resistance of the floors and the base are arbitrarily located.

2. Three dimensional shear building representation is used for the superstructure, hence:

(a) Floor decks are rigid, walls and columns are inextensible,

(b) Each floor has three degrees of freedom, X and Y translations and rotation about a vertical axis. These degrees of freedom are attached to the center of mass of each floor.

In option two, mass information of the superstructure, eigenvalues and eigenvectors of the superstructure normalized with respect to the mass matrix have to be input (see APPENDIX A) in addition to the other information. In this option, the stiffness matrix of the superstructure is not explicitly assembled. The following additional assumptions are made:

1. Eigenvalue analysis of the superstructure is done using other programs.

2. The output comprised of displacement, velocity, acceleration and base shear time history are at the centers of mass of each floor and the base. Using this output, the program used for eigenvalue analysis can be used to arrive at the member forces in the superstructure.

The present phase of the research effort in progress is directed towards interfacing ETABS [43] to Program 3D-BASIS.

1.4 Report Outline

Section 2 deals with mathematical modeling of superstructure, isolation elements, hysteretic model used for their representation and validation of the hysteretic model and equations of motion. Section 2 also describes the solution procedure involving Newmark integration scheme and fourth order Runge-kutta scheme, with pseudo load formulation for handling negative stiffness encountered in velocity-dependent frictional interfaces and rigorous mathematical approach for solving equations of motion. Section 3 deals with numerical verification. The report is concluded with discussions in Section 4.

SECTION 2
MATHEMATICAL MODELING OF SUPERSTRUCTURE BASE ISOLATION ELEMENTS AND DYNAMIC ANALYSIS

2.1 Superstructure

Multistory buildings with eccentric centers of mass and resistance respond in coupled lateral torsional motions to earthquake ground motion, even when the motion is uniform over the base and contains no rotational components [6,25,33]. Analysis of such buildings requires torsional degrees of freedom in addition to translational degrees of freedom. Hence, a three-dimensional building with three degrees of freedom per floor is assumed to adequately represent the elastic superstructure. As explained in section 3, two options exist in Program 3D-BASIS. In option one, the elastic superstructure is assumed to be a three-dimensional shear building, and in option two, the elastic superstructure is assumed to be a truly three-dimensional building. In this section, the superstructure stiffness matrix needed for option one is described. Figure 2-1, 2-2 and 2-3 show the salient features of the idealized system.

2.1.1 Idealized System

The N-story idealized superstructure consists of rigid floor slabs (and rigid base slab) supported on massless axially inextensible columns and walls. It is assumed that the centers of mass of the floors and the base lie on the same vertical axis and that the principal axes of resistance of all stories are identically oriented. However, the centers of resistance need not lie on one vertical axis.

The static eccentricities, e_{xl} and e_{yl}, between the center of resistance and center of mass are defined by:

$$e_{xl} = \frac{1}{K_{yl}} \sum_{i} X_{il} k_{iy} \qquad (2.1.1)$$

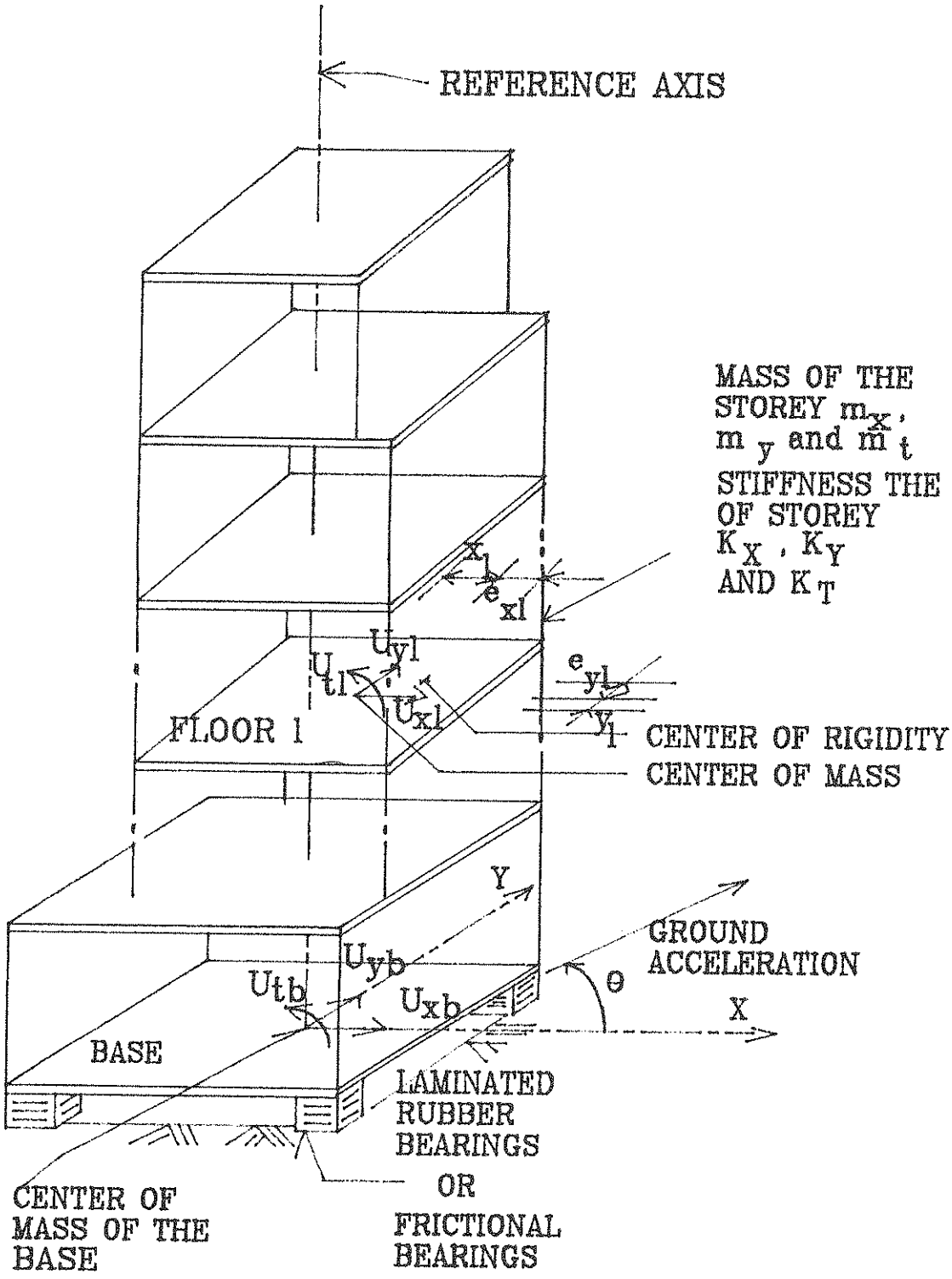

Figure 2-1 **Base Isolated Structure Excited By Multidirectional Ground Motion**

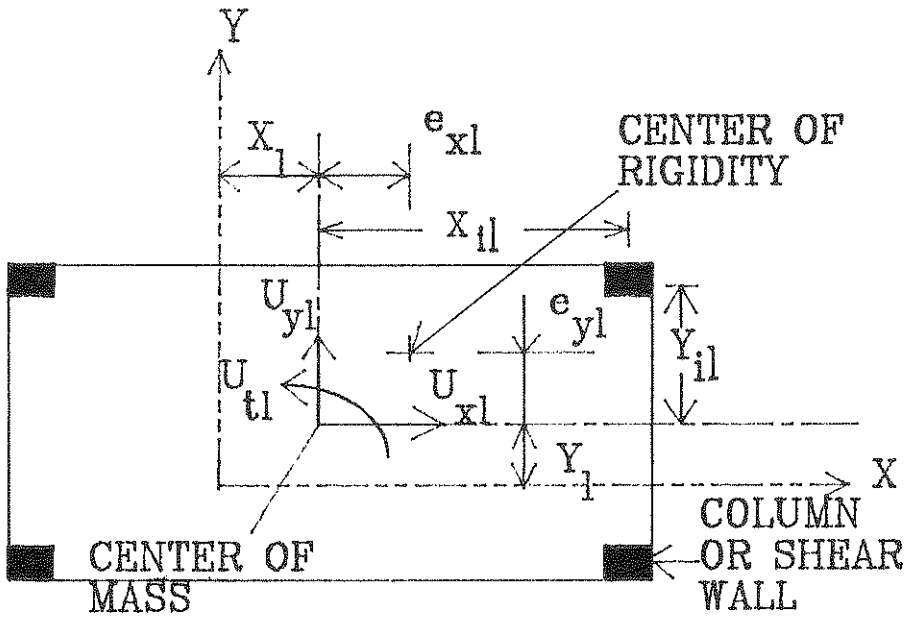

Figure 2-2 **Plan of Floor l**

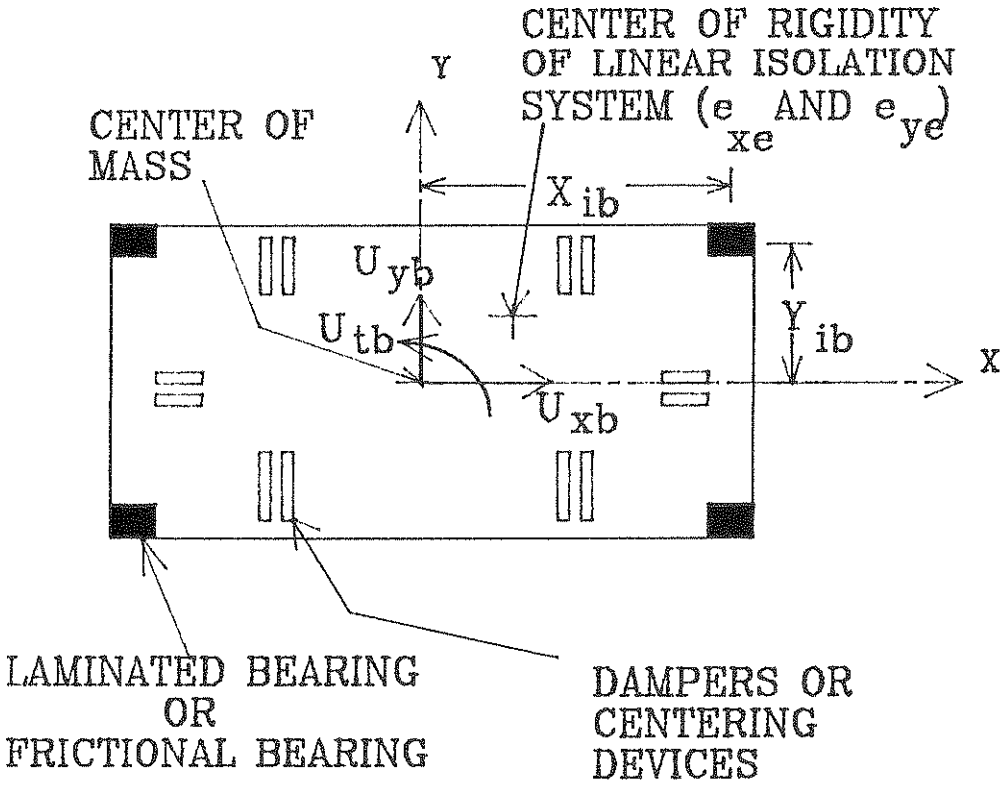

Figure 2-3 **Plan of Base**

TABLE 2-I
SUPERSTRUCTURE STIFFNESS MATRIX FOR OPTION ONE

K_{xn}	0	$-K_{xn}e_{yn}$	$-K_{xn}$	0	$K_{xn}e_{yn}$						
0	K_{yn}	$K_{yn}e_{xn}$	0	$-K_{yn}$	$-K_{yn}e_{xn}$		0			0	
$-K_{xn}e_{yn}$	$K_{yn}e_{xn}$	K_{tn}	$K_{xn}e_{yn}$	$-K_{yn}e_{xn}$	$-K_{tn}$						
			$K_{xn}+K_{xn-1}$	0	$-K_{xn}e_{yn}-K_{xn-1}e_{yn-1}$						
	SYM		0	$K_{yn}+K_{yn-1}$	$K_{yn}e_{xn}+K_{yn-1}e_{xn-1}$		SYM			0	
			$-K_{xn}e_{yn}-K_{xn-1}e_{yn-1}$	$K_{yn}e_{xn}+K_{yn-1}e_{xn-1}$	$K_{tn}+K_{tn-1}$						
						$K_{x3}+K_{x2}$	0	$-K_{x3}e_{y3}-K_{x2}e_{y2}$			
	0			SYM		0	$K_{y3}+K_{y2}$	$K_{y3}e_{x3}+K_{y2}e_{x2}$		SYM	
						$-K_{x3}e_{y3}-K_{x2}e_{y2}$	$K_{y3}e_{x3}+K_{y2}e_{x2}$	$K_{t3}+K_{t2}$			
									$K_{x2}+K_{x1}$	0	$-K_{x2}e_{y2}-K_{x1}e_{y1}$
	0			0			SYM		0	$K_{y2}+K_{y1}$	$K_{y2}e_{x2}+K_{y1}e_{x1}$
									$-K_{x2}e_{y2}-K_{x1}e_{y1}$	$K_{y2}e_{x2}+K_{y1}e_{x1}$	$K_{t2}+K_{t1}$

$$e_{yl} = \frac{1}{K_{xl}} \sum_i Y_{il} k_{ix} \qquad (2.1.2)$$

where, $K_{xl} = \sum_i k_{ix}$ and $K_{yl} = \sum_i k_{iy}$

k_{ix} and k_{iy} represent the translational stiffnesses of the resisting elements (column or wall) of l^{th} story along the principal axes of resistance X and Y, respectively. X_{il} and Y_{il} define the location of the i^{th} resisting element with respect to the origin at the center of mass. The torsional stiffness of the l^{th} story is defined with respect to the center of mass:

$$K_{tl} = \sum_i k_{ix} Y_{il}^2 + \sum_i k_{iy} X_{il}^2 \qquad (2.1.3)$$

where, X_{il} and Y_{il} define the location of the i^{th} resisting element with respect to the origin at the center of mass. The resulting stiffness matrix of the superstructure is presented in Table 2-I. The associated mass matrix is diagonal and involves the masses and rotational moments of inertia of each floor.

2.2 Isolation devices and Mathematical Model For Behavior of Such Devices

Isolation devices are modeled by elements that exhibit elastic, inelastic or hysteretic, frictional and viscous behavior.

Elastic element - Used to approximately simulate the behavior of elastomeric bearings.

Hysteretic element - Used to simulate the behavior of high damping rubber bearings, lead-rubber bearings, lead extrusion devices, and mild steel dampers in the form of torsional or flexural beams [26,27,28].

Frictional element - Used to simulate the behavior Teflon-steel interfaces and other frictional interfaces [15,32,44,13,14].

Viscous element - To simulate energy dissipation in viscoelastic dampers and hydraulic dampers.

2.2.1 Elastic Elements

Elastic elements contribute horizontal stiffness in specific directions. They are modeled as elastic springs in global X an Y directions at specified locations.

2.2.2 Uni-axial Hysteretic Elements

A number of models have been employed to model the force deformation relationship in inelastic structural elements under harmonic or transient dynamic loading.

Two distinct types of models are those described by algebraic equations, such as Ramberg-Osgood model [9], bilinear and elastoplastic models, and those by differential equations, such as Wen's model [8,10,11]. The advantages of models described by differential equations are:

(a) Ability to reproduce variety of behaviors ranging from simple elastoplastic to general hysteretic behavior. This wide range of behavior can be produced by selection of parameters that appear in the governing differential equations.

(b) High computational efficiency which stems from the fact that tracing of the hysteresis loops in these models is not necessary.

The modified viscoplasticity model used in this algorithm for modeling hysteretic elements, is an extension of Wen's model and produces kinematic hardening.

This model has been adopted because of its computational efficiency. This model of hysteresis was originally proposed by Bouc et al. and subsequently extended by Wen et al.[8]. According to this model, the restoring force, F_h , in a hysteretic system is described by [8]:

$$F_h = \alpha \frac{F^y}{U^y} U + (1 - \alpha) F_y Z \qquad (2.2.1)$$

where, α is the post yielding to elastic stiffness ratio, F^y is the yield force, U^y is the yield displacement, U is the displacement and Z is a hysteretic dimensionless quantity. The first

term of the restoring force represents the linear elastic component and the second term of the restoring force represents the hysteretic elasto-plastic component. The hysteretic dimensionless quantity Z is governed by the following equation:

$$\dot{Z}U^{y} = \{A - |Z|^{\eta}(\gamma Sign(\dot{U}Z) + \beta)\}\dot{U} \qquad (2.2.2)$$

where, γ, β, η, and A are dimensionless quantities that control the shape of the hysteresis loop, $\dot{U}$ stands for the velocity. Constantinou et al.[11] have shown that when A = 1 and $\beta + \gamma = 1$, the model of equations (2.2.1) and (2.2.2) reduces to a model of viscoplasticity that was proposed by Ozdemir [10]. The model exhibits rate dependency, which reduces with increasing values of the exponent η and/or increasing ductility ratio.

2.2.3 Inelastic Bi-axial Behavior of Hysteretic Elements and Bi-axial Hysteretic Element to Model High Damping Rubber Bearings, Lead-Rubber Bearings and Steel Dampers

Analytical [22,40] and experimental results [40] have shown that inelastic bi-axial behavior is important. In general plane motion, each isolation bearing undergoes displacement in two orthogonal directions with rotation in the same plane. This motion will be resisted by forces in the two orthogonal directions and torque in plane, which in turn, contribute to the overall resisting forces at the center of mass of the base.

Considering the interaction between forces in X and Y directions only,the bi-axial behavior is modeled using coupled differential equations proposed by Park et al.[22] and extended by Kunnath and Reinhorn[46]. The restoring forces are:

$$\begin{Bmatrix} F_x \\ F_y \end{Bmatrix} = \begin{pmatrix} \alpha_x \dfrac{F_x^y}{U_x^y} & 0 \\ 0 & \alpha_y \dfrac{F_y^y}{U_y^y} \end{pmatrix} \begin{Bmatrix} U_x \\ U_y \end{Bmatrix} + \begin{pmatrix} (1-\alpha_x)F_x^y & 0 \\ 0 & (1-\alpha_y)F_y^y \end{pmatrix} \begin{Bmatrix} Z_x \\ Z_y \end{Bmatrix} \qquad (2.2.3)$$

where, α_x and α_y are the post yielding to elastic stiffness ratio in X and Y directions, F_x^y and F_y^y are the yield forces, U_x^y and U_y^y are the yield displacements, in X and Y direction, respectively. The first term represents the linear elastic component and the second term

represents the elasto-plastic component of the restoring force. Z_x and Z_y, the hysteretic dimensionless quantities, are governed by the following coupled differential equations which account for the interaction between the X and Y directions:

$$\begin{Bmatrix} \dot{Z}_x U_x^y \\ \dot{Z}_y U_y^y \end{Bmatrix} = AI \begin{Bmatrix} \dot{U}_x \\ \dot{U}_y \end{Bmatrix} - \begin{pmatrix} Z_x^2(\gamma Sign(\dot{U}_x Z_x) + \beta) & Z_x Z_y(\gamma Sign(\dot{U}_y Z_y) + \beta) \\ Z_x Z_y(\gamma Sign(\dot{U}_x Z_x) + \beta) & Z_y^2(\gamma Sign(\dot{U}_y Z_y) + \beta) \end{pmatrix} \begin{Bmatrix} \dot{U}_x \\ \dot{U}_y \end{Bmatrix} \tag{2.2.4}$$

The resultant resisting force at each pad opposes the instantaneous incremental displacement, computed at each time step of solution. This resultant resisting force is at an angle θ, to the X axis, at each instant. In general plane motion of a pad without rotation, at each instant of time, the pad relative velocity components $\dot{U}_x$ and $\dot{U}_y$, can be used to establish instantaneous resultant velocity $\dot{U}$ and angle θ with respect to the X-axis:

$$\theta = \tan^{-1}(\dot{U}_y / \dot{U}_x) \tag{2.2.5}$$

$$\dot{U} = (\dot{U}_x^2 + \dot{U}_y^2)^{1/2} \tag{2.2.6}$$

Equations (2.2.4) can be written in the following form:

$$(\beta + \gamma)\left\{ Z_x^2 + Z_x Z_y \frac{dU_y}{dU_x} \right\} + \frac{dZ_x}{dU_x} U_x^y = A \tag{2.2.7}$$

$$(\beta + \gamma)\left\{ Z_y^2 + Z_x Z_y \frac{dU_x}{dU_y} \right\} + \frac{dZ_y}{dU_y} U_y^y = A \tag{2.2.8}$$

Noting that after yielding:

$$\frac{dZ_x}{dU_x} = 0 \tag{2.2.9}$$

$$\frac{dZ_y}{dU_y} = 0 \tag{2.2.10}$$

equations (2.2.7) and (2.2.8) can be expressed as:

$$Z_x^2 + \frac{dU_y}{dU_x} Z_x Z_y = \frac{A}{\beta + \gamma} \tag{2.2.11}$$

$$Z_y^2 + \frac{dU_x}{dU_y} Z_x Z_y = \frac{A}{\beta + \gamma} \tag{2.2.12}$$

where:

$$\frac{dU_y}{dU_x} = \tan\theta \tag{2.2.13}$$

$$\frac{dU_x}{dU_y} = \cot\theta \tag{2.2.14}$$

The system of equations (2.2.11) and (2.2.12) have the solution:

$$Z_x = \cos\theta \tag{2.2.15}$$

$$Z_y = \sin\theta \tag{2.2.16}$$

provided that $A/(\beta + \gamma) = 1$. Substituting for Z_x and Z_y in equation (2.2.3), the elastic and elasto-plastic components of the restoring force, in X and Y direction after yield are obtained.

The interaction between the forces and moments in X, Y and Z directions at each bearing is important. In this report, interaction between only in plane forces in X and Y directions is considered. Contribution of the torsional moment of each individual bearing is negligible, hence it is neglected.

For an isotropic system, where stiffness and strength in the two orthogonal directions are the same, the interaction curve for F_x and F_y is of circular shape. For an orthotropic system, where stiffness and strength in the two orthogonal directions are different, the interaction curve for Fx and Fy deviates from the circular shape.

The shear stiffness degradation observed in high damping rubber bearings is modeled by varying α, the post yielding to elastic stiffness ratio. This bi-axial hysteretic model is used in Program 3D-BASIS for modeling lead-rubber bearings, high damping bearings and steel dampers.

2.2.4 Uni-axial Frictional Elements

In asymmetric structures, each sliding bearing undergoes different motion requiring multiple stick-slip conditions. The use of coulomb model [13,14,16,21] under these conditions is complicated. Hence the modified viscoplasticity model [45] is used in modeling frictional elements.

Experimental studies have shown that the coefficient of friction depends on velocity and bearing pressure [15,32,44]. The coefficient of sliding friction [32] at sliding velocity $\dot{U}$ may be approximated by the following equation:

$$\mu_s = f_{max} - \Delta f \exp(-a|\dot{U}|) \qquad (2.2.17)$$

where, f_{max} is the coefficient of friction at large velocity of sliding, Δf is the difference between f_{max} and the coefficient of sliding friction at very low velocity and a is a constant.

The frictional force F_f, in the modified viscoplasticity model [45] is given by:

$$F_f = \mu_s W Z \qquad (2.2.18)$$

where, μ_s is the coefficient of friction which varies with velocity, Z is defined by equation(2.2.2) and W is the weight or normal force at the friction interface. It should be noted that Z takes values of ± 1.0 during sliding (postyielding with low or negative stiffness) phase. During sticking (elastic behavior with high elastic stiffness generating near stick conditions) phase, the absolute value of Z is less than unity. The conditions of stick-slip are accounted for by equation(2.2.2). Quantity Z may be regarded as continuous approximation to the unit step function [45]. Limitations of the viscoplasticity model is its inability to reproduce truly rigid-plastic behavior. But, since Teflon-steel interfaces undergo very small elastic displacement before sliding [32], small value of yield displacement Y, of the order of 0.005 inches can be reasonably assumed and, hence, the viscoplasticity model can be used. The model exhibits insignificant rate dependency for such low yield displacement and the resulting ductility ratio and for $\eta = 2$, $\beta = 0.1$, and $\gamma = 0.9$. Hysteresis loops which are in good

agreement with experimental results [32] are produced by this model. Variation of coefficient of friction, μ_s, with bearing pressure is incorporated by adjusting, μ_s, based on bearing pressure. The normal force at the interface is updated at every step.

Break away friction is incorporated by adjusting, μ_s, to a higher value for times prior to initial sliding:

$$\mu_s = b(f_{max} - D_f) \qquad for \qquad |Z| \leq 0.999 \tag{2.2.19}$$

Initial sliding commences for values of $|Z| > 0.999$. Also $b > 1$, $(f_{max} - D_f)$ is the coefficient of sliding friction at essentially zero velocity of sliding. After sliding commences equation (2.2.17) gives the coefficient of friction. Increase in friction that follows momentary sticking is not accounted for.

2.2.5 Friction in Arbitrary Plane Motion and Bi-axial Friction Element to Model Teflon-steel Interfaces.

Plane motion friction [16,21] arises in base isolated structures with non-symmetric structural systems, and in systems excited by multidirectional ground motion. Asymmetric behavior is furthermore produced by differences in the frictional properties of Teflon bearings[45]. In general, a Teflon-steel interface will undergo displacement in the two orthogonal directions with rotation in the same plane. This motion will give rise to frictional forces in the two orthogonal directions and torque.

Friction forces generated at each interface, in X and Y directions, contribute to the overall restoring forces, force in X and Y direction and torsional moment, at the center of mass of the base. As in base isolated structures with elastomeric bearings, the contribution of torsional moment resistance of each interface is negligible as compared to the overall torsional moment resistance at the center of mass of the base, hence it is neglected.

The resultant resisting friction force at each pad opposes the instantaneous incremental displacement, computed at each time step of solution. This resultant frictional force is at an angle θ, to the X axis, at each instant. In general, plane motion of a Teflon-steel interface

without rotation, at each instant of time, the interface relative velocity components $\dot{U}_x$ and $\dot{U}_y$, can be used to establish instantaneous resultant velocity $\dot{U}$ and angle θ with respect to the X-axis:

$$\theta = \tan^{-1}(\dot{U}_y/\dot{U}_x) \qquad (2.2.20)$$

$$\dot{U} = (\dot{U}_x^2 + \dot{U}_y^2)^{1/2} \qquad (2.2.21)$$

The frictional forces F_x and F_y (exerted at the interface) are given by:

$$F_x = \mu_s W \cos\theta \qquad (2.2.22)$$

$$F_y = \mu_s W \sin\theta \qquad (2.2.23)$$

in which μ_s is described by equation (2.2.17). Parameters f_{max}, D_f and a depend, in general, on the direction of sliding. For an isotropic interface, μ_s, is independent of angle θ, the interaction curve for F_x and F_y, is of circular shape. For anisotropic interface, the interaction curve deviates from circular shape[45].

The interaction between the two frictional forces in X and Y directions and torque is of prime importance in the development of a model of friction in plane motion. Constantinou et al. [45] has shown that torque or equivalently the rotation at the interface does not have any interaction with the frictional forces in X and Y directions.

The model of friction in plane motion [45] is based on the coupled differential equations(2.2.4). These equations are used to account for the conditions of separation and reattachment of the Teflon-steel interface. During sliding, Z_x and Z_y attain their maximum values and the following conditions apply:

$$\frac{dZ_x}{dU_x} = \frac{dZ_y}{dU_y} = 0 \qquad (2.2.24)$$

Equation (2.2.4) can be expressed as:

$$Z_x^2 + \frac{dU_y}{dU_x} Z_x Z_y = \frac{A}{(\beta + \gamma)} \qquad (2.2.25)$$

$$Z_y^2 + \frac{dU_x}{dU_y} Z_x Z_y = \frac{A}{(\beta + \gamma)} \qquad (2.2.26)$$

where:

$$\frac{dU_y}{dU_x} = \tan\theta, \qquad \frac{dU_x}{dU_y} = \cot\theta \qquad (2.2.27)$$

The system of equations (2.2.25) and (2.2.26) have the solution

$$Z_x = \cos\theta, \qquad Z_y = \sin\theta \qquad (2.2.28)$$

provided that $A/(\beta + \gamma) = 1$. In this way, components of frictional force in the two orthogonal directions are expressed as:

$$F_x = \mu_s W Z_x \qquad (2.2.29)$$

$$F_y = \mu_s W Z_y \qquad (2.2.30)$$

which are identical to equations(2.2.22) and (2.2.23). It should be noted that this is true only when the ratio $A/(\beta + \gamma)$ is equal to unity. As discussed earlier, this condition reduces the uni-axial version of the model to one of the theory of viscoplasticity.

This model is used for modeling frictional elements, with friction in plane motion, in Program 3D-BASIS. The variation of coefficient of sliding friction with velocity ,bearing pressure, and breakaway friction is accounted for.

2.2.6 Comparison of Numerical Simulation and Experimental Results of Hysteretic and Frictional Elements

Two comparisons are considered:

1. Comparison with experimental tests conducted at Kajima corporation [40], Japan, on high damping rubber bearing and steel damper are considered.

2. Comparison with experimental results obtained by Constantinou et al. [32], for Teflon-steel interface is considered. The modified viscoplasticity model [32] described in section 2.2.4 is used for numerical simulation.

Friction in plane motion is considered.

Kajima's [40] tests were conducted on a high damping rubber bearing and steel damper. These specimens were of 1/7 scale. The steel damper is shown in figure 2-4. The vertical actuator in the test set up was controlled to hold the axial load at 4 ton(8.8 Kips), for the high damping rubber bearing, or controlled to hold the effective height of the steel damper. The horizontal actuators were controlled to obtain the desired motion in the horizontal plane.

The steel damper, shown in figure 2-4, had an effective height of 10 cm(3.937 in), elastic horizontal stiffness of 2.58 ton/cm(14.417 Kip/in), yield force of 0.286 ton(0.6292 Kip), and yield displacement of 0.111 cm(0.0437 in).

The high damping rubber bearing had 24 layers of 50 hardness rubber of 1.2 mm(0.0472 in) thickness, with 24 steel insert plates of 0.5 mm(0.01968 in) thickness. Design dead weight was 4 ton(8.8 Kips), post yielding horizontal stiffness was 0.281 ton/cm(1.5702 Kip/in), and vertical stiffness was 0.451 ton/cm(2.5201 Kip/in).

The properties used for simulation of the uni-axial and bi-axial hysteresis loops are extracted from the experimental results. The bi-axial hysteretic model is used for this comparison.

The following parameters are used for simulation of results for steel damper, elastic horizontal stiffness of 2.58 ton/cm (14.417 Kip/in), yield force of 0.286 ton(0.6292 Kips), yield displacement of 0.111 cm(0.0437 in), $\alpha = 0.023$, $\beta = 0.1$, $\gamma = 0.9$ and $\eta = 2$. The amplitude of input motion is as shown in figures 2-5,2-6,2-7 and 2-8, the frequency is 0.25 Hz.

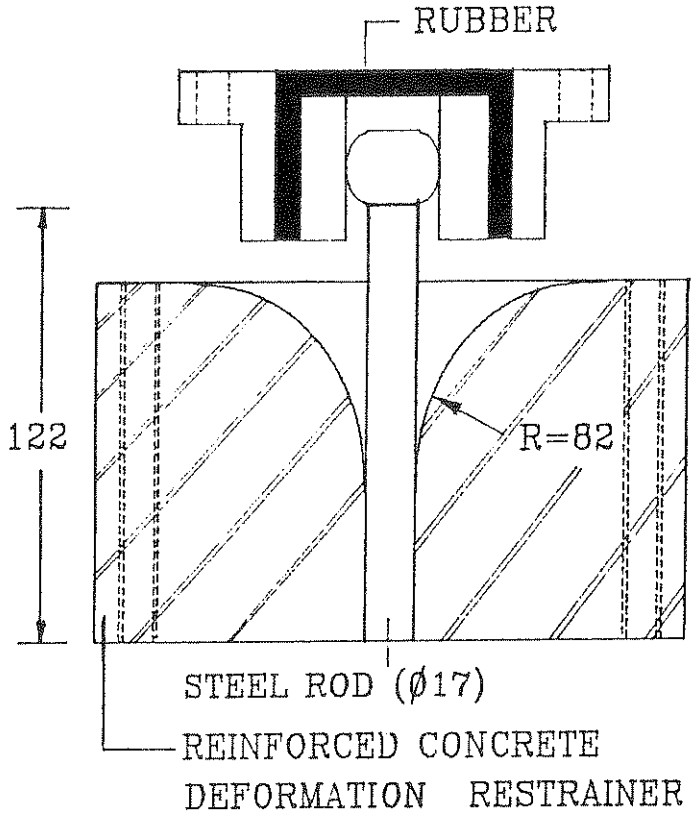

Figure 2-4 1/7 Scale Model of Kajima's Steel Damper used for Bi-directional tests. Units are Tons (1 Ton = 2.2 Kips) and Cm.

The Y direction sinusoidal motion frequency in the 8-shaped locus pattern is 0.5 Hz. Strain hardening is adopted by increasing the yield force and yield displacement as this was observed in the experimental results.

Figures 2-5, 2-6, 2-7 and 2-8 show the comparison of experimental and simulated response for unidirectional, circular, elliptical and 8-shaped locus patterns, respectively.

The following parameters are used for simulation of results for high damping rubber bearing. Elastic horizontal stiffness of 1.1 ton/cm(6.1468 Kip/in), yield force 0.165 ton/cm(0.922 Kip/in), yield displacement of 0.15 cm(0.05906 in), $\alpha = 0.3$, $\beta = 0.1$, $\gamma = 0.9$ and $\eta = 2$. The amplitude of input motion is as shown in figures 2-9, 2-10, 2-11 and 2-12, the frequency is 0.25 Hz. The Y direction sinusoidal motion frequency in the 8-shaped locus pattern is 0.5 Hz. Shear stiffness degradation of 50% at 100% strain is adopted. Shear stiffness degradation is incorporated as follows:

$$\alpha_x^* = \alpha_x\left(0.5 + 0.5e^{(-5|U_x|/t_s)}\right) \qquad (2.2.34)$$

where U_x is the X direction displacement, t_s is the thickness of the rubber, α_x is postyielding to preyielding stiffness ratio, α_x^* is the modified α_x. The same modification is adopted for the Y direction.

Figures 2-9, 2-10, 2-11 and 2-12 show the comparison of experimental and simulated response for unidirectional, circular, elliptical and 8-shaped locus patterns, respectively.

To study the effect of interaction between forces in the X and Y direction, the steel damper is subjected to a locus pattern with constant velocity. The velocity in both X and Y directions is 2 cm/sec (5.08 in/sec). Amplitude of motion is 3 cm (1.181 in). Figures 2-13 and 2-14 show the force-displacement relationship in X and Y directions, respectively. From point 5 to 6, displacement is increased only in the X direction, maintaining the same displacement in the Y direction. As expected, the resistance in the X direction is increased from point 5 to 6 in figure 2-13. However, the resistance in the Y direction is clearly reduced from point 5 to 6 in figure 2-14, despite no change in deformation in that direction. Hence the lateral resistance of a direction is reduced with displacement in the orthogonal direction. This clearly indicates the bi-axial interaction.

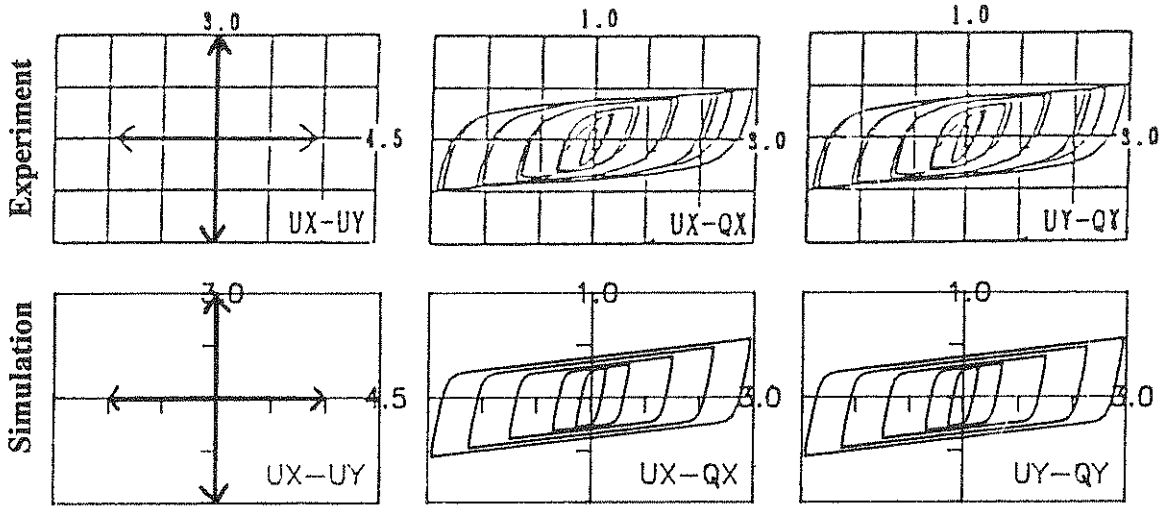

Figure 2-5 Comparison of Experimental and Simulated Results of the Bi-directional Tests on a 1/7 Scale Model of Kajima's Steel Damper for Uni-directional Motion. Units are Tons (1 Ton = 2.2 Kips) and Cm.

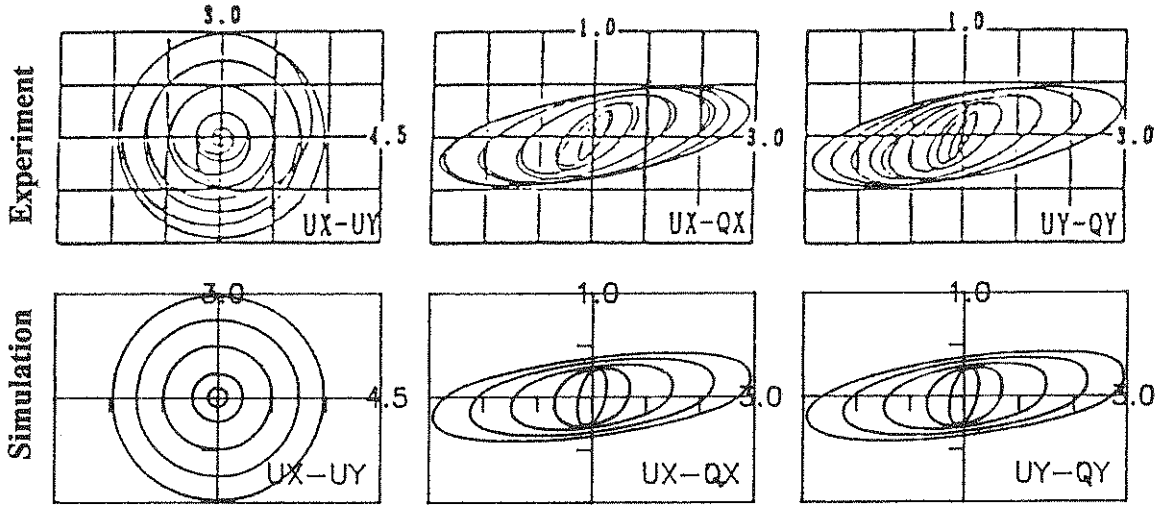

Figure 2-6 Comparison of Experimental and Simulated Results of the Bi-directional Tests on a 1/7 Scale Model of Kajima's Steel Damper for Circular Motion. Units are Tons (1 Ton = 2.2 Kips) and Cm.

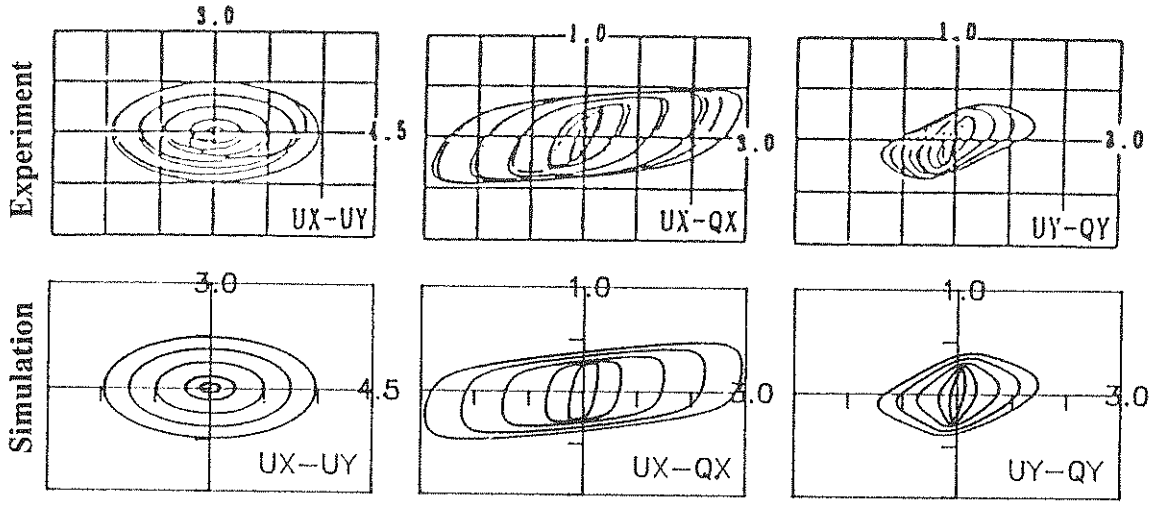

Figure 2-7 Comparison of Experimental and Simulated Results of the Bi-directional Tests on a 1/7 Scale Model of Kajima's Steel Damper for Elliptical Motion. Units are Tons (1 Ton = 2.2 Kips) and Cm.

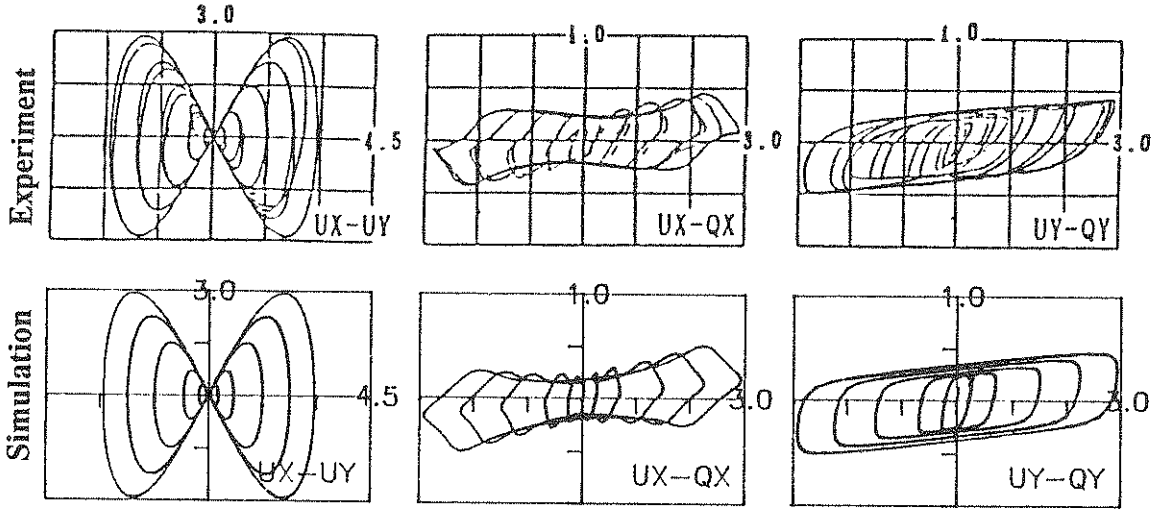

Figure 2-8 Comparison of Experimental and Simulated Results of the Bi-directional Tests on a 1/7 Scale Model of Kajima's Steel Damper for 8-Shaped Motion. Units are Tons (1 Ton = 2.2 Kips) and Cm.

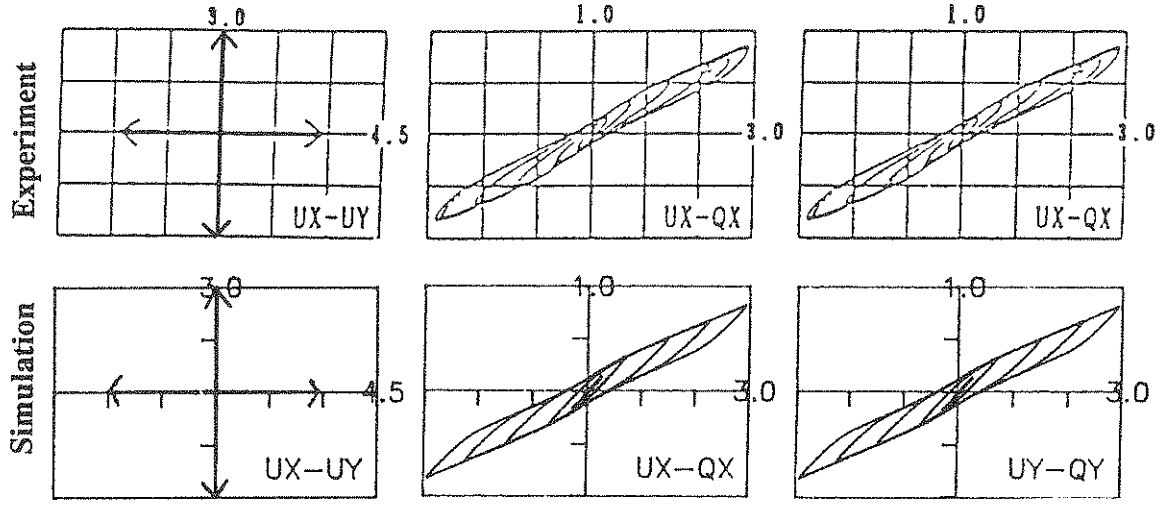

Figure 2-9 Comparison of Experimental and Simulated Results of the Bi-directional Tests on a 1/7 Scale Model of Kajima's High Damping Rubber Bearing for Uni-directional Motion. Units are Tons (1 Ton = 2.2 Kips) and Cm.

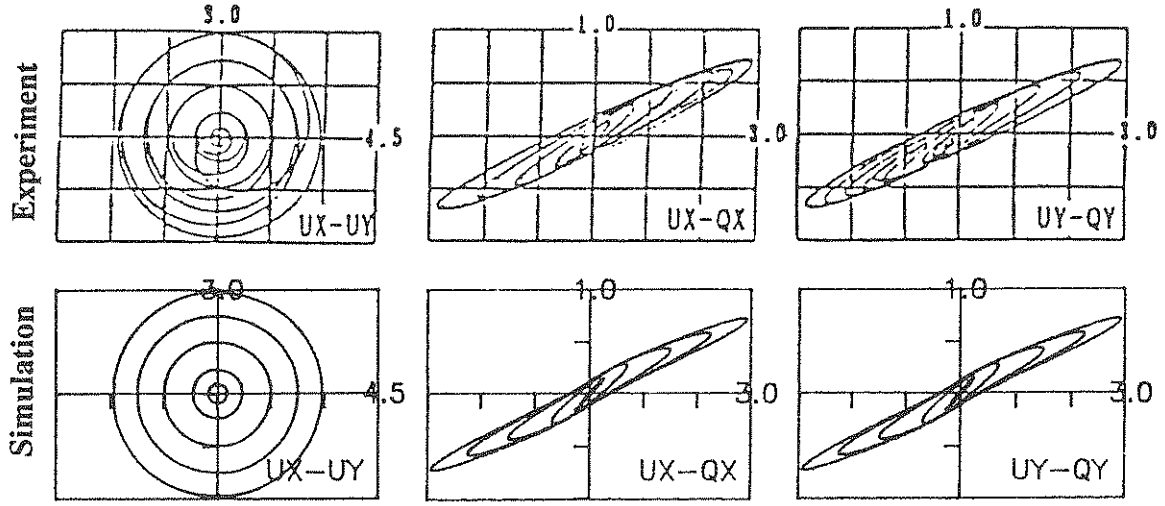

Figure 2-10 Comparison of Experimental and Simulated Results of the Bi-directional Tests on a 1/7 Scale Model of Kajima's High Damping Rubber Bearing for Circular Motion. Units are Tons (1 Ton = 2.2 Kips) and Cm.

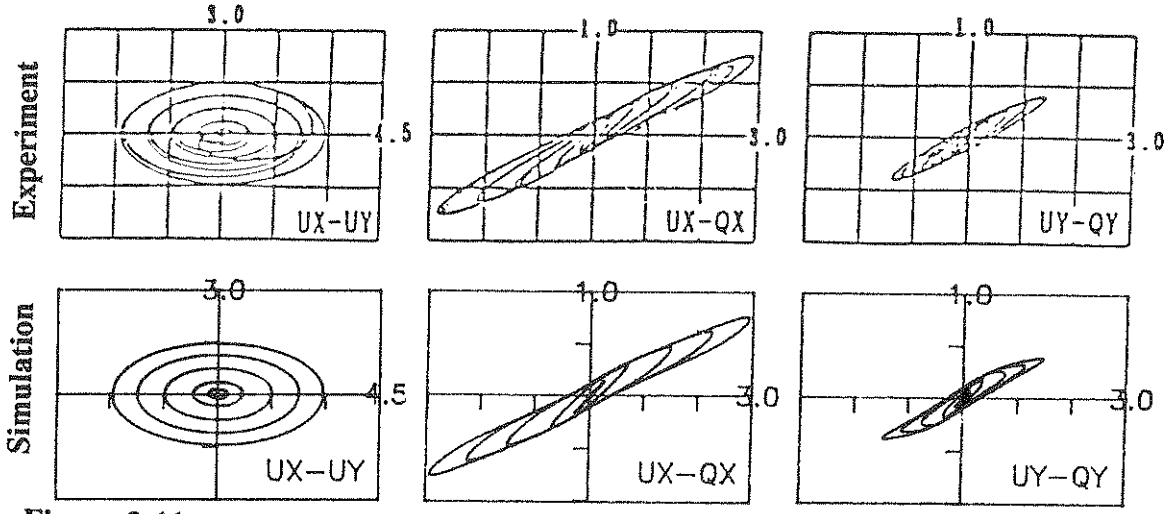

Figure 2-11 Comparison of Experimental and Simulated Results of the Bi-directional Tests on a 1/7 Scale Model of Kajima's High Damping Rubber Bearing for Elliptical Motion. Units are Tons (1 Ton = 2.2 Kips) and Cm.

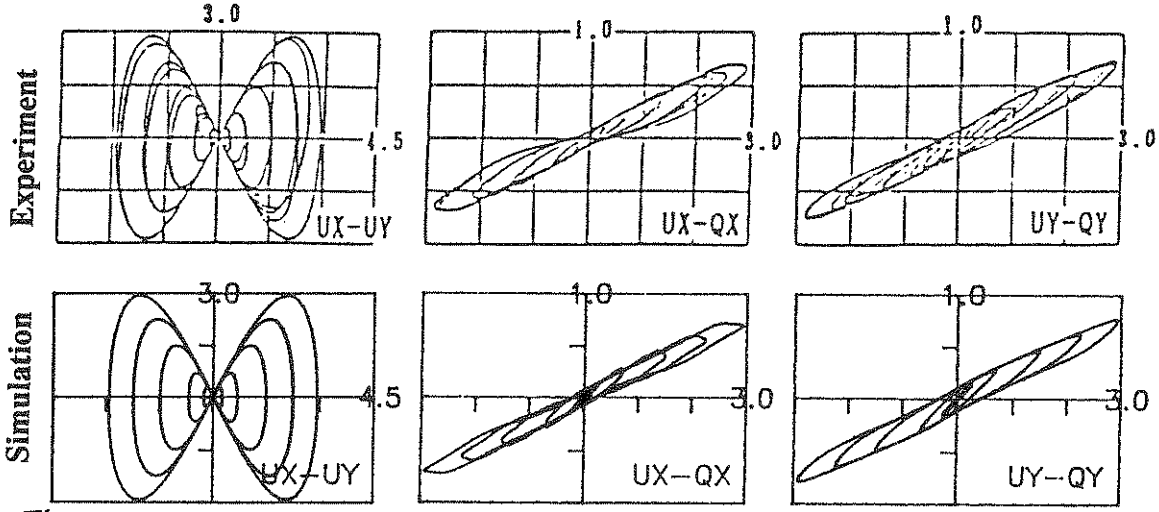

Figure 2-12 Comparison of Experimental and Simulated Results of the Bi-directional Tests on a 1/7 Scale Model of Kajima's High Damping Rubber Bearing for 8-Shaped Motion. Units are Tons (1 Ton = 2.2 Kips) and Cm.

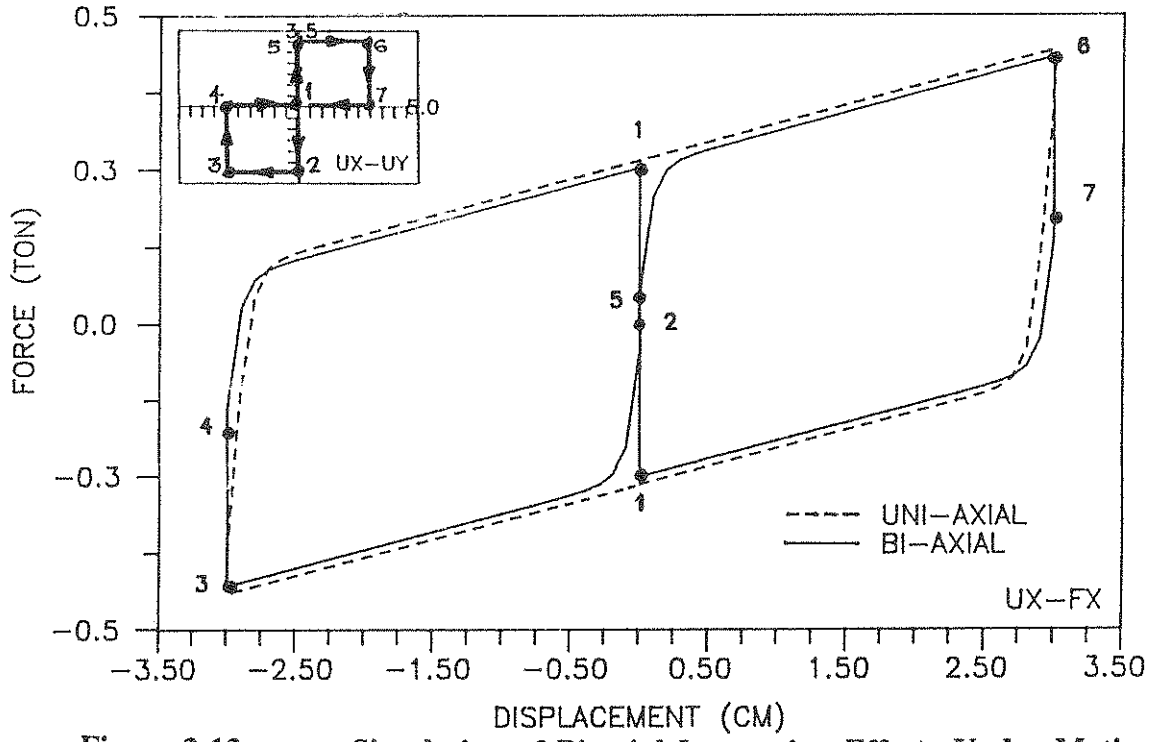

Figure 2-13 **Simulation of Bi-axial Interaction Effects Under Motion of Constant Velocity (Shown in upper left corner) on Kajima's Steel Damper. Units are Tons (1 Ton = 2.2 Kips) and Cm.**

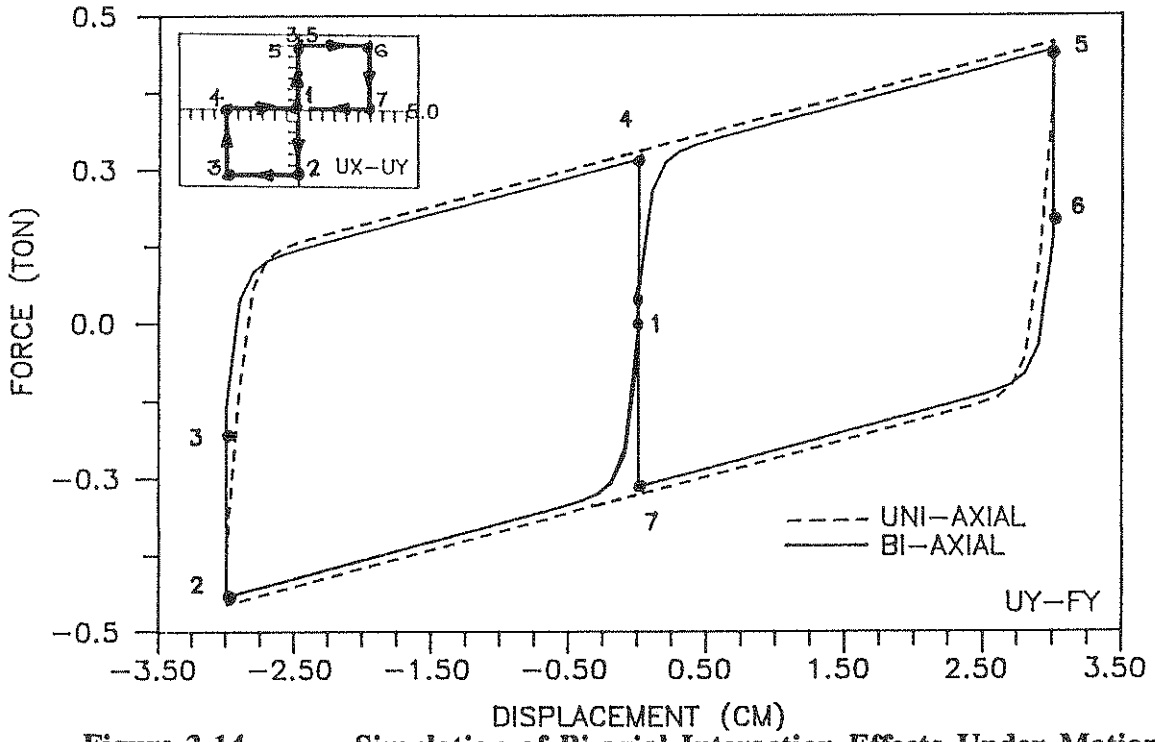

Figure 2-14 **Simulation of Bi-axial Interaction Effects Under Motion of Constant Velocity (Shown in upper left corner) on Kajima's Steel Damper. Units are Tons (1 Ton = 2.2 Kips) and Cm.**

The marked similarity of the two hysteresis loops with those of Otani's [41] bi-directional tests (shown in figure 2-15) on reinforced concrete column specimen B8-0 is noted. The same locus pattern shown in figures 2-13 and 2-14 was used for this test.

The Teflon-steel interface experiment [32] was conducted on a highly polished stainless steel-unfilled Teflon interface at 1000 psi pressure. The input was a sinusoidal wave of 1.0 inch amplitude and frequency 0.16 Hz. Figure 2-16 shows the experimental hysteresis loops. The following parameters are used for the hysteretic model, $\beta = 0.1$, $\gamma = 0.9$, $\eta = 2$, and $U^y = 0.01$ in. Figure 2-16 shows the simulated hysteresis loops.

Friction in plane motion is considered. The model developed for plane motion friction is used for this study. Isotropic interface condition (same coefficient of friction in all directions) is considered. The parameters used above for steel-unfilled Teflon interface at 1000 psi pressure are used for this analytical study. The amplitude of input motion is as shown in figures 2-17, 2-18 and 2-19, the frequency is 0.16 Hz. The Y direction sinusoidal motion frequency for 8-shaped locus pattern was 0.32 Hz. The simulated hysteresis loops are shown in figures 2-17, 2-18 and 2-19. To compare the model without bi-axial interaction, two uni-axial models described in section 2.2.4, are used in X and Y directions, independently. The simulated results are shown in dotted lines in figures 2-17, 2-18 and 2-19.

2.2.7 Validation of the Bi-axial Hysteretic and Friction Element

The validation of the proposed bi-axial model for hysteretic and friction element should be based on experimental data. Such an assessment requires identification of the model parameters and validation of the model. A complete validation of the model requires experimental data with bi-directional motion. In the case of bi-axial hysteretic model for rubber bearings and steel dampers Kajima's [40] and Otani's [41] tests are available for qualitative validation. However, in the case of friction in plane motion, no bi-directional tests are available.

The bi-axial model clearly simulates satisfactory hysteresis loops in the case of rubber bearings and steel dampers. Validation of the proposed model in this case is provided by:

(a) When uni-directional motion is imposed in an arbitrary direction, the resulting restoring force is in the same direction and has the same magnitude as that of a uni-axial element in that direction.

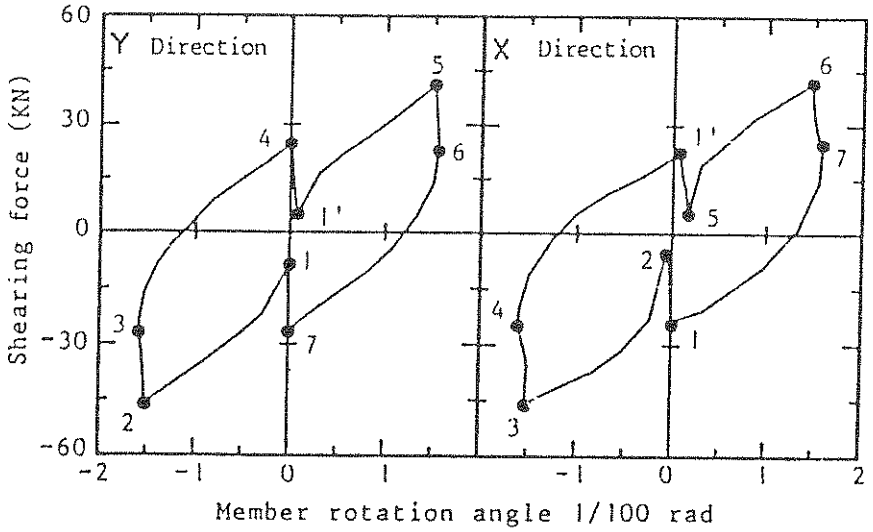

Figure 2-15 Otani's Bi-directional Tests on Reinforced Concrete Column Specimen B8-0.

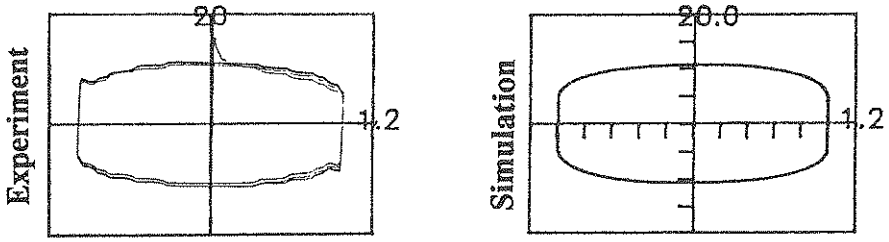

Figure 2-16 Comparison of Results of Experiment No. 62 Conducted on Unfilled Teflon- steel Interface at 1000 psi Pressure for Motion of Low Velocity by Constantinou et al. and Simulated Results. Units are Kips and In.

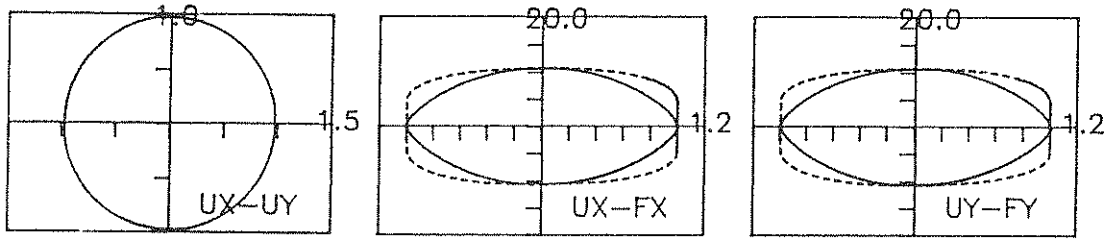

--- Uni-Axial
—— Bi-Axial

Figure 2-17 Simulation of Friction Behavior of Unfilled Teflon-steel Interface Under Bi-directional Circular Motion of Low Velocity at 1000 psi Pressure. Units are Kips and In.

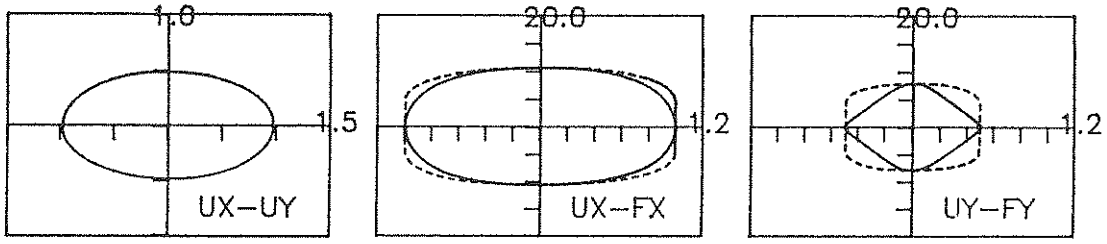

---- Uni-Axial
—— Bi-Axial

Figure 2-18 Simulation of Friction Behavior of Unfilled Teflon-steel Interface Under Bi-directional Elliptical Motion of Low Velocity at 1000 psi Pressure. Units are Kips and In.

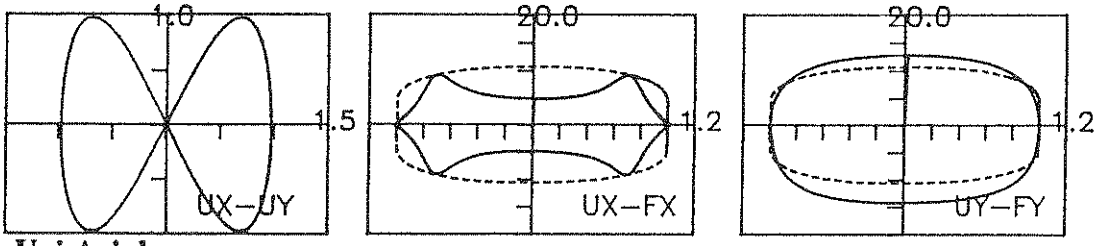

---- Uni-Axial
—— Bi-Axial

Figure 2-19 Simulation of Friction Behavior of Unfilled Teflon-steel Interface Under Bi-directional 8-Shaped Motion of Low Velocity at 1000 psi Pressure. Units are Kips and In.

The model is capable of producing this behavior by virtue of equations (2.2.3),(2.2.4),(2.2.15) and (2.2.16).

(b) When multidirectional motion with out-of-phase components is imposed, the resulting force-displacement loops exhibit a marked similarity with experimental results from testing of high damping rubber bearing and steel damper developed by Kajima Corporation, Japan [40].

(c) When motion of constant velocity is imposed, the force-displacement loops exhibit a marked similarity with experimental results from testing of a reinforced concrete column specimen by Otani [41].

Figure 2-20 shows the simulated force-displacement loops and the force response of Kajima's steel damper, simulated using uni-axial model independently in X and Y directions, and bi-axial model, under bi-directional 8-shaped motion in which

$$U_x = U_0 \sin \omega t, \quad U_y = U_0 \sin 2\omega t$$

with U_0= 3 cm and $\omega = 1.5707 rad/\sec(0.25 Hz)$. The isotropic case is considered. The parameters of the steel damper and the model used for simulation are as described before for the bi-directional test shown in Figure 2-8. Further validation of the proposed model is provided by:

(a) The bi-axial force in the X direction approaches the uni-axial force in the X direction when the elasto-plastic component of the bi-axial force in the Y direction approaches zero value, indicating very little interaction. This can be observed at points 2 and 4 in figure 2-20(b). The elasto-plastic component of the bi-axial force in X direction, near zero value, approaches the elasto-plastic component of the uni-axial force in X direction. This can be observed at point 3 in figure 2-20(b).

In the case of friction in arbitrary plane motion, the assessment and validation should be based on experimental data with bi-directional motion. The identification of the model parameters for uni-directional motion, in both parallel to lay and perpendicular to lay directions, has been investigated by Constantinou et al. [32]. In lieu of experimental data under bi-directional motion, the following indirect validation of the proposed model is provided:

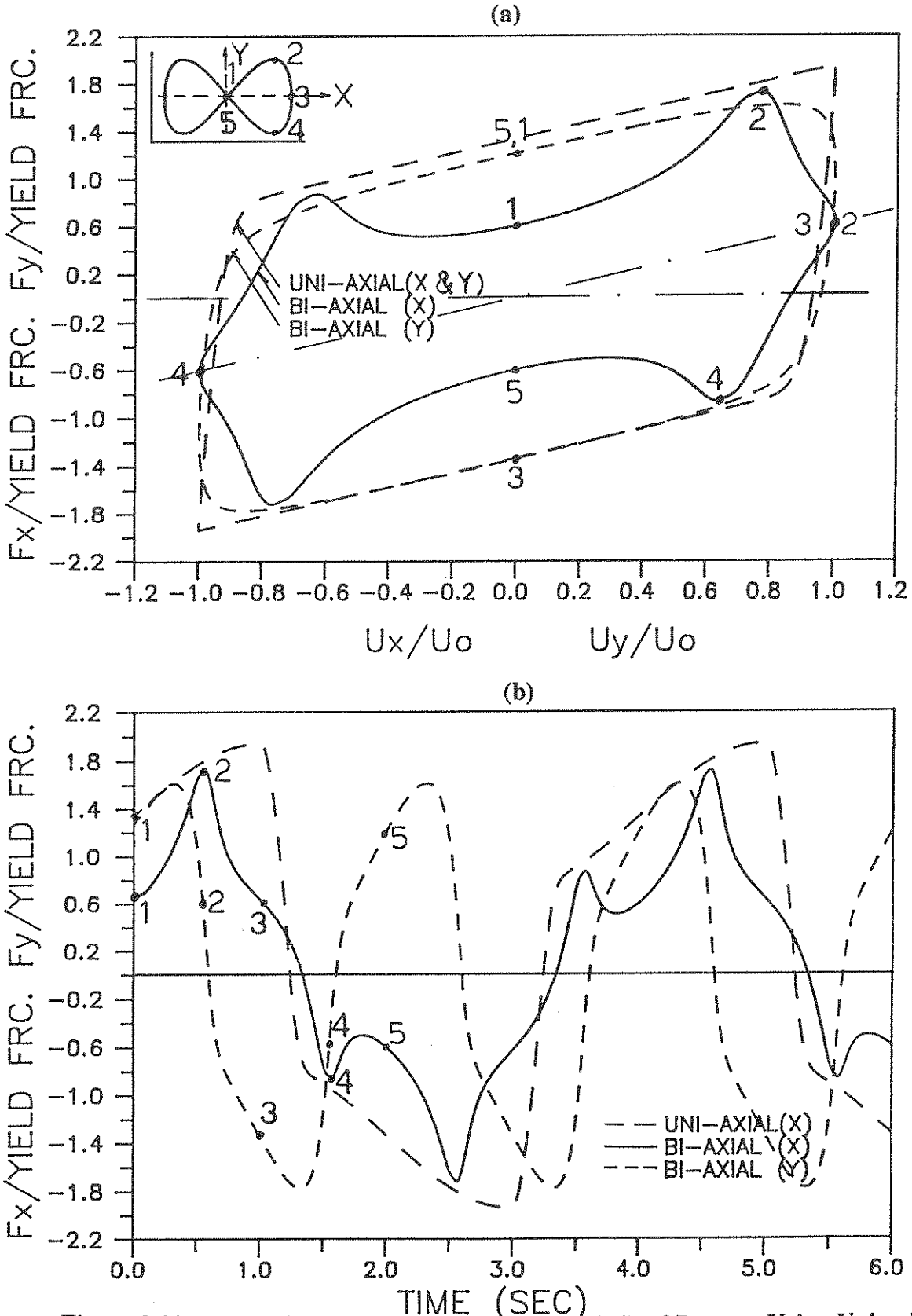

Figure 2-20 **Simulated Response of Kajima's Steel Damper Using Uni-axial and Bi-axial Models Under Bi-directional 8-Shaped Motion (a) Force-Displacement Response (8-Shaped Motion Shown in the Upper Left Corner) (b) Force Response.**

(a) When uni-directional motion is imposed in an arbitrary direction, the resulting frictional force is in the same direction and has the same magnitude as that of a uni-axial element in that direction. The model is capable of producing this behavior by virtue of equations (2.2.22) and (2.2.23).

(b) When multi-directional motion with out-of-phase components is imposed, the resulting force-displacement loops exhibit a marked similarity with experimental results from testing of steel damper developed by Kajima Corporation, Japan [40].

Figure 2-21 shows the simulated force-displacement loops and the force response of unfilled Teflon-steel interface used by Constantinou et al. [32], simulated using uni-axial model independently in X and Y directions, and bi-axial model, under bi-directional 8-shaped motion in which

$$U_x = U_0 \sin \omega t, \quad U_y = U_0 \sin 2\omega t$$

with $U_0 = 1$ in and $\omega = 1.0 rad/\sec(0.16 Hz)$. The isotropic case is considered. The parameters of unfilled Teflon-steel interface and the model used for simulation are as described before for the uni-directional test shown in figure 2-19. Further validation of the proposed model is provided by:

(a) The bi-axial force in the X direction approaches the uni-axial force in the X direction when the bi-axial force in the Y direction approaches zero value, indicating very little interaction. This can be observed at points 2 and 4 in figure 2-21(b). The forces in figure 2-21 are normalised by the normal force or weight W at the interface. The bi-axial force in X direction, near zero value, approaches the uni-axial force in X direction. This can be observed at point 3 in figure 2-21(b).

Hence the proposed bi-axial model is adopted for the hysteretic element and the frictional element.

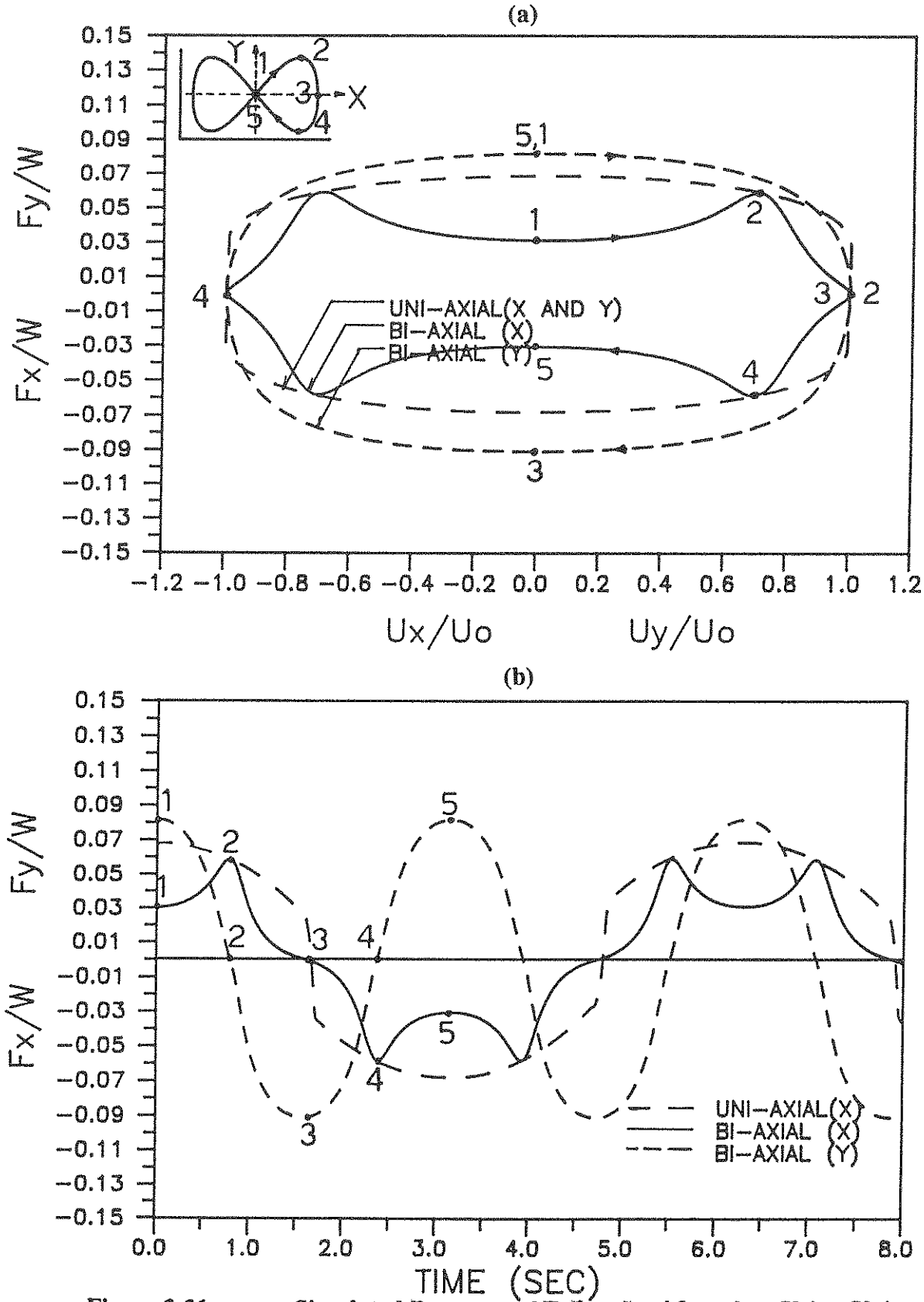

Figure 2-21 **Simulated Response of Teflon-Steel Interface Using Uni-axial and Bi-axial Models Under Bi-directional 8-Shaped Motion of Low Velocity at 1000 psi Pressure (a) Force-Displacement Response (8-Shaped Motion Shown in the Upper Left Corner) (b) Force Response.**

2.3 Equations of Motion and Modal Reduction

2.3.1 Equations of Motion

The superstructure consists of a three-dimensional elastic shear building, as explained in Section 2.1. The linear and nonlinear isolation elements are restricted to the base. A typical base isolated multistory building and the displacement coordinates that will be used in the formulation are shown in figure 2-1, 2-2, 2-3 and 2-22. Figure 2-22 shows the superstructure relative displacement as U_l and does not carry either the subscript x or y along with the subscript l, as this is a general elevation of the isolated building.

The equation of motion for the **superstructure**, with respect to the vertical axis at the center of mass of the base, is as follows:

$$\mathbf{M}_{nxn}\ddot{\mathbf{u}}_{nx1} + \mathbf{C}_{nxn}\dot{\mathbf{u}}_{nx1} + \mathbf{K}_{nxn}\mathbf{u}_{nx1} = -\mathbf{M}_{nxn}\mathbf{R}_{nx3}\{\ddot{\mathbf{u}}_g + \ddot{\mathbf{u}}_b\}_{3x1} \qquad (2.3.1)$$

Where:

M = Diagonal mass matrix =

$$\begin{pmatrix} m_{xn} & . & . & . & . & . & . & . \\ . & m_{yn} & . & . & . & . & . & . \\ . & . & m_{tn} & . & . & . & . & . \\ . & . & . & . & . & . & . & . \\ . & . & . & . & . & m_{x1} & . & . \\ . & . & . & . & . & . & m_{y1} & . \\ . & . & . & . & . & . & . & m_{t1} \end{pmatrix}$$

C = Damping matrix

K = Stiffness matrix (see Table 2-I)

$$\mathbf{R} = \begin{pmatrix} \mathbf{R}_n^* \\ . \\ . \\ \mathbf{R}_l^* \\ . \\ \mathbf{R}_1^* \end{pmatrix}$$

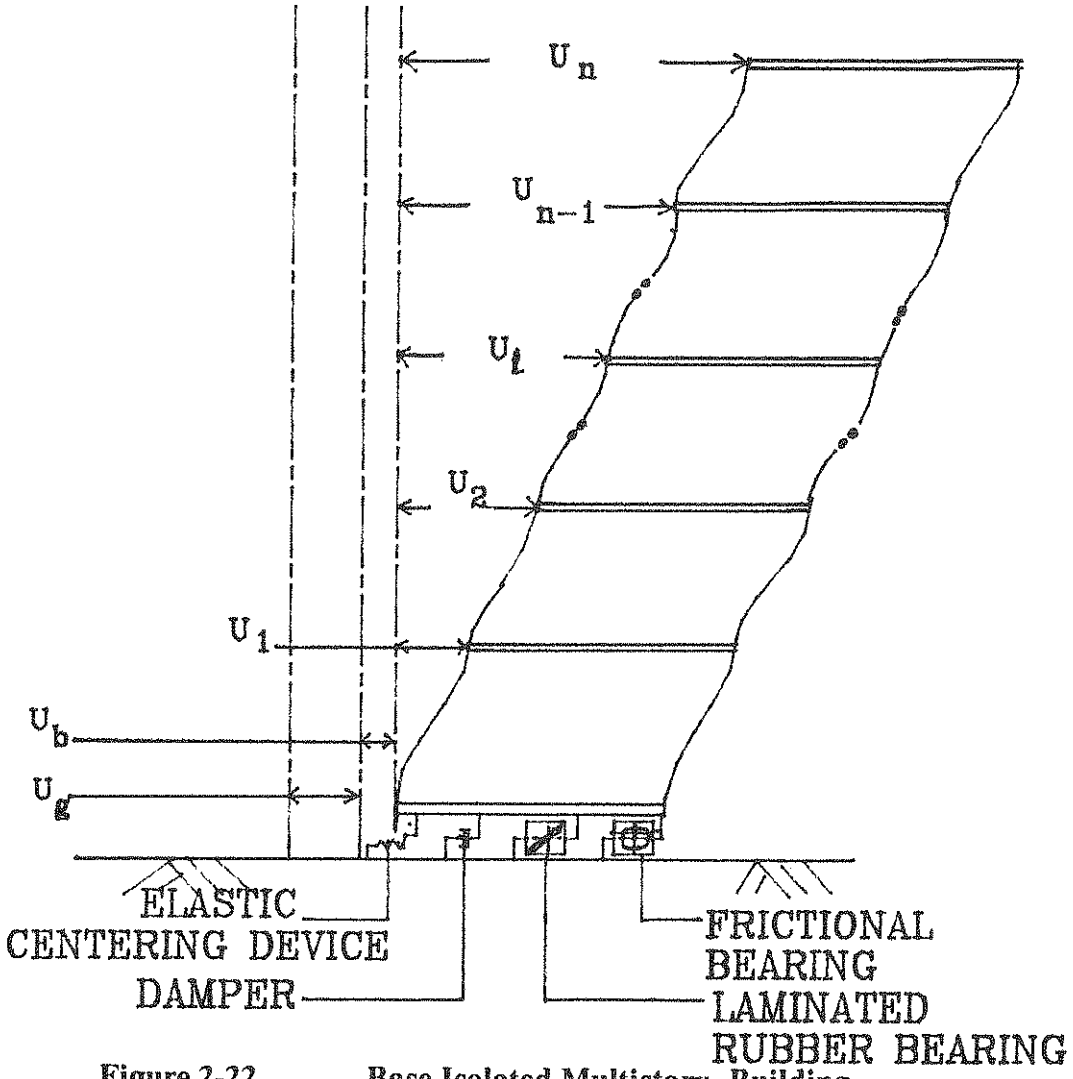

Figure 2-22 **Base Isolated Multistory Building**

Where:

$$\mathbf{R}_l^* = \begin{pmatrix} 1 & 0 & -Y_l \\ 0 & 1 & X_l \\ 0 & 0 & 1 \end{pmatrix}$$

where:

X_l = the distance to the center of mass of l^{th} floor from the center of mass of the base in X direction.

Y_l = the distance to the center of mass of l^{th} floor from the center of mass of the base in Y direction.

$\ddot{\mathbf{u}}$ = Relative acceleration, relative to base

$$\ddot{\mathbf{u}} = \begin{Bmatrix} \ddot{\mathbf{u}}_{xn} \\ \ddot{\mathbf{u}}_{yn} \\ \ddot{\mathbf{u}}_{tn} \\ \cdot \\ \cdot \\ \cdot \\ \ddot{\mathbf{u}}_{xl} \\ \ddot{\mathbf{u}}_{yl} \\ \ddot{\mathbf{u}}_{tl} \end{Bmatrix}$$

$\dot{\mathbf{u}}$ = Relative velocity, relative to base

$\mathbf{u}$ = Relative displacement, relative to base

$\ddot{\mathbf{u}}_b$ = Base acceleration, relative to ground

$\ddot{\mathbf{u}}_g$ = Ground acceleration

For computational efficiency, the superstructure is reduced using modal reduction. The modal reduction was found to be more accurate than alternative reduction using Ritz vectors [19]. The reduction is obtained as follows:

$$\mathbf{u} = \Phi \mathbf{u}^* \qquad (2.3.2)$$

where:

$\mathbf{u}^*$ = Modal displacement, relative to base

$\mathbf{u}$ = Relative displacement, relative to base

Φ = Modal matrix

The reduced equation of motion in modal coordinates is obtained using equation(2.3.2) in equation (2.3.1) and premultiplying equation (2.3.1) by Φ^T:

$$[\Phi^T \mathbf{M} \Phi]_{nxn} \ddot{\mathbf{u}}^*_{nx1} + [\Phi^T \mathbf{C} \Phi]_{nxn} \dot{\mathbf{u}}^*_{nx1} + [\Phi^T \mathbf{K} \Phi]_{nxn} \mathbf{u}^*_{nx1} = -[\Phi^T \mathbf{M R}]_{nx3} \{\ddot{\mathbf{u}}_g + \ddot{\mathbf{u}}_b\}_{3x1} \tag{2.3.3}$$

for modal matrix normalized with respect to mass matrix, we obtain:

$$[I]_{nxn} \ddot{\mathbf{u}}^*_{nx1} + [2\zeta_i \omega_i]_{nxn} \dot{\mathbf{u}}^*_{nx1} + [\omega_i^2]_{nxn} \mathbf{u}^*_{nx1} = -[\Phi^T \mathbf{M R}]_{nx3} \{\ddot{\mathbf{u}}_g + \ddot{\mathbf{u}}_b\}_{3x1} \tag{2.3.4}$$

where:

ζ_i = Modal damping factor for the i th mode

ω_i = Natural frequency of the i th mode

The equation of motion for the **base** with respect to the vertical axis at the center of mass of the base, is as follows:

$$\mathbf{M}_{s\,3xn}\{\{\ddot{\mathbf{u}}\} + \mathbf{R}\{\ddot{\mathbf{u}}_b + \ddot{\mathbf{u}}_g\}\}_{nx1} + \mathbf{M}_{b\,3x3}\{\ddot{\mathbf{u}}_b + \ddot{\mathbf{u}}_g\}_{3x1} + \mathbf{C}_{b\,3x3}\{\dot{\mathbf{u}}_b\}_{3x1} + \mathbf{K}_{b\,3x3}\{\mathbf{u}_b\}_{3x1} + \{\mathbf{f}_N\}_{3x1} = 0 \tag{2.3.5}$$

where:
$$\mathbf{M}_s = \begin{pmatrix} m_{xn} & 0 & 0 & \cdots & m_{x1} & 0 & 0 \\ 0 & m_{yn} & 0 & \cdots & 0 & m_{y1} & 0 \\ 0 & 0 & m_{tn} & \cdots & 0 & 0 & m_{t1} \end{pmatrix}$$

$= \mathbf{R}^T \mathbf{M}$

$$\mathbf{M}_b = \begin{pmatrix} m_{bx} & 0 & 0 \\ 0 & m_{by} & 0 \\ 0 & 0 & m_{bt} \end{pmatrix}$$

$\mathbf{C}_b$ = Damping matrix of the base

$\mathbf{K}_b$ = Stiffness matrix of elastic elements at various locations at the base

$\mathbf{f}_N = \{\mathbf{f}_{Hysteretic} + \mathbf{f}_{Friction}\}$

$\mathbf{f}_{Hysteretic}$ = Restoring force from hysteretic elements

$\mathbf{f}_{Friction}$ = Restoring force from frictional elements

$\mathbf{u}, \mathbf{u}_b, \mathbf{u}_g$,are as defined in equation (2.3.1)

Rewriting the equation (2.3.5):

$$[\mathbf{R}^T\mathbf{M}]_{3xn}\ddot{\mathbf{u}}_{nx1} + [\mathbf{R}^T\mathbf{M}]_{3xn}\mathbf{R}_{nx3}\{\ddot{\mathbf{u}}_b + \ddot{\mathbf{u}}_g\}_{3x1} + \mathbf{M}_{b\,3x3}\{\ddot{\mathbf{u}}_b + \ddot{\mathbf{u}}_g\}_{3x1} + \mathbf{C}_{b\,3x3}\dot{\mathbf{u}}_{b\,3x1} + \mathbf{K}_{b\,3x3}\mathbf{u}_{b\,3x1} + \mathbf{f}_{N\,3x1} = 0 \qquad (2.3.6)$$

Using modal reduction, from equation (2.3.2):

$$\mathbf{R}^T_{3xn}\mathbf{M}_{nxn}\Phi_{nxn}\ddot{\mathbf{u}}^*_{nx1} + [\mathbf{R}^T\mathbf{M}\mathbf{R} + \mathbf{M}_b]_{3x3}\{\ddot{\mathbf{u}}_b + \ddot{\mathbf{u}}_g\}_{3x1} + \mathbf{C}_{b\,3x3}\dot{\mathbf{u}}_{b\,3x1} + \mathbf{K}_{b\,3x3}\mathbf{u}_{b\,3x1} + \mathbf{f}_{N\,3x1} = 0 \qquad (2.3.7)$$

Combining equations (2.3.4) and (2.3.7):

$$\begin{pmatrix} [\mathbf{I}] & [\Phi^T\mathbf{M}\mathbf{R}] \\ [\mathbf{R}^T\mathbf{M}\Phi] & [\mathbf{R}^T\mathbf{M}\mathbf{R} + \mathbf{M}_b] \end{pmatrix}_{(n+3)x(n+3)} \begin{Bmatrix} \ddot{\mathbf{u}}^* \\ \ddot{\mathbf{u}}_b \end{Bmatrix}_{(n+3)x1} + \begin{pmatrix} [2\xi_i\omega_i] & 0 \\ 0 & [\mathbf{C}_b] \end{pmatrix}_{(n+3)x(n+3)} \begin{Bmatrix} \dot{\mathbf{u}}^* \\ \dot{\mathbf{u}}_b \end{Bmatrix}_{(n+3)x1}$$
$$+ \begin{pmatrix} [\omega_i^2] & 0 \\ 0 & [\mathbf{K}_b] \end{pmatrix}_{(n+3)x(n+3)} \begin{Bmatrix} \mathbf{u}^* \\ \mathbf{u}_b \end{Bmatrix}_{(n+3)x1} + \begin{Bmatrix} 0 \\ \mathbf{f}_N \end{Bmatrix}_{(n+3)x1} = -\begin{bmatrix} \Phi^T\mathbf{M}\mathbf{R} \\ \mathbf{R}^T\mathbf{M}\mathbf{R} + \mathbf{M}_b \end{bmatrix}_{(n+3)x3} \ddot{\mathbf{u}}_{g\,3x1} \qquad (2.3.8)$$

the reduced equation of motion for the superstructure and the base is as follows:

$$\mathbf{M}^{*}\ddot{\mathbf{u}}_{t}^{c} + \mathbf{C}^{*}\dot{\mathbf{u}}_{t}^{c} + \mathbf{K}^{*}\mathbf{u}_{t}^{c} + \mathbf{f}_{t} = \mathbf{p}_{t} \qquad (2.3.9)$$

where: $\mathbf{u}_{t}^{c} = \begin{Bmatrix} \mathbf{u}^{*} \\ \mathbf{u}_{b} \end{Bmatrix}_{t}$

2.4 Numerical Solution

2.4.1 Numerical Solution of the Differential Equations of Motion

The reduced equations of motion are solved numerically by discretizing them in time, with the exact solution $\mathbf{u}(t)$, $\dot{\mathbf{u}}(t)$, and $\ddot{\mathbf{u}}(t)$ approximated by $\mathbf{u}_{t}$, $\dot{\mathbf{u}}_{t}$, and $\ddot{\mathbf{u}}_{t}$, respectively. The step-by-step integration procedure starts with the known initial conditions and marches forward in time giving the solution at discrete time intervals. The process for a nonlinear system has two distinct phases. The first phase is the linearization phase, in which the equations are linearized about the current state by retaining only the first order terms of the Taylor series expansion. Estimates of the solution at the next step are then obtained by using these linearized equations. The second phase is the state determination phase, in which the internal forces in equilibrium with the new state of motion are calculated. In the first phase, Newmark's method is used and in the second phase, the internal forces in the hysteretic or frictional elements are computed using a fourth order Runge-Kutta scheme.

The equation of motion at time $\tau = t + \Delta t$, from equation (2.3.9):

$$\mathbf{M}^{*}\ddot{\mathbf{u}}_{\tau}^{c} + \mathbf{C}^{*}\dot{\mathbf{u}}_{\tau}^{c} + \mathbf{K}^{*}\mathbf{u}_{\tau}^{c} + \mathbf{f}_{\tau} = \mathbf{p}_{\tau} \qquad (2.4.1)$$

where: $\mathbf{u}_{\tau}^{c} = \mathbf{u}_{t}^{c} + \Delta\mathbf{u}^{c}$

$$\dot{\mathbf{u}}_{\tau}^{c} = \dot{\mathbf{u}}_{t}^{c} + \Delta\dot{\mathbf{u}}^{c}$$

$$\ddot{\mathbf{u}}_{\tau}^{c} = \ddot{\mathbf{u}}_{t}^{c} + \Delta\ddot{\mathbf{u}}^{c}$$

$$\mathbf{f}_{\tau} = \mathbf{f}_{t} + \Delta\mathbf{f}$$

$$\tau = t + \Delta t$$

$$\mathbf{M}^*\{\ddot{\mathbf{u}}_t^c + \Delta\ddot{\mathbf{u}}^c\} + \mathbf{C}^*\{\dot{\mathbf{u}}_t^c + \Delta\dot{\mathbf{u}}^c\} + \mathbf{K}^*\{\mathbf{u}_t^c + \Delta\mathbf{u}^c\} + \mathbf{f}_t + \Delta\mathbf{f} = \mathbf{p}_\tau \qquad (2.4.2)$$

subtracting equation (2.3.9) from equation (2.4.2):

$$\mathbf{M}^*\Delta\ddot{\mathbf{u}}^c + \mathbf{C}^*\Delta\dot{\mathbf{u}}^c + \mathbf{K}^*\Delta\mathbf{u}^c + \Delta\mathbf{f} = \mathbf{p}_\tau - \mathbf{p}_t \qquad (2.4.3)$$

bringingΔ f to the right hand side to facilitate handling negative stiffness in frictional element:

$$\mathbf{M}^*\Delta\ddot{\mathbf{u}}^c + \mathbf{C}^*\Delta\dot{\mathbf{u}}^c + \mathbf{K}^*\Delta\mathbf{u}^c = \mathbf{p}_\tau - \mathbf{p}_t - \Delta\mathbf{f} \qquad (2.4.4)$$

where: $\mathbf{p}_t = \mathbf{M}^*\ddot{\mathbf{u}}_t^c + \mathbf{C}^*\dot{\mathbf{u}}_t^c + \mathbf{K}^*\mathbf{u}_t^c + \mathbf{f}_t$

2.4.2 Newmark's Method

Newmarks generalized acceleration method [17] in incremental form is used for integration of the equation of motion. This single step method assumes that the increments in velocity and acceleration are related to the increment in displacement and state of motion at time t, as follows:

$$\Delta\dot{\mathbf{u}}^c = \frac{\gamma_N}{\beta_N\Delta t}\Delta\mathbf{u}^c - \frac{\gamma_N}{\beta_N}\dot{\mathbf{u}}_t^c - \left(\frac{\gamma_N}{2\beta_N} - 1\right)\Delta t\,\ddot{\mathbf{u}}_t^c \qquad (2.4.5)$$

$$\Delta\ddot{\mathbf{u}}^c = \frac{1}{\beta_N(\Delta t)^2}\Delta\mathbf{u}^c - \frac{1}{\beta_N\Delta t}\dot{\mathbf{u}}_t^c - \frac{1}{2\beta_N}\ddot{\mathbf{u}}_t^c \qquad (2.4.6)$$

where: Δt = time step of integration

γ_N = Parameter that produces numerical (or algorithmic) damping within time step Δt.

for $\gamma_N < \frac{1}{2}$, artificial negative damping results

for $\gamma_N > \frac{1}{2}$, artificial positive damping results

for $\gamma_N = \frac{1}{2}$, no numerical damping results

β_N = parameter which controls the variation of acceleration within time step Δt.
for $\beta_N = 0$, constant acceleration results

for $\beta_N = \frac{1}{4}$, average acceleration results

for $\beta_N = \frac{1}{6}$, linear acceleration results.

substituting equation (2.4.5) and equation (2.4.6) into equation (2.4.4) and simplifying gives:

$$\left[\frac{1}{\beta_N(\Delta t)^2}\mathbf{M}^* + \frac{\gamma_N}{\beta_N \Delta t}\mathbf{C}^* + \mathbf{K}^*\right]\Delta \mathbf{u}^c = \mathbf{p}_\tau - \mathbf{p}_t - \Delta \mathbf{f}$$

$$+ \mathbf{M}^*\left\{\frac{1}{\beta_N \Delta t}\dot{\mathbf{u}}_t^c + \frac{1}{2\beta_N}\ddot{\mathbf{u}}_t^c\right\} + \mathbf{C}^*\left\{\frac{\gamma_N}{\beta_N}\dot{\mathbf{u}}_t^c + \Delta t\left(\frac{\gamma_N}{2\beta_N} - 1\right)\ddot{\mathbf{u}}_t^c\right\} \qquad (2.4.7)$$

$$\mathbf{K}_t^P \Delta \mathbf{u}^c = \mathbf{q}_t \qquad (2.4.8)$$

error involved is Δt^3 for average acceleration and Δt^4 for linear acceleration.

2.4.3 Computation of Forces in Hysteretic and Frictional Elements

An explicit fourth order Runge-Kutta scheme is used for computation of forces in hysteretic and frictional elements. An estimate of velocity at $\frac{\Delta t}{2}$ is obtained using linear acceleration variation over time interval Δt. An error of Δt^5 is involved.

2.5.1 Pseudo Load Formulation and Time Marching Algorithm for Accuracy and Efficiency

Frictional element with velocity dependent coefficient of sliding friction, involves negative stiffness in sliding mode (Postyielding with low and negative stiffness) and very high stiffness,in stick mode (elastic behavior with high elastic stiffness generating near stick conditions). Since negative stiffness is involved, nonlinear stiffness formulation is not adopted. The nonlinear restoring force term is brought on to the right hand side and used as a pseudo load [38].

For accurate solution of stiff differential equations, predictor-corrector methods like Gears method [39] are used. In the algorithm reported in this report, simple Pseudo load formulation with one-point iteration is used. To maintain comparable accuracy of predictor-corrector methods, a very small time step of the order of $5x10^{-5}$ seconds is used where negative stiffness or where very large stiffness occurs.

Time marching with a varying time step at low structure velocities (in stick-slip transition) is adopted. The time step is varied using an exponential formulation:

$$\Delta t_{st} = \Delta t_{sl}\left[1 - \exp\left(\frac{-\dot{U}^2}{a}\right)\right] \quad for \dot{U} > \dot{U}_{min} \qquad (2.5.1)$$

Where:

Δt_{st} = Variable reduced time step used for 'stick' mode (high elastic stiffness and negative stiffness) at low velocity.

Δt_{sl} = Constant time step used for slip mode (low stiffness).

a = constant to control the velocity range over which the time step reduction occurs. A default value of 1 is adopted.

$\dot{U}$ = Velocity at the sliding interface.

$$\Delta t_{st,\,min} = \Delta t_{sl}\left[1 - \exp\left(\frac{-\dot{U}^2_{min}}{a}\right)\right] \quad for \dot{U} < \dot{U}_{min} \qquad (2.5.2)$$

Where:

$\Delta t_{st,\,min}$ = Smallest time step used for the stick mode.

$\dot{U}_{min}$ = 0.1 inches/second is adopted.

A sample plot of the time step variation with velocity is shown in figure 2-23. The values of Δt_{st} and $\dot{U}_{min}$ above for stick-sliding conditions do not depend on structural characteristics. The value of Δt_{sl} can be varied depending on the dynamic characterstics of the structural system following standard requirements for numerical accuracy and stability. In program 3D-BASIS the exponential formulation is used to establish the time step at every 0.1 in/sec. The time step at these intervals are used instead of a continuously changing time step, based on the velocity.

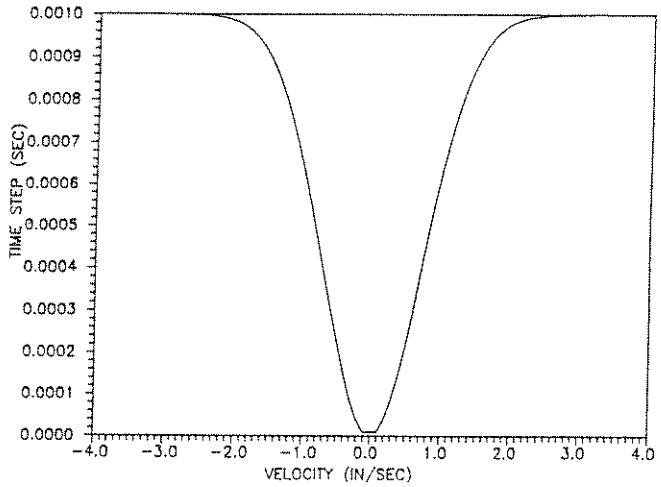

Figure 2-23 **Time Step Variation Under Low Velocity**

2.5.2 Rigorous Mathematical Solution For Validation of the Proposed Pseudo Load Formulation

In the case involving friction, the second order ordinary differential equations of motion are reduced to first order ordinary differential equations. These equations, along with the equations governing hysteretic model behavior, are solved by adaptive integration. Gear's [39] method of solving 'stiff' differential equations is adopted.

Gear's [39] method for 'stiff' differential equations of the form $y' = f(y, t)$, uses a p^{th} order predictor formula of the form:

$$y_{n,(0)} = \alpha_1 y_{n-1} + \ldots + \alpha_p y_{n-p} + \eta_1 h y'_{n-1} \qquad (2.5.3)$$

and a corrector

$$y_{n,(m+1)} = \alpha^*_1 y_{n-1} + \ldots\ldots + \alpha^*_p y_{n-p} + \eta^*_0 h f(y_{n,(m)}, t_n) \qquad (2.5.4)$$

The integration error involved when iterated to convergence is $C^s_{p+1} h^{p+1} y^{p+1}(t_n) + O(h^{p+2})$ where $C^s_{p+1} = 1/(p+1)$. Where p is the order of the predictor equation, α, η, α^* and η^*_0 are constants, h is the step size.

Numerical solutions for comparison with pseudo load formulation were obtained using DIVPAG subroutine of the International Mathematical and Statistical Library (IMSL) which uses Gear's[39] method.

Constantinou et al. [32] has used this approach for analysis of base isolated structures on friction interfaces.

Numerical verification in section 3 shows the comparison of results of the two methods.

2.6 Computational Algorithm for Solution

2.6.1 Formulation

The reduced equation of motion equation (2.4.4) has a nonlinear term on the right hand side which is treated as pseudo load:
rewriting equation (2.4.4)

$$\mathbf{M}^*\Delta\ddot{\mathbf{u}}^c + \mathbf{C}^*\Delta\dot{\mathbf{u}}^c + \mathbf{K}^*\Delta\mathbf{u}^c = \mathbf{p}_\tau - \mathbf{M}^*\ddot{\mathbf{u}}_t^c - \mathbf{C}^*\dot{\mathbf{u}}_t^c - \mathbf{K}^*\mathbf{u}_t^c - \mathbf{f}_t - \Delta\mathbf{f} \qquad (2.6.1)$$

denoting:

$$\mathbf{f}_t + \Delta\mathbf{f} = \mathbf{f}_{t+\Delta t} \qquad (2.6.2)$$

equation (2.6.1) becomes:

$$\mathbf{M}^*\Delta\ddot{\mathbf{u}}^c + \mathbf{C}^*\Delta\dot{\mathbf{u}}^c + \mathbf{K}^*\Delta\mathbf{u}^c = \mathbf{p}_\tau - \mathbf{M}^*\ddot{\mathbf{u}}_t^c - \mathbf{C}^*\dot{\mathbf{u}}_t^c - \mathbf{K}^*\mathbf{u}_t^c - \mathbf{f}_{t+\Delta t} \qquad (2.6.3)$$

Using first order Taylor's series expansion:

$$\mathbf{f}_{t+\Delta t} \sim \mathbf{f}_t + \frac{\delta}{\delta t}\mathbf{f}_t \Delta t \qquad (2.6.4)$$

Approximating the partial derivative by a first-order backwards difference expression:

$$\mathbf{f}_{t+\Delta t} \sim 2\mathbf{f}_t - \mathbf{f}_{t-\Delta t} \qquad (2.6.5)$$

This expression has an inherent error of order $(\Delta t)^2$. Since iteration is done at every step to satisfy a specified tolerance level, this is acceptable.

2.6.2 Computational Procedure

1. State of motion is initialized by specifying initial displacement, initial velocity and initial acceleration.

2. In the first step to start the solution, initial stiffness of hysteretic and/or frictional elements is used i.e., the nonlinear term is retained on the left hand side as in equation (2.4.3). Note $\Delta\mathbf{f} = \mathbf{K}_t^N \Delta\mathbf{u}^c$.

3. Newmarks method is used for integration of equations of motion. $\mathbf{K}_t^P$ in equation (2.4.8) is computed. Gaussian elimination is used for triangularisation of $\mathbf{K}_t^P$ in the first step(and the triangularised form is used repeatedly for solution until the time step of computation is changed based on velocity as explained in section 2.5.1).

Incremental displacement $\Delta\mathbf{u}^c$, is computed by using forward reduction and

backsubstitution. State of motion is updated as follows:

$$\ddot{\mathbf{u}}_{\tau}^{c} = \ddot{\mathbf{u}}_{t}^{c} + \Delta\ddot{\mathbf{u}}^{c}$$

$$\dot{\mathbf{u}}_{\tau}^{c} = \dot{\mathbf{u}}_{t}^{c} + \Delta\dot{\mathbf{u}}^{c}$$

$$\mathbf{u}_{\tau}^{c} = \mathbf{u}_{t}^{c} + \Delta\mathbf{u}^{c}$$

$$\tau = t + \Delta t$$

where:

$\Delta\ddot{\mathbf{u}}^{c}$, $\Delta\dot{\mathbf{u}}^{c}$ are calculated from equation(2.4.5) and equation(2.4.6) knowing $\Delta\mathbf{u}^{c}$ from equation(2.4.8).

4. Using the nonlinear force at time t and the nonlinear force at time $t - \Delta t$, the nonlinear force F_x and F_y, at each pad at $t + \Delta t$ is estimated as explained in section 2.6.1. From these forces at individual pads, $\mathbf{f}_{\tau(i)}$ resultant force vector at the center of mass of the base is computed.

5. Using the estimated nonlinear resultant force vector as pseudo load, as in equation (2.6.3), the incremental displacement $\Delta\mathbf{u}^{c}$ at $t + \Delta t$ is computed, using forward reduction and backsubstitution.

6. Using the incremental displacement $\Delta\mathbf{u}^{c}$ computed in step 5, the state of motion at time t is updated to the state of motion at time $t + \Delta t$ and the nonlinear force at each individual pad is computed, using fourth order Runge-Kutta scheme. The resultant force vector $\mathbf{f}_{\tau(i+1)}$ at the center of mass of the base is computed.

7. The difference $\mathbf{f}^{e}$, between the computed force in step 6 and the estimated force in step 4, is computed. The normalized relative error is computed as follows:

$$\text{Error} = \frac{\|\mathbf{f}^{e}\|_2}{FMNORM}$$

Where, $FMNORM$ =Reference moment for convergence since the story torque is the dominating element in the vector $\mathbf{f}$ and $\|\mathbf{f}\|_2$ denotes the euclidean norm of vector $\mathbf{f}$, i.e.,

$$\|\mathbf{f}\|_2 = \sqrt{f_x^2 + f_y^2 + f_t^2}$$

If error $\leq$ tolerance, no iteration is needed, the state of motion computed in step 6 is carried along with the estimated nonlinear force in step 4 used for its computation, and computations at the next time step are started from step 4, or else iteration procedure is started as in step 8, using the nonlinear force $\mathbf{f}_{\tau(i+1)}$ and the state of motion at time t.

8. Iteration within time step :

(a) Using the nonlinear force $\mathbf{f}_{\tau(i+1)}$ computed in step 6 as pseudo load and the state of motion at time t, the incremental displacement $\Delta \mathbf{u}^c$ at $t + \Delta t$ is computed.

(b) Using the incremental displacement computed in step 8a, the state of motion at time t is updated to the state motion at time $t + \Delta t$ and the resultant force vector $\mathbf{f}_{\tau(i+2)}$ is computed, using fourth order Runge-Kutta scheme.

(c) The normalized relative error is computed and checked against specified tolerance as in step 7, if satisfied, the state of motion computed in step 8b, is carried on to the next step along with the nonlinear force $\mathbf{f}_{\tau(i+1)}$ used for its computation and computations at the next time step are started from step 4, if not the iteration procedure is continued from step 8a, using the nonlinear force $\mathbf{f}_{\tau(i+2)}$ and the state of motion at time t until convergence is reached or maximum number of iterations specified is exceeded, in which case the program is terminated with an error message.

SECTION 3
NUMERICAL VERIFICATION

The earthquake response of a two story steel moment-resisting frame building shown in figure 3-1 is considered. First story height is 26.67 ft(320 inches) and second story height is 10 ft.(120 inches). First story height is chosen to simulate a soft first story. First story columns are assumed to be stable. Columns are spaced at 30 ft.(360 inches) in X direction and 15 ft.(180 inches) in Y direction. Columns are assumed to be square sections. The first story columns have A = 11.6 in^2,$I_x = I_y = 250\ in^4$, J = 0.25 in^4 and weight = 40 lbs/ft. The second story columns have A = 11.1 in^2,$I_x = I_y = 106\ in^4$, J = 0.56 in^4 and weight = 38 lbs/ft. All beams are considered rigid (very stiff) and the floor slab is assumed rigid in the X-Y plane. The mass of the floors are lumped at the four corners. Total weight of the structure is 156 Kips. Total mass in X and Y directions at the first floor is 272 lb-sec^2/in. Total mass in X and Y directions at the second floor is 132 lb-sec^2/in. A 5% eccentricity in Y direction is used by offsetting the center of mass of the building at both floors, from the center of rigidity or the geometric center of the building.

A base isolated building on four elastomeric bearings with damper is shown in figure 3-6. The bearings exhibit bilinear hysteretic behavior. The elastic stiffness of each bearing in X and Y directions is 2.73 Kips/in, with a yield displacement of 1 in. The yield force is 7% of the total weight of the structure including the base. A 5% eccentricity in Y direction is used by offsetting the center of mass of the building at the first floor and the base, from the center of rigidity or the geometric center of the building. Total mass in X and Y directions at the base is 272 lb-sec^2/in. Total mass in X and Y directions at the first floor is 132 lb-sec^2/in.

Comparison of the structure response computed using 3D-BASIS with response computed using various programs is considered.

3.1 Elastic Analysis

3.1.1 Comparison with GTSTRUDL

Comparison of the structure response with the response computed using GTSTRUDL [34] is considered. The structure shown in figure 3-1 described above is considered.

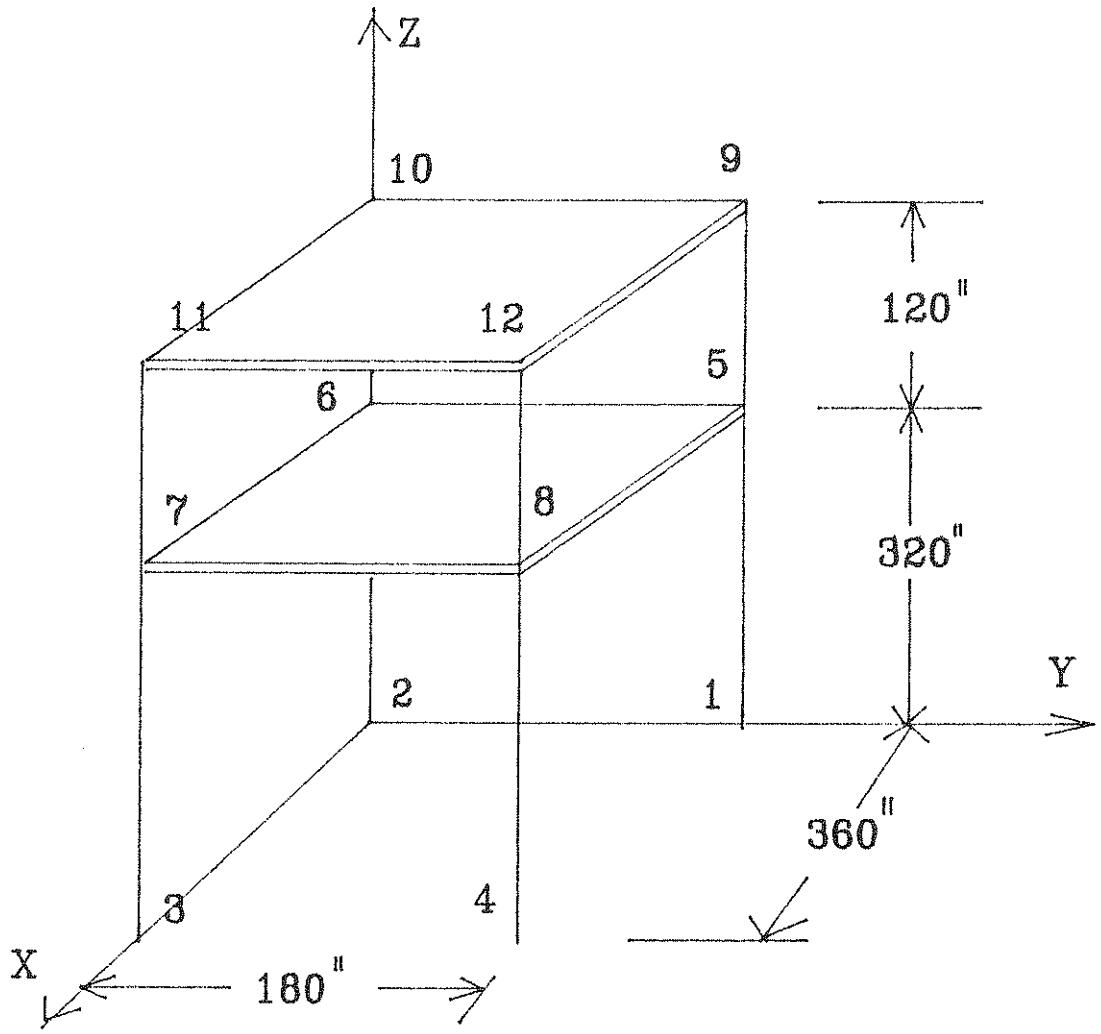

Figure 3-1 **Two Story Steel Moment-resisting Frame Building**

Superstructure damping of 2% of critical is used in all modes. 15 seconds of the 1940 El Centro earthquake, north-south component, is input in the X direction. Figures 3-2 and 3-4 show the X direction relative base displacement response time history, at node 8 and 12, respectively. Figures 3-3 and 3-5 show the X direction shear force response time history in the first story column at node 8 and in the second story column at node 12, respectively. The difference (less than 15%) in shear force response at node 12 may be due to exact finite element representation used in GTSTRUDL analysis against shear building representation used in 3D-BASIS analysis. However, the displacement response at node 12 compares well. The response at node 8 compares well. Substantially lower force level at node 12 is to be noted as the effect of a soft first story, as in base isolation.

3.2 Inelastic Analysis

3.2.1 Comparison with DNA

Comparison of inelastic structure response with the response computed using the program Dynamic Nonlinear Analysis (DNA) [36,42] is considered. The base isolated building shown in figure 3-6 and described previously is considered. A post yielding stiffness of 1.6% of elastic stiffness is used. 15 seconds of the 1940 El Centro earthquake north-south component is input in the X direction. Superstructure damping of 2% of critical is used in all modes. Figure 3-7 and 3-9 show the X and Y direction relative base displacement response time history at node 8, respectively. Figure 3-8 and 3-10 show the X and Y direction shear force response time history in the bearing at node 8, respectively. In this comparison, inelastic bi-axial interaction effects are neglected. The permanent drift in the X direction is due to the near elasto-plastic properties assumed for the elastomeric bearings with damper. The X direction peak base displacement response is nearly doubled from the elastic response, while peak shear force at node 8 is reduced, indicating the effect of isolation. The difference (less than 5%) in the Y direction response may be due to the exact finite element representation used in DNA analysis, against shear building representation used in 3D-BASIS analysis. The peak response in the X direction compares well. The Y direction response is smaller than the Y direction response of the elastic structure shown in figure 3-1. This reduction in torsional response is the effect of base isolation.

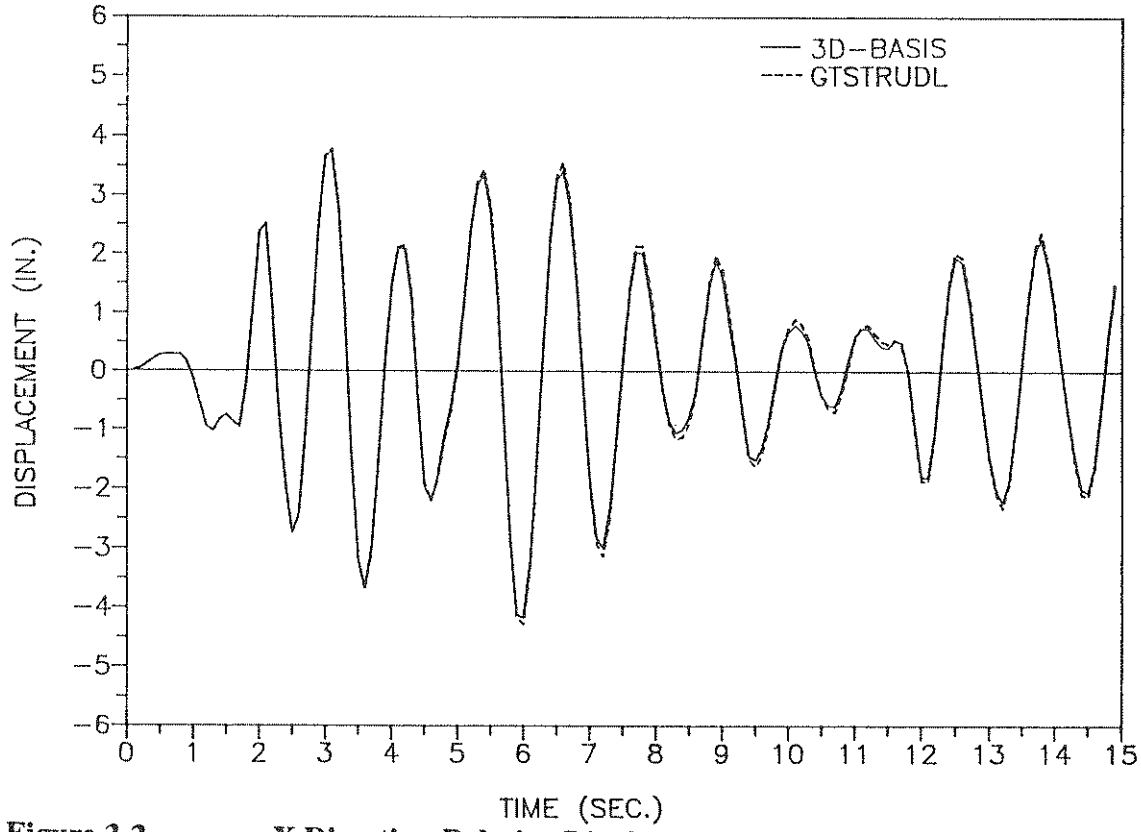

Figure 3-2 X Direction Relative Displacement Response at Node 8 of the Two Story Building Subjected to EL CENTRO Earthquake (S00E component) in X Direction

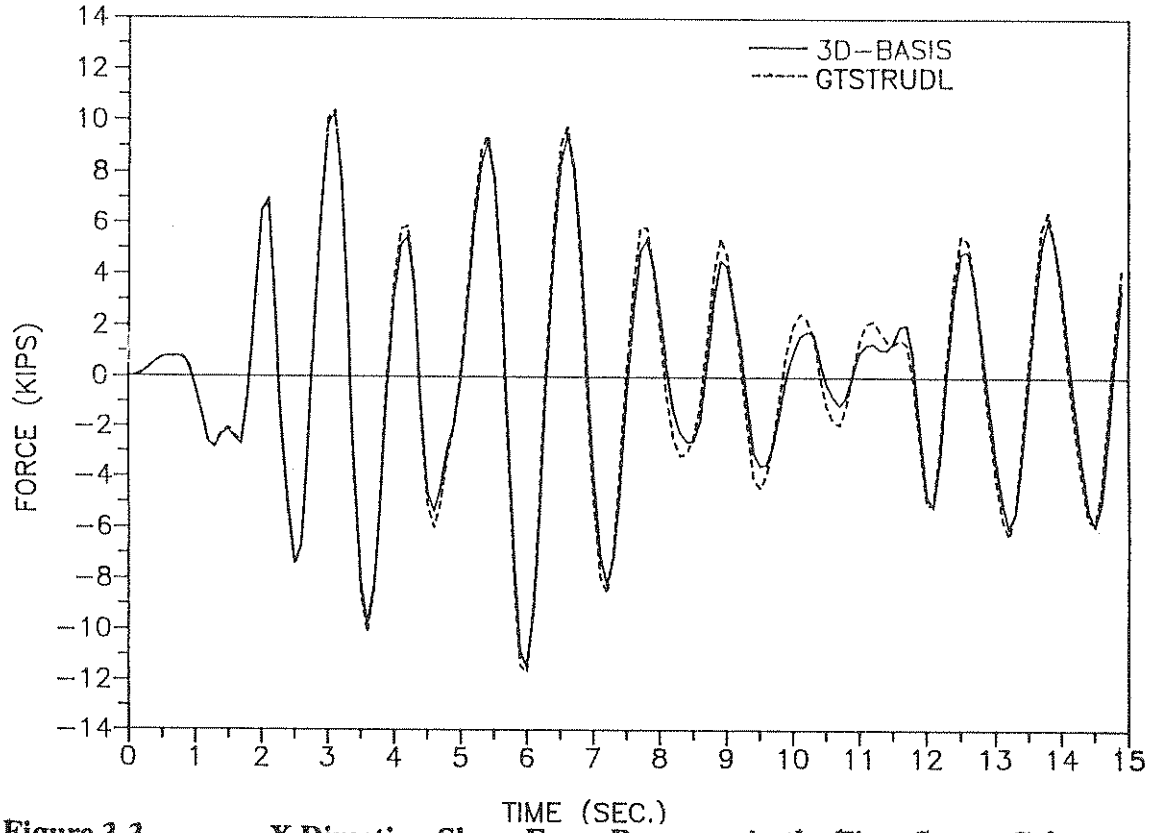

Figure 3-3 X Direction Shear Force Response in the First Story Column at Node 8 of the Two Story Building Subjected to EL CENTRO Earthquake (S00E component) in X Direction

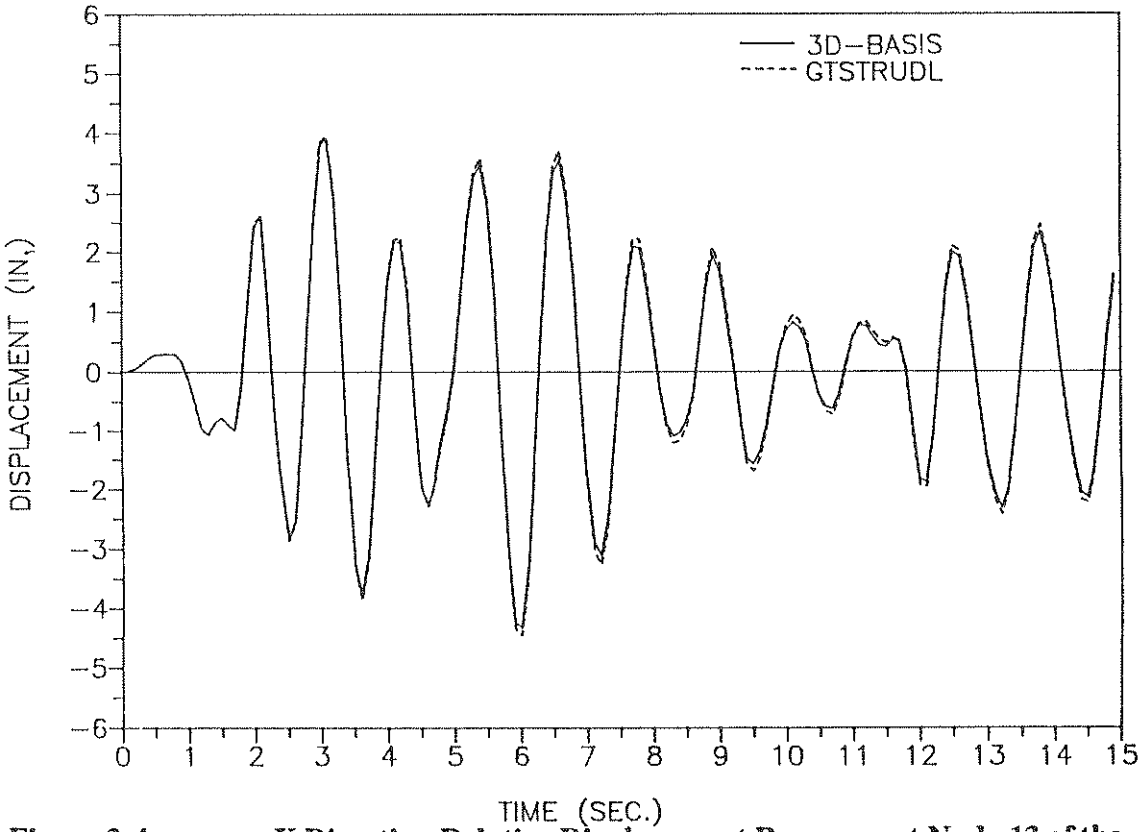

Figure 3-4 X Direction Relative Displacement Response at Node 12 of the Two Story Building Subjected to EL CENTRO Earthquake (S00E component) in X Direction

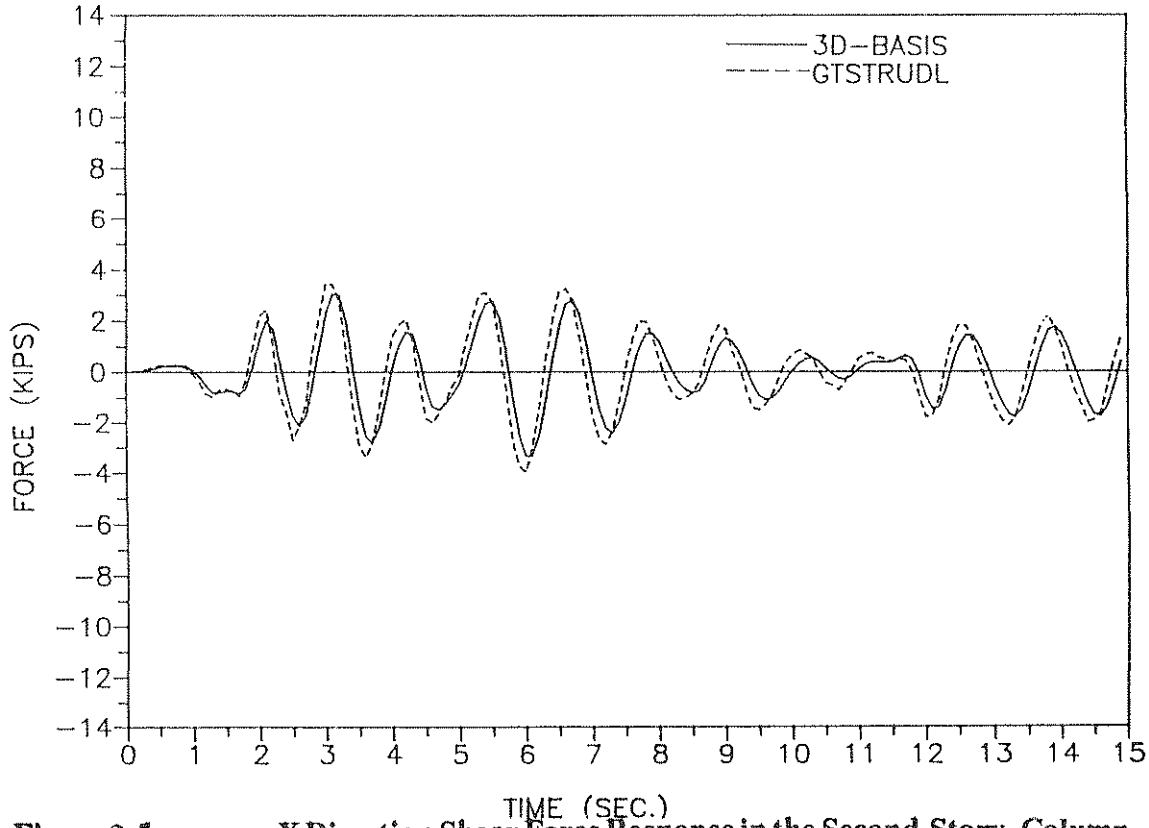

Figure 3-5 X Direction Shear Force Response in the Second Story Column at Node 12 of the Two Story Building Subjected to EL CENTRO Earthquake (S00E component) in X Direction

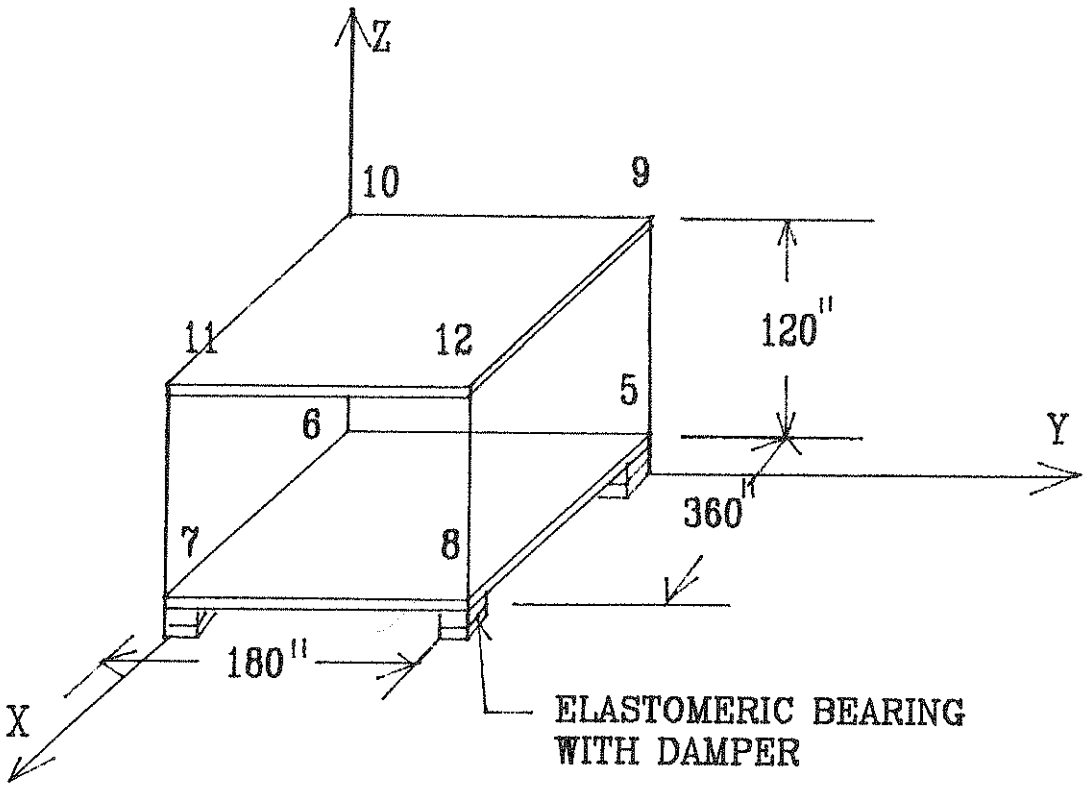

Figure 3-6 **Base Isolated Building on Four Elastomeric Bearings with damper.**

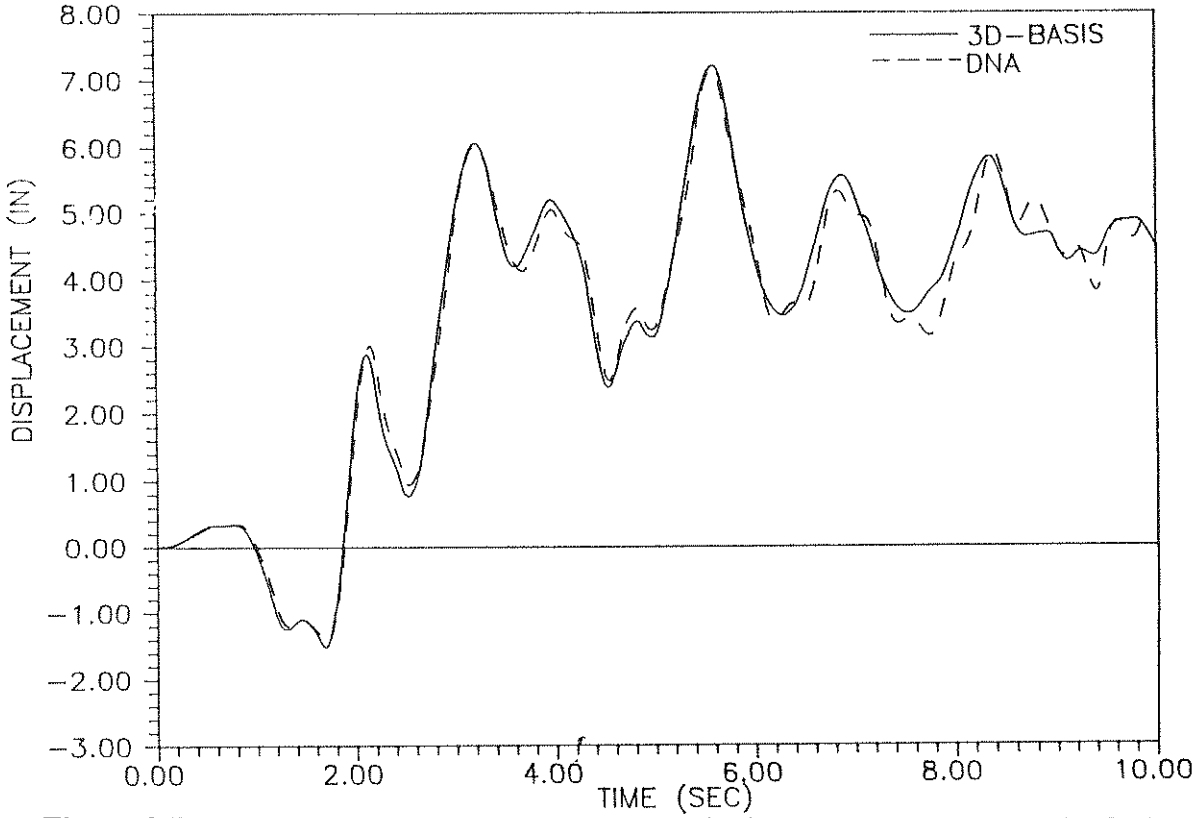

Figure 3-7 X Direction Relative Base Displacement Response at Node 8 of the Base Isolated Building Subjected to EL CENTRO Earthquake (S00E component) in X Direction

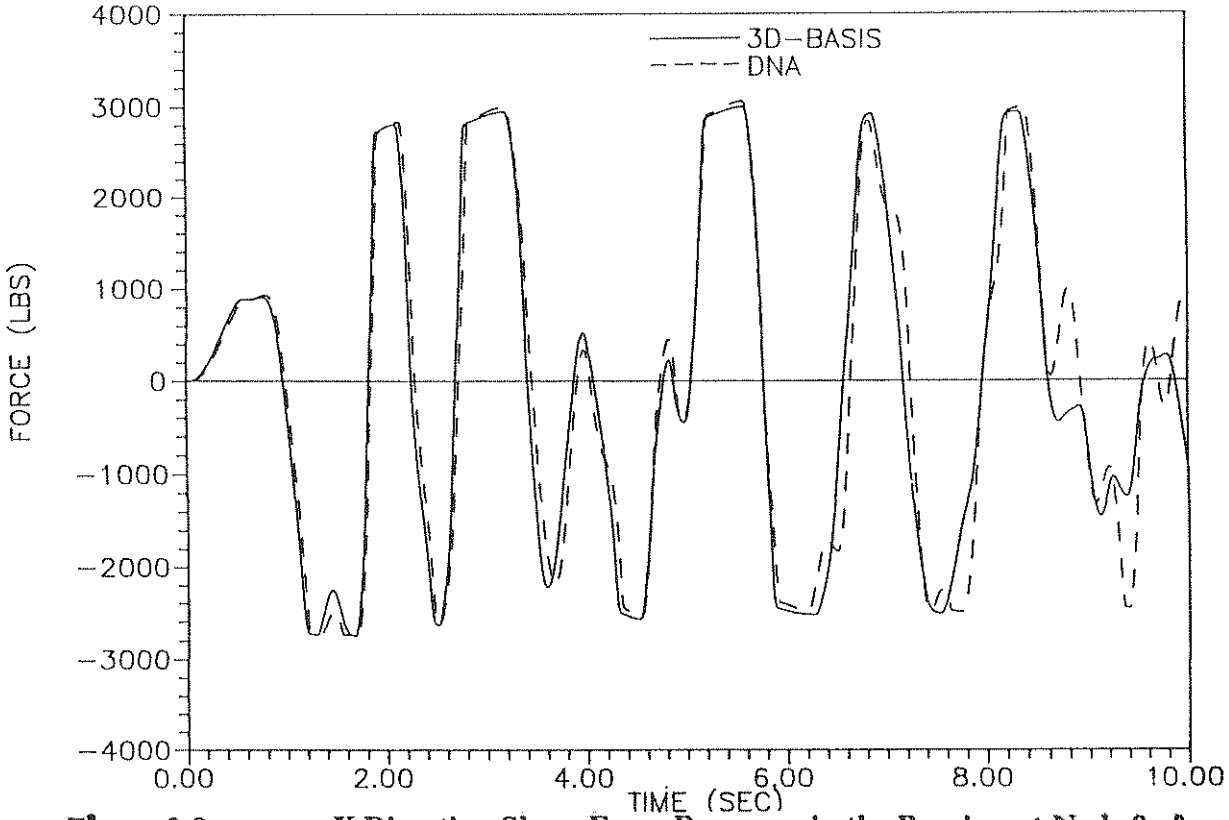

Figure 3-8 X Direction Shear Force Response in the Bearing at Node 8 of the Base Isolated Building Subjected to EL CENTRO Earthquake (S00E component) in X Direction

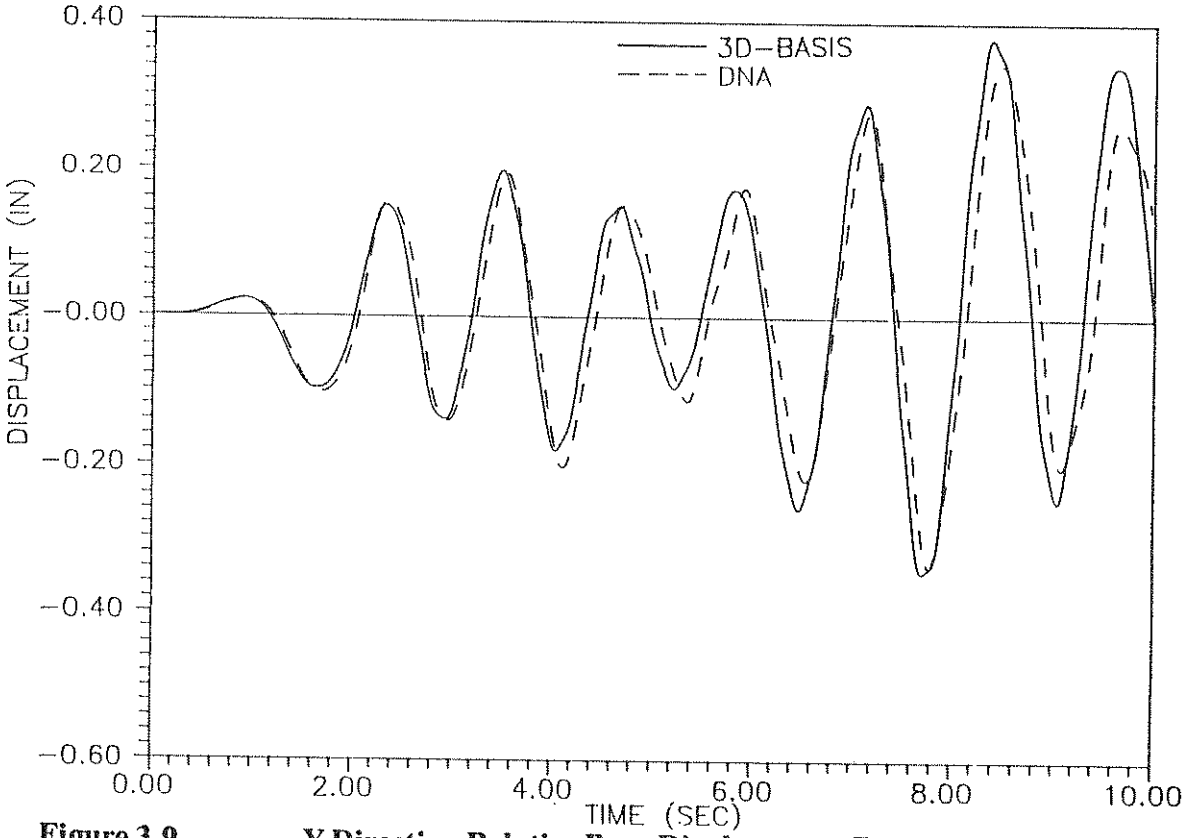

Figure 3-9 Y Direction Relative Base Displacement Response at Node 8 of the Base Isolated Building Subjected to EL CENTRO Earthquake (S00E component) in X Direction

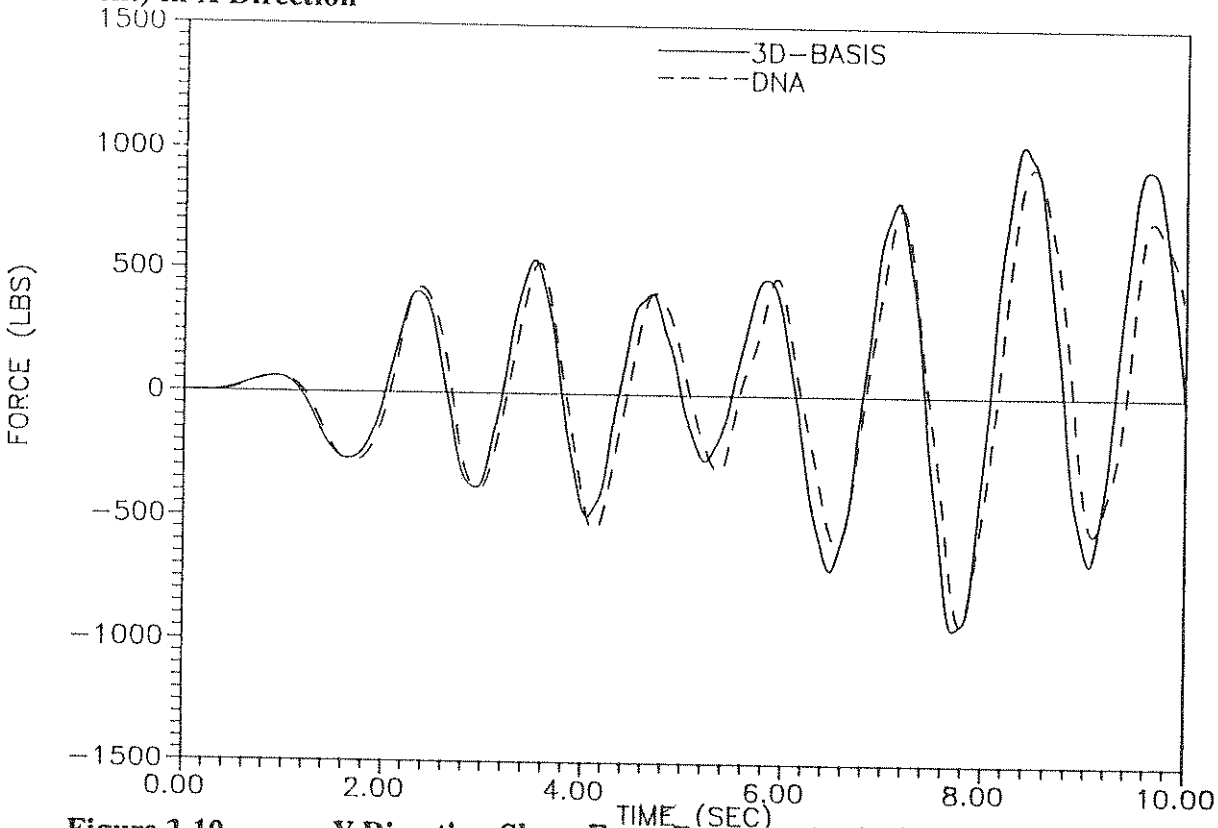

Figure 3-10 Y Direction Shear Force Response in the Bearing at Node 8 of the Base Isolated Building Subjected to EL CENTRO Earthquake (S00E component) in X Direction

3.2.2 Comparison with ANSYS

Comparison of the structure response with the response computed using ANSYS [35] is considered. The base isolated structure shown in figure 3-6 and described previously is considered. A postyielding stiffness of 10% of elastic stiffness is used. The acceleration input in the X direction is as shown in Figure 3-11. The acceleration history was chosen to have the force always in one direction (even though unrealistic) after unloading-reloading inelastic response. This is because of the different material model used in ANSYS. Peak acceleration used is 0.15g. The total length of input acceleration time history is 4 seconds. Superstructure damping of 2% of critical is used in all modes. Figures 3-12 and 3-14 show the X and Y direction relative base displacement response time history at node 8, respectively. Figures 3-13 and 3-15 show the X and Y direction shear force response time history in the bearing at node 8, respectively. The differences (less than 3%) in the response may be due to the exact finite element representation used in ANSYS analysis, against the shear building representation used in 3D-BASIS analysis. In this comparison, inelastic bi-axial interaction effects are neglected. The analysis is unrealistic because of the input acceleration used, but is for comparison only.

3.2.3 Comparison with DRAIN-2D

Comparison of the structure response with the response computed using DRAIN-2D [37] is considered. The base isolated structure shown in figure 3-6 and described previously is considered. The 5% eccentricity in Y direction is not considered. The building and the base isolation system centers of mass and rigidity are considered coincident to produce a planar response, which can be computed by DRAIN-2D. A post yielding stiffness of 10% of elastic stiffness is used. Superstructure damping of 2% of critical is used in all modes. 15 seconds of the 1940 El Centro earthquake, north-south component, is input in the X direction. Figure 3-16 shows the X direction relative base displacement response time history at node 8. Figure 3-17 shows the X direction total shear force response time history in the four bearings. Y direction response is zero. In this case, the permanent drift in the X direction is absent and the peak displacement is reduced, because of the postyielding stiffness of 10% of elastic stiffness used. The peak responses compare well.

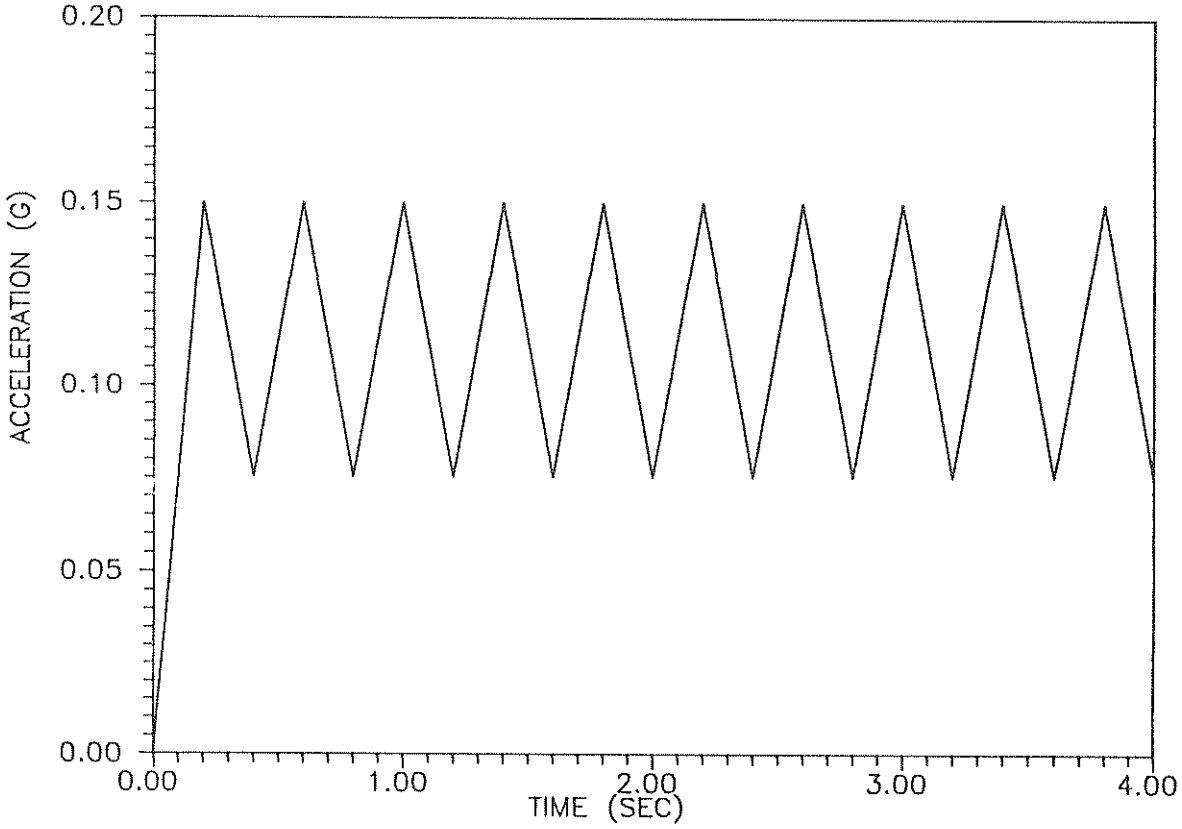

Figure 3-11 Ground Acceleration Input to the Base Isolated Building in X Direction for Comparison With ANSYS

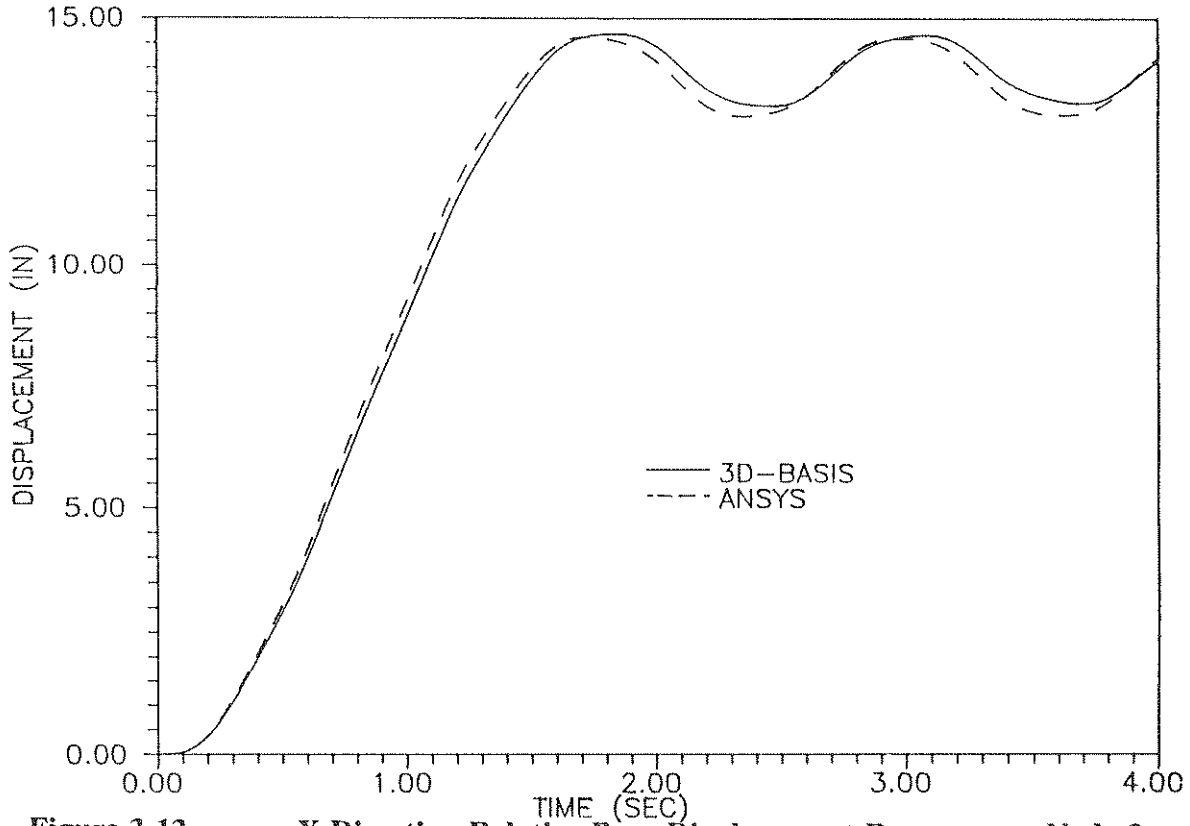

Figure 3-12 X Direction Relative Base Displacement Response at Node 8 of the Base Isolated Building Subjected to Ground Acceleration Shown in Fig. 3-11 in X Direction

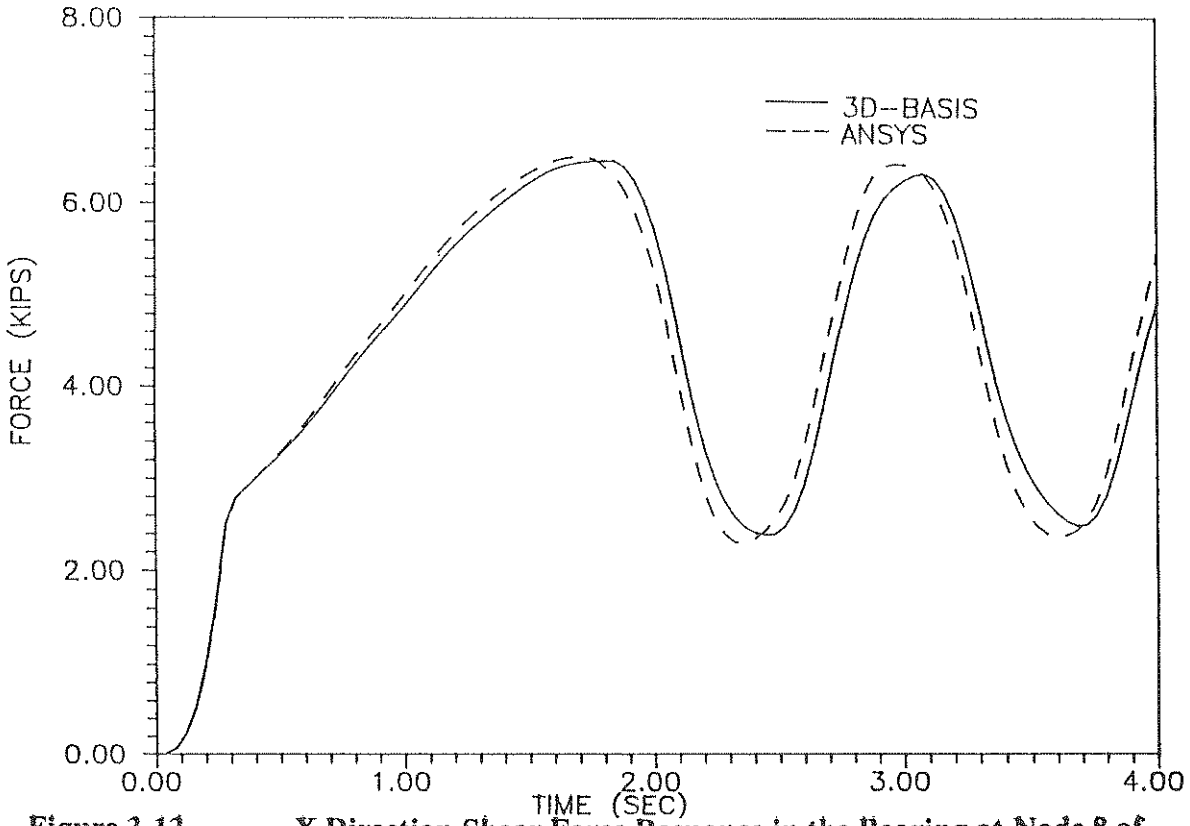

Figure 3-13 X Direction Shear Force Response in the Bearing at Node 8 of the Base Isolated Building Subjected to Ground Acceleration Shown in Fig. 3-11 in X Direction

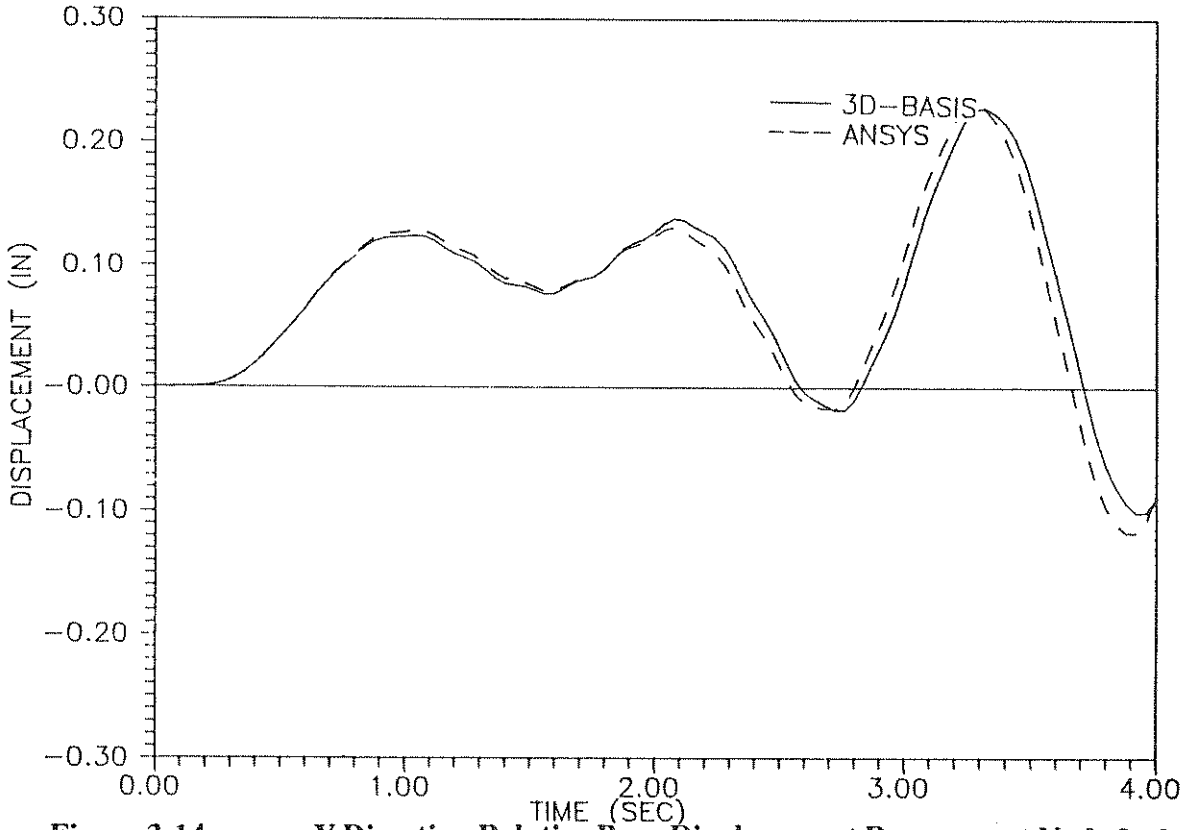

Figure 3-14 Y Direction Relative Base Displacement Response at Node 8 of the Base Isolated Building Subjected to Ground Acceleration Shown in Fig. 3-11 in X Direction

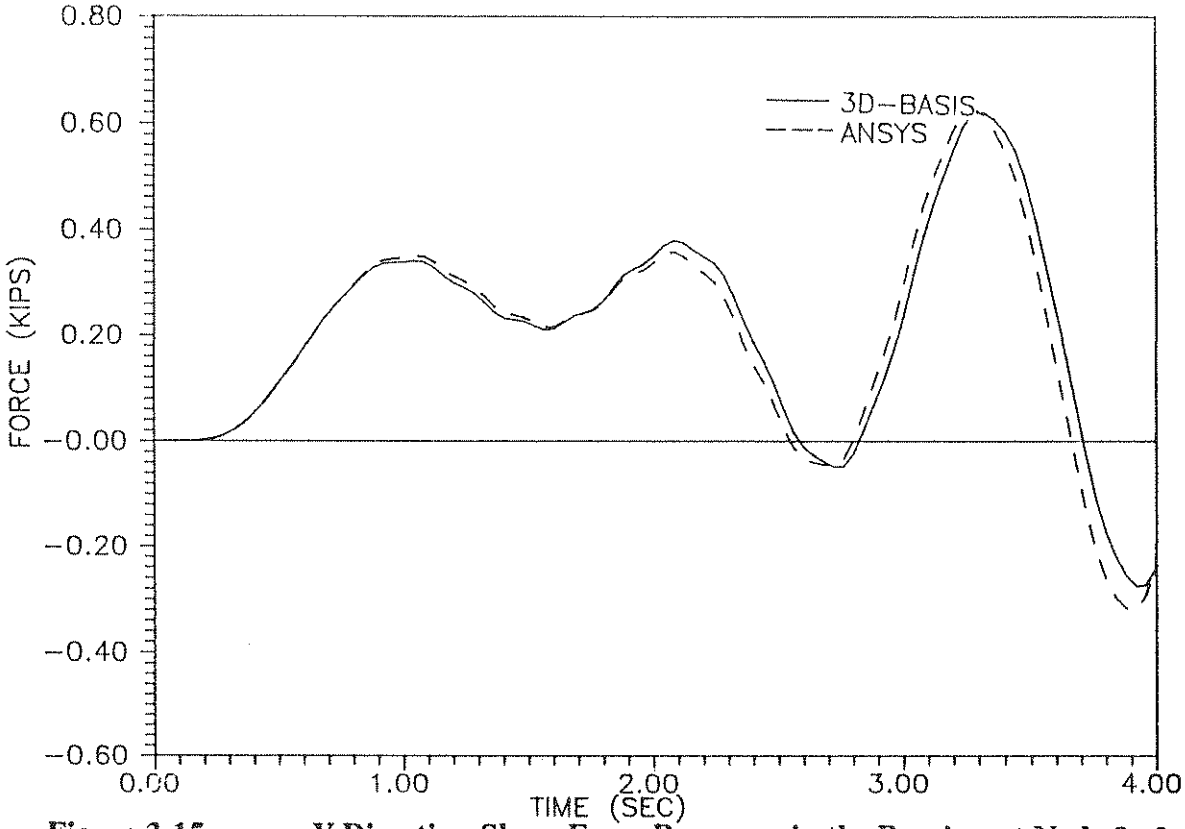

Figure 3-15 Y Direction Shear Force Response in the Bearing at Node 8 of the Base Isolated Building Subjected to Ground Acceleration Shown in Fig. 3-11 in X Direction

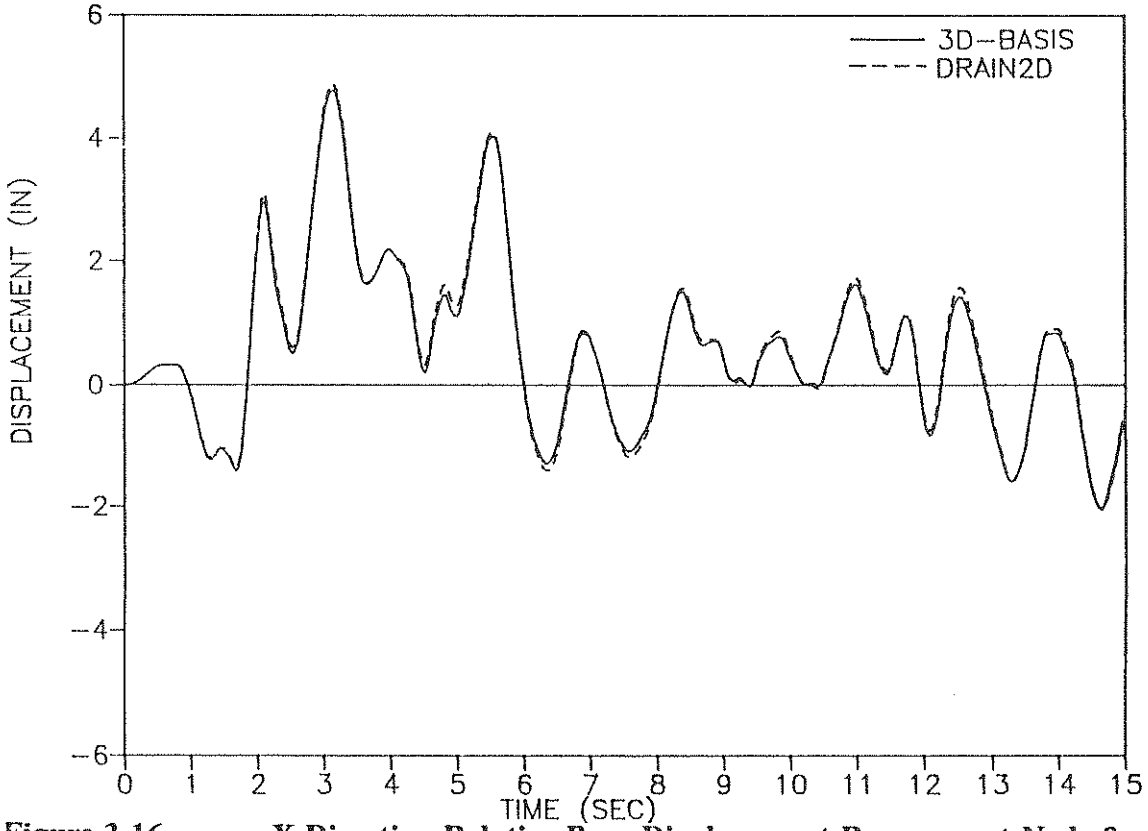

Figure 3-16 X Direction Relative Base Displacement Response at Node 8 of the Base Isolated Building Subjected to EL CENTRO Earthquake (S00E component) in X Direction

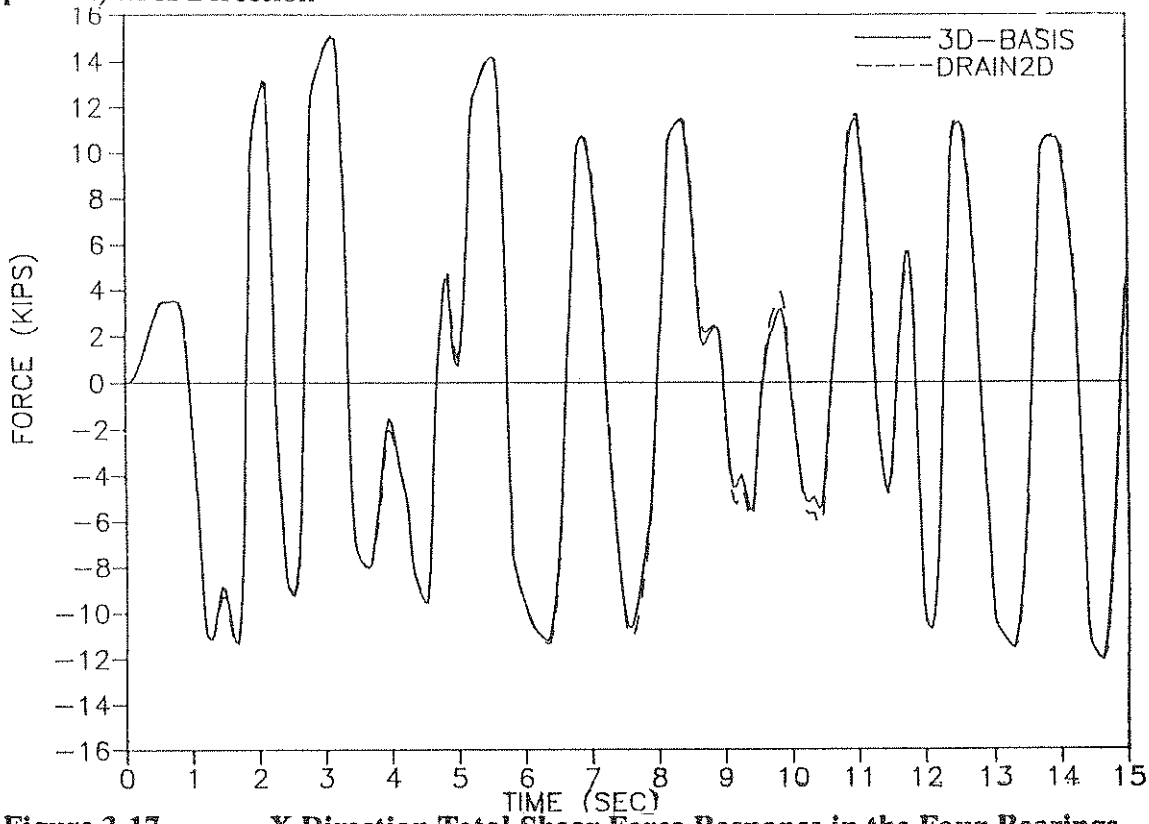

Figure 3-17 X Direction Total Shear Force Response in the Four Bearings of the Base Isolated Building Subjected to EL CENTRO Earthquake (S00E component) in X Direction

3.2.4 Comparison with Rigorous Mathematical Solution

Comparison of the response with a rigorous mathematical solution using Gears method, presented in section 2.5.2 [39] is considered. Constantinou et al. [32] has used rigorous mathematical solution for solving structural systems with frictional elements. The response of a rigid structure supported on Teflon bearings is considered. The bearing pressure at the friction interface was 1000 psi. Input motion is sinusoidal acceleration of the ground, with peak amplitude $\ddot{U}_{g0} = 0.25g$ and a frequency of $\omega = \pi$ rad/sec. For 1000 psi Teflon-steel bearing [32], $f_{max} = 0.1193, \Delta f = 0.0927$ and a = 0.6 in equation (2.2.17) is used. Figures 3-18 and 3-19 show the non-dimensional sliding displacement U, and the non-dimensional total acceleration $\ddot{U}$, time histories of the rigid structure, respectively. There is virtually no difference in response computed from the two methods.

Comparison of the response of a six-story steel moment-resisting frame building is considered. Floor height is 12 ft. and columns are spaced at 16 ft. on center in both directions. A slice of the building, involving one bay of 16 ft. width and 48 ft. length, supported by eight columns is analyzed. A computer model of the building was developed for determining the dynamic characterstics. The model has been condensed to one with six degrees of freedom, representing the lateral displacement of each floor. The dynamic characterstics of the condensed model are presented in Table 3-I. Typical floor weight (including framing, etc.) is 105 Kips. A quarter scale artificial mass model of this building has been constructed for shake table testing. The identified frequencies and mode shapes of the scaled structure agree well with those in Table 3-I. The isolation system for this building consists of sliding unfilled Teflon bearings and rubber springs. Bearing pressure of 1000 psi is considered. The rubber springs do not carry any vertical load and provide a total horizontal stiffness of K_b. The weight of the structure, including the base is, 672 Kips. The rigid body mode period of 2 secs. is chosen for the sliding isolated structure. Furthermore, the rubber springs provide an equivalent viscous damping factor in the rigid body mode of vibration equal to 0.05. Damping in the superstructure is assumed to be 2% of critical in all modes. The time scale of ground motions used are scaled by 50% to satisfy similitude requirements.

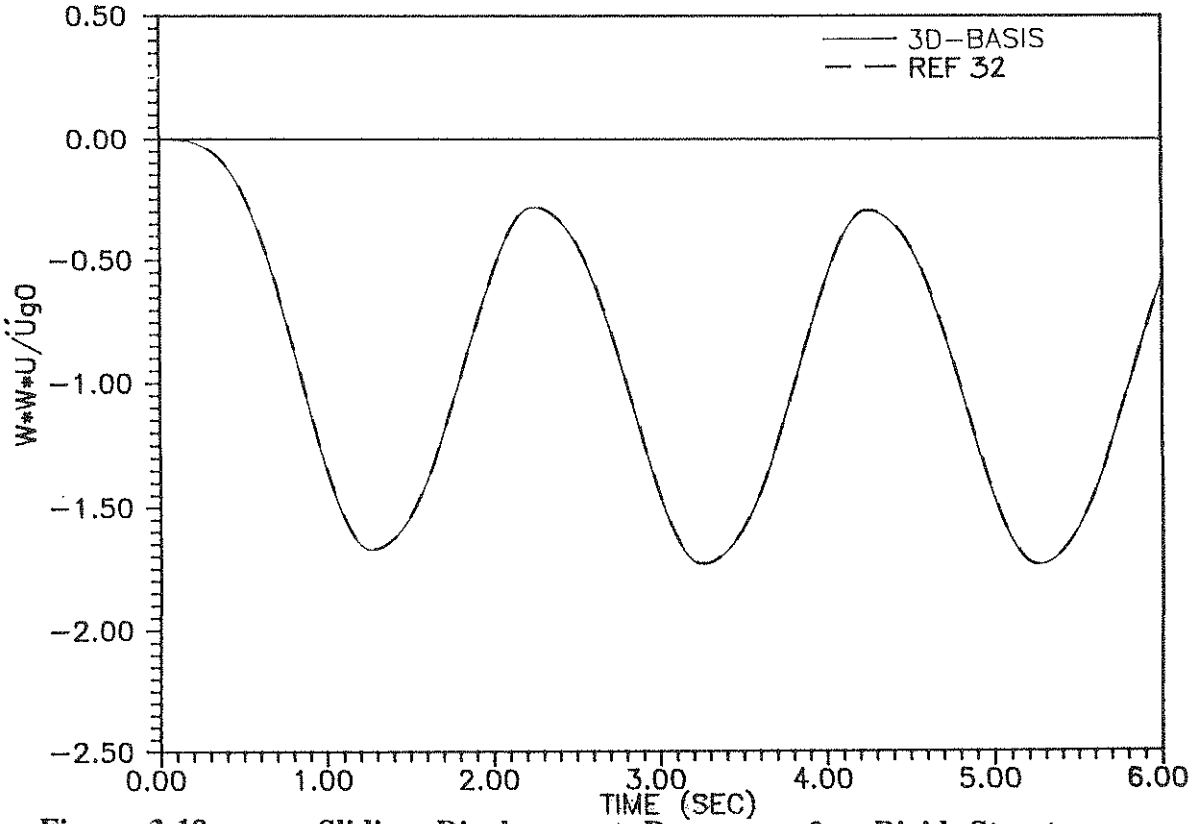

Figure 3-18 Sliding Displacement Response of a Rigid Structure on Teflon-steel Interface Subjected to Sinusoidal Ground Acceleration $\ddot{U}_{go}$ = 0.25g of Frequency π Rad/Sec

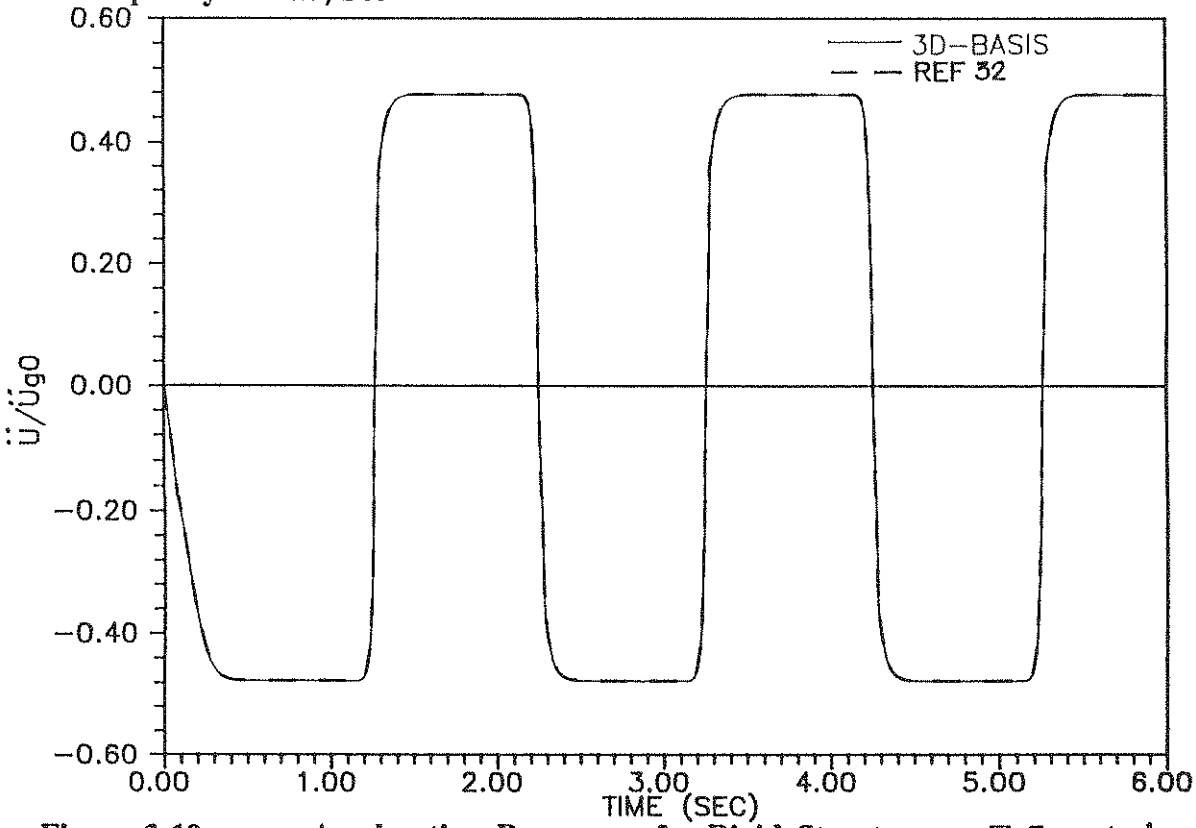

Figure 3-19 Acceleration Response of a Rigid Structure on Teflon-steel Interface Subjected to Sinusoidal Ground Acceleration $\ddot{U}_{go}$ = 0.25g of Frequency π Rad/Sec

TABLE 3-I CHARACTERISTICS OF 6-STORY BUILDING (VALUE IN PARENTHESIS IS EXPERIMENTAL EXTRAPOLATED TO PROTOTYPE)

MODE	FREQUENCY (Hz)	MODE SHAPE					
		FLOOR 1	FLOOR 2	FLOOR 3	FLOOR 4	FLOOR 5	FLOOR 6
1	1.07 (1.17)	0.164	0.395	0.611	0.791	0.923	1
2	3.38 (3.86)	0.520	1	0.956	0.386	-0.401	-0.996
3	6.02 (6.64)	-0.804	-0.863	0.230	1	0.383	-0.817
4	8.99 (9.52)	1	0.104	-0.996	0.24	0.980	-0.619
5	12.01 (12.40)	1	-0.769	-0.027	0.805	-0.946	0.397
6	14.41 (14.46)	0.679	-0.919	1	-0.879	0.580	-0.196

TABLE 3-II
DYNAMIC CHARACTERISTICS OF 3-STORY BUILDING

MODE	FREQUENCY (Hz)	MODE SHAPE		
		FLOOR 1	FLOOR 2	FLOOR 3
1	2.246	0.1101	0.2408	0.3293
2	6.836	0.3158	0.1569	-0.2328
3	11.621	0.2516	-0.3043	0.1506

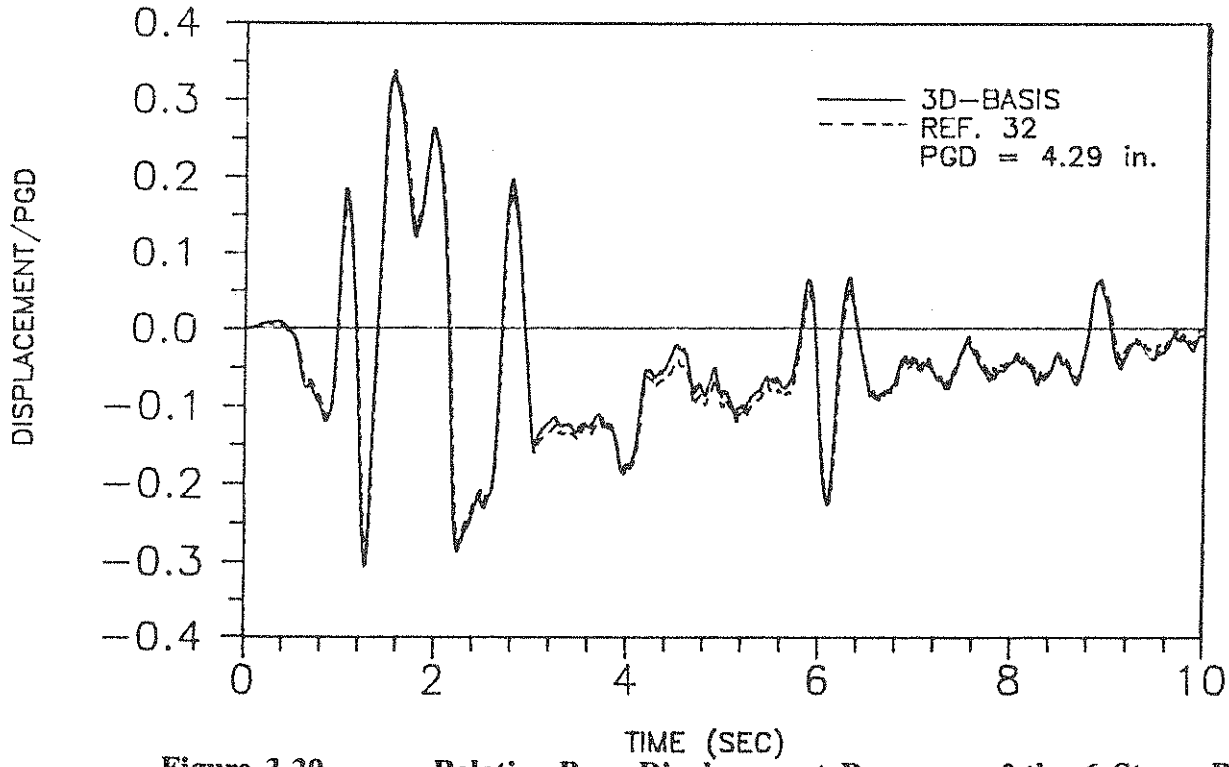

Figure 3-20 Relative Base Displacement Response of the 6-Story Base Isolated Building Subjected to EL CENTRO Earthquake (S00E component)

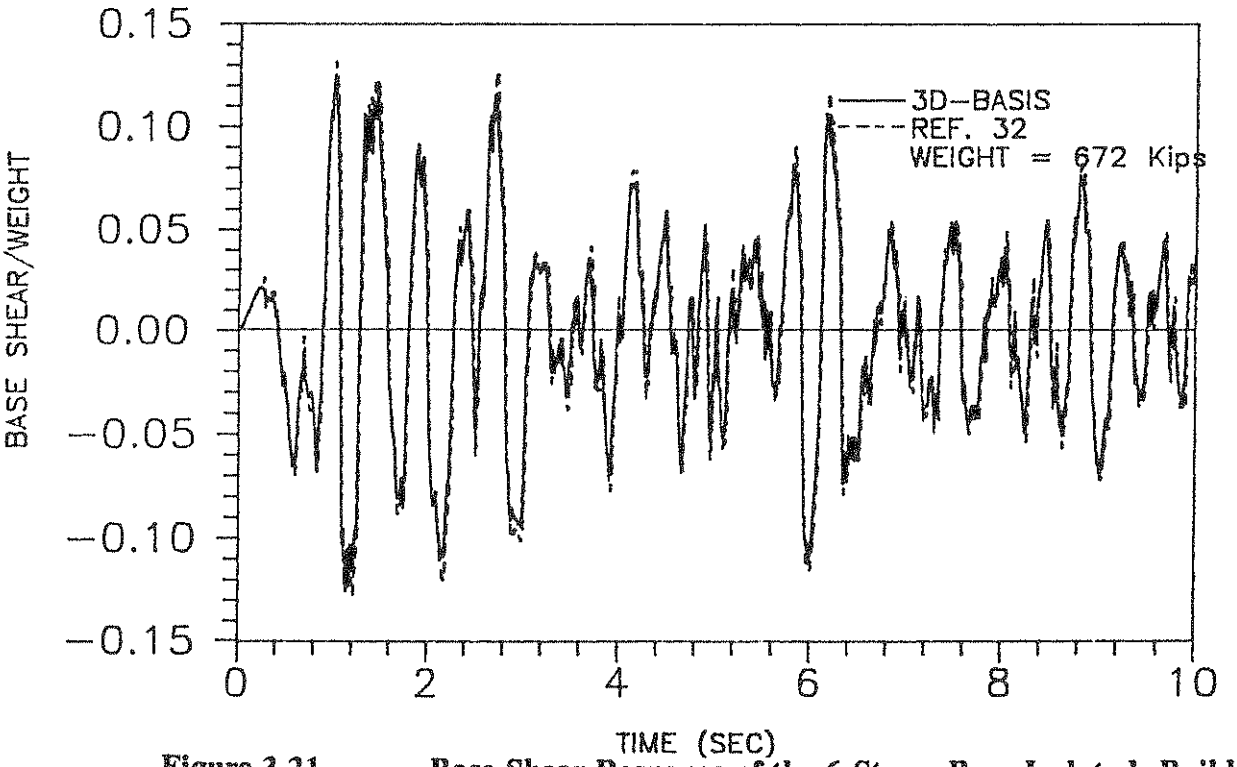

Figure 3-21 Base Shear Response of the 6-Story Base Isolated Building Subjected to EL CENTRO Earthquake (S00E component)

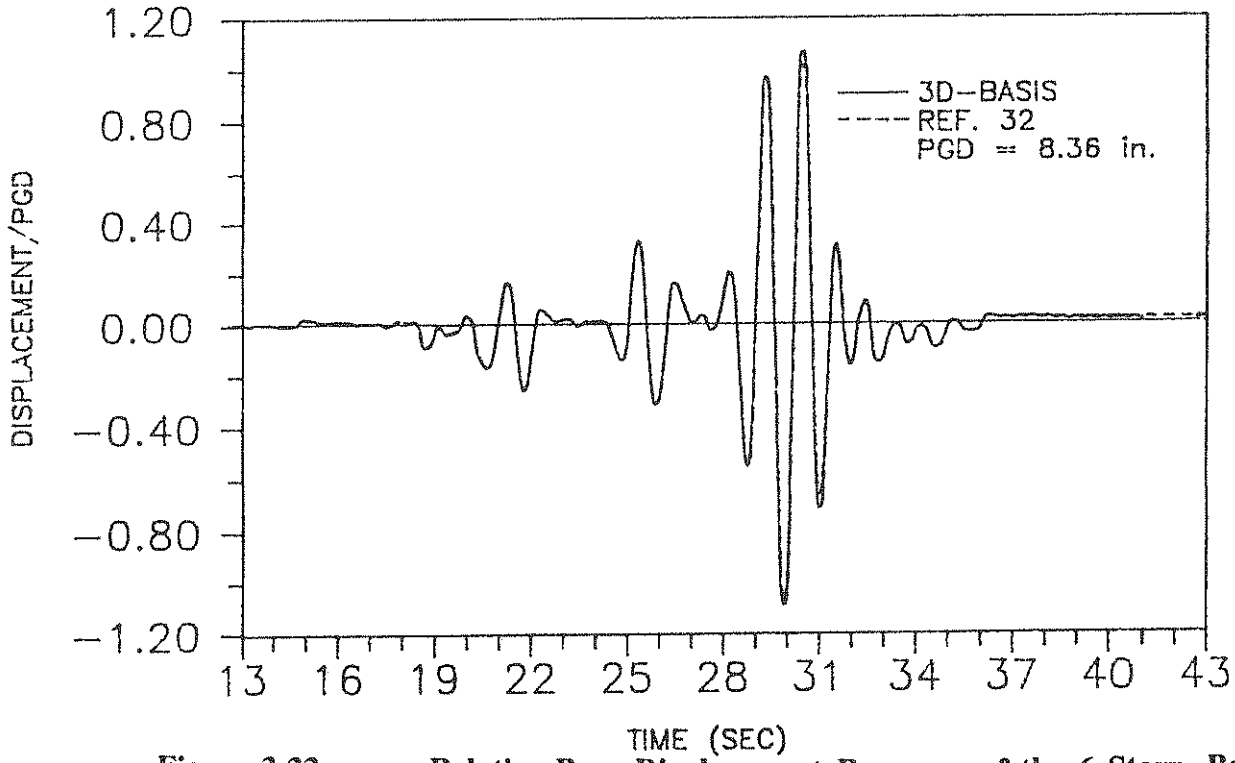

Figure 3-22 Relative Base Displacement Response of the 6-Story Base Isolated Building Subjected to MEXICO CITY Earthquake (N90W component)

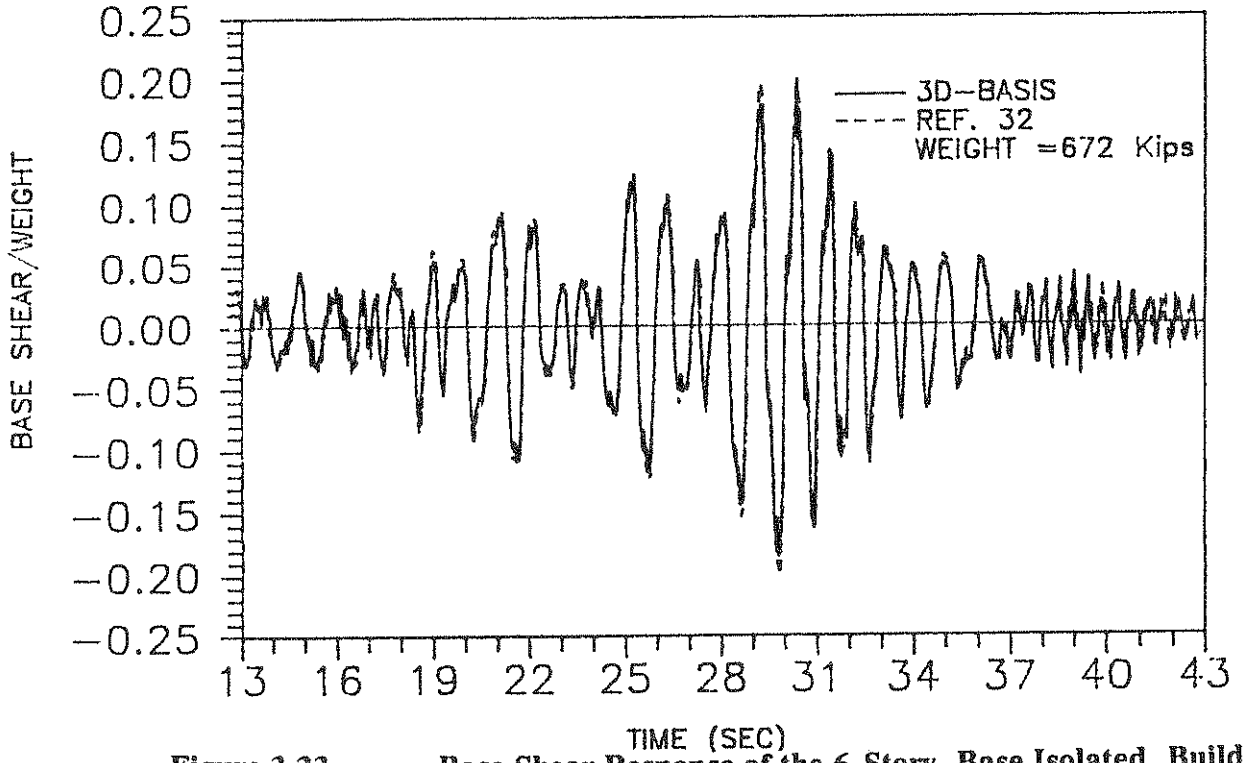

Figure 3-23 Base Shear Response of the 6-Story Base Isolated Building Subjected to MEXICO CITY Earthquake (N90W component)

Figures 3-20 and 3-21 show the relative base displacement and base shear time history, respectively, for 10 secs. of time scaled north-south component of the 1940 El Centro earthquake. Figures 3-22 and 3-23 show the relative base displacement and base shear time history, respectively, for time scaled east-west component of the 1985 Mexico City earthquake. The duration of time scaled Mexico City earthquake used is from 13 sec. to 37.5 sec. with free vibration of 5 sec. The peak response compares well, but the response in the vicinity of stick-slip condition is different (by 2 to 3%). This is due to the difference in accuracy achieved in computation by the two methods.

3.2.5 Comparison with Experimental Results

Comparison of the measured response of a quarter scale base isolated three-story moment-resisting steel frame building model is considered. The model [44] was supported by linear roller bearings. The dynamic characterstics of the model, obtained through system identification, with a lateral degree of freedom per floor, is presented in Table 3-II. The foundation base of the model was guided between stationary rails, padded on either sides (two interfaces) of the base with Merriman Co. G12 friction resistant interfaces. The pads were pressed against the foundation base by prestressing rods. The prestressing force was monitored throughout the test. The interface against which the pads were pressing was a polished steel surface. Thus controlled friction force was introduced into the system. A horizontal flat plate beam fixed to the ground and connected at 1/3 and 2/3 span to the foundation base was used as an additional spring with centering capability. The elastic stiffness of this device was measured to be 1.856 Kips/in. The system was tested for scaled 1940 El Centro Earthquake, north-south component, on the shake table. The amplitude was scaled to 25% of its original amplitude and the time scale was scaled by 50% to satisfy simulitude requirements. The artificial weight of each floor was 2.163 Kips and that of the base was 1.8036 Kips. For the particular test under consideration, the identified coefficient of sliding friction was 5% and the prestressing force was 2 Kips. Thus the maximum friction force was 0.2 Kips. The following parameters are used for simulation, $f_{max} = 0.024, \Delta f = 0.015$ and a = 0.65 in equation (2.2.17) for the friction interface at the base of the building. Figure 3-24 shows the measured base displacement and figure 3-25 shows the computed response.

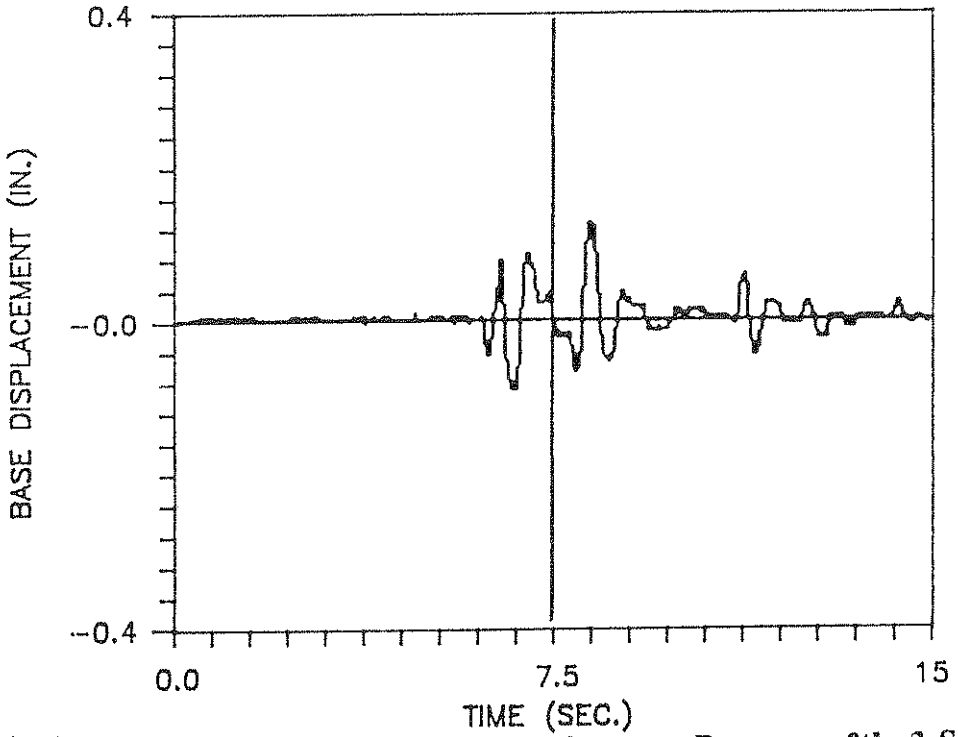

Figure 3-24 Measured Relative Base Displacement Response of the 3-Story Base Isolated Building Model Subjected to Scaled EL CENTRO Earthquake

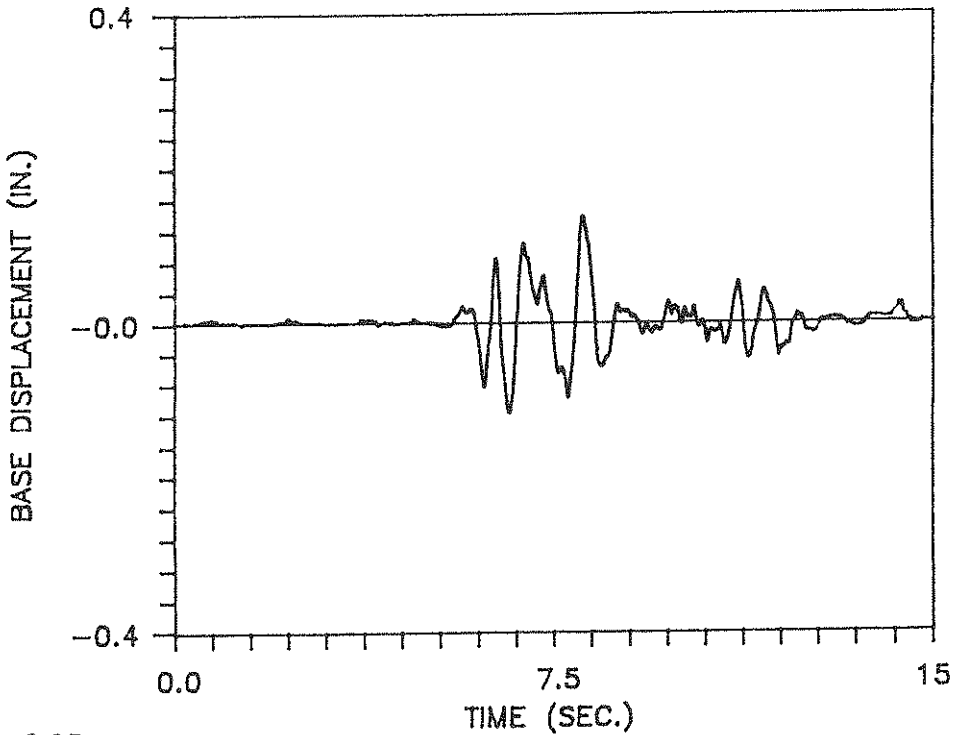

Figure 3-25 Computed Relative Base Displacement Response of the 3-Story Base Isolated Building Model Subjected to Scaled EL CENTRO Earthquake

3.2.6 Comparison with 3 Story Model

Comparison of the response with the response computed in reference 18, in which the response of a 3 story model was investigated, is considered. Centers of mass and rigidity are considered coincident. 15 secs. of the 1940 El Centro earthquake, north-south component, scaled to 75% of its original amplitude(span 750), is input. Figure 3-26 shows the base displacement response time history. The differences in the response may be due to the difference in the input acceleration time history of El Centro (span 750) used in computation of the response.

3.2.7 Response Using Bi-axial Element Under Bi-directional Motion

The base isolated structure shown in figure 3-6 and described previously is considered. A post yielding stiffness of 20% of elastic stiffness is used. Superstructure damping of 2% of critical is used in all modes. 70 seconds of the 1985 Mexico City earthquake, N90W component is input in the X direction, S00E component is input in the Y direction. In this case, inelastic bi-axial interaction is considered. Figure 3-27 shows the corner Y direction base displacement. The bi-axial interaction causes more displacement, since the restoring force is reduced due to the interaction.

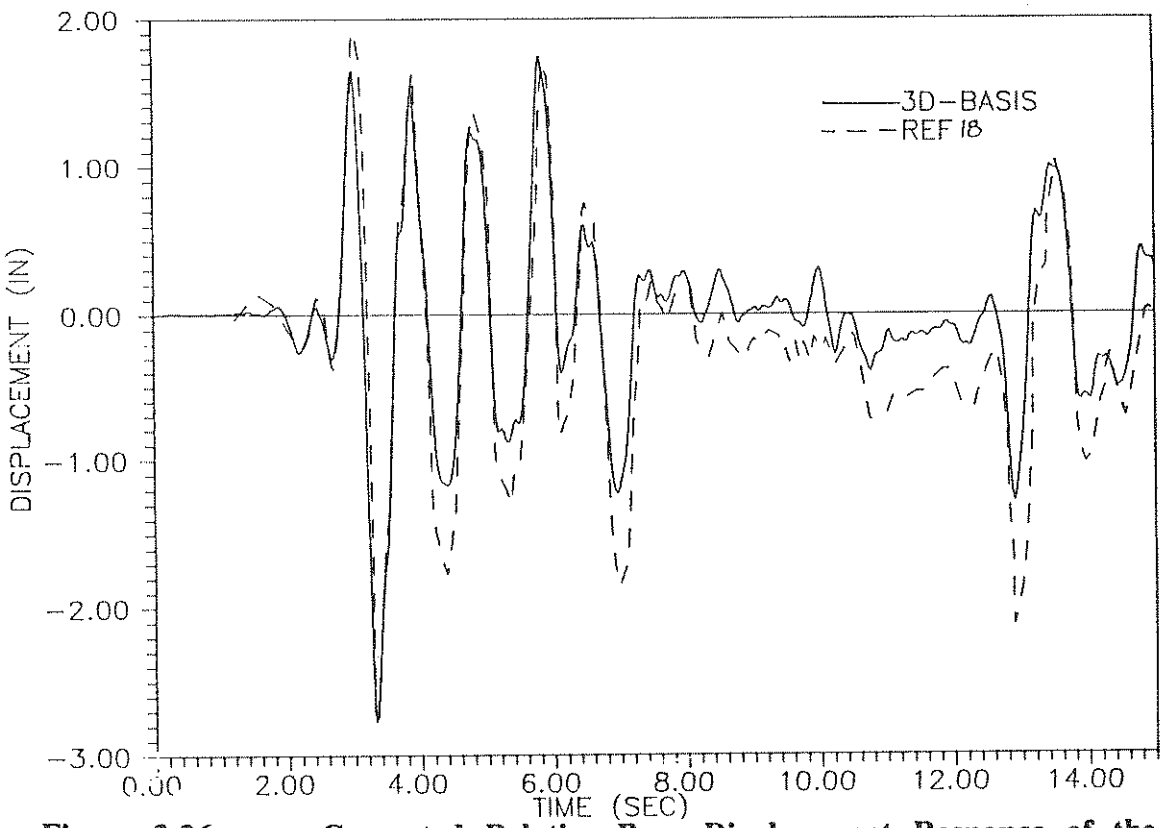

Figure 3-26 Computed Relative Base Displacement Response of the 3-Story Base Isolated Building Model Subjected to Scaled EL CENTRO Earthquake

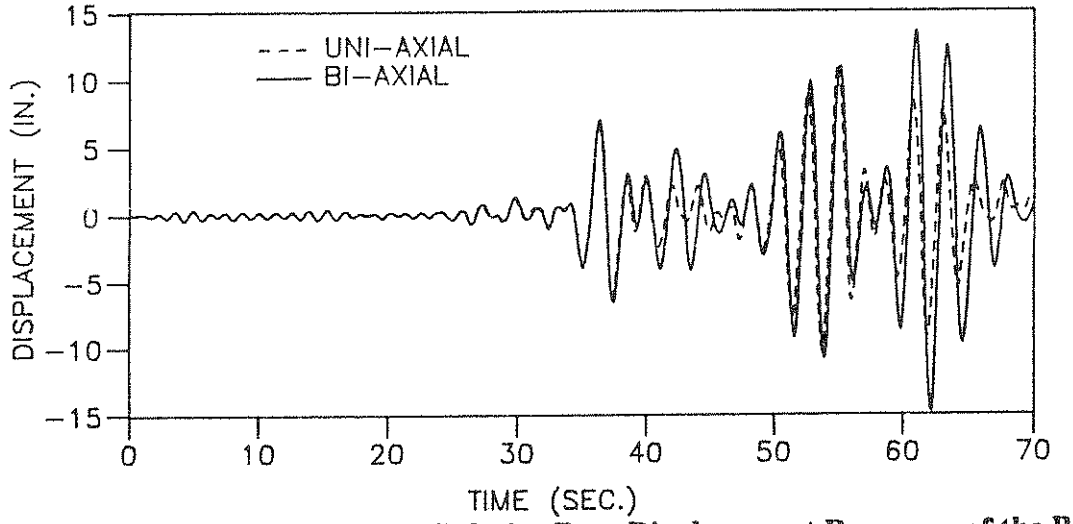

Figure 3-27 Y Direction Relative Base Displacement Response of the Base Isolated Building Subjected to Bi-Directional Input of MEXICO CITY Earthquake (N90W in X Direction and S00E in Y Direction)

SECTION 4
CONCLUSIONS

The report summarizes the development of a computational model for base isolated structures and the computer program 3D-BASIS. This program can perform nonlinear transient dynamic analysis of three dimensional multistory base isolated buildings. The report presents the developement of the bi-axial hysteretic model used for representing hysteretic isolation elements like high damping rubber bearings, lead-rubber bearings, steel dampers, and frictional elements like Teflon-steel interfaces.

The comparison of hysteresis loops from numerical simulation, with hysteresis loops from Kajima's [40] bi-directional tests on high damping rubber bearing and steel damper, and Constantinou et al. [32] uni-directional tests on Teflon-steel interface, indicate good agreement.

The verification done to ensure efficiency and accuracy shows good agreement. Comparable results obtained using two different solution procedures, as in the comparison with rigorous mathematical procedure, is notable.

The program in its present form has nonlinear elements like frictional elements and high damping rubber bearing elements with bi-axial interaction. The two options, available in the program described in section 1.3, are for representing the superstructure to the desired detail. Modifications of the program under progress include:

1. Interfacing the ETABS program [43] with 3D-BASIS for truely three dimensional representation of the superstructure. This is being done externally, at present by using option two described in section 1.3, by doing an eigenvalue analysis of the superstructure using ETABS and using the required number of frequencies and mode shapes for 3D-BASIS analysis.

2. A graphics preprocessor and postprocessor for analysis.

The program is expected to contribute significantly to the development of simpler response computation methods useful for code development, and to establish better understanding of the behavior of three dimensional multistory structures on high damping rubber bearings, lead-rubber bearings and friction interfaces.

The program is available for use on DEC/VAX computers. A microcomputer version is in the development stage.

SECTION 5
REFERENCES

1. Kelly, J. M. "Aseismic Base Isolation: Review and Bibliography," Soil Dynamics and Earthquake Engineering, 5, 4, 202-217, 1986.

2. Kelly, J. M. "Aseismic Base Isolation," Shock and Vibration Digest, 17, 7, 3-14, 1985.

3. Buckle, I. G. "Development and Application of Base Isolation and Passive Energy Dissipation: A World Overview," Proc. ATC-17 Seminar on Base Isolation and Passive Energy Dissipation, San Fransisco, CA, 153-174, 1986.

4. Way, D. and Jeng, V. "NPAD - A Computer Program for the Analysis of Base Isolated Structures," ASME Pressure Vessels and Piping Conference, PVP - VOL. 147, Pittsburgh, 65-69, 1988.

5. Tarics, G. A., Way, D., and Kelly, J. M. "The Implementation of Base Isolation for the Foothill Communities Law and Justice Center," Report to the National Science Foundation, November, 1984

6. Kan, C. L. and Chopra, A. K. "Elastic Earthquake Analysis of Torsionally Coupled Multistory Buildings," Earthquake Engineering and Structural Dynamics, 5, 4, 395-412, 1977.

7. Arya, A. S. "Sliding Concept for Mitigation of Earthquake Disaster to Masonry Buildings," 8 th World Conference on Earthquake Engineering, San Francisco, 5, 951-958, 1984.

8. Wen, Y. K. "Method of Random Vibration of Hysteretic Systems," Journal of Engineering Mechanics Division, ASCE, 102, EM2, 249-263, 1976.

9. Ramberg, W. and Osgood, W. R. "Description of Stress-Strain Curves by Three Parameters," Technical note 902, National Advisory Committee on Aeronautics, July, 1943.

10. Ozedmir, H. "Nonlinear Transient Dynamic Analysis of Yielding Structures," Ph. D. Thesis, University of California, Berkeley, CA, 1976.

11. Constantinou, M. and Adnane, M. "Dynamics of Soil-Base-Isolated-Structure Systems, Report 4: Evaluation of Two Models For Yielding Systems," Report to the National Science Foundation, September, 1987.

12. Su, L., Ahmadi, G. and Tadjbakhsh, I. G. "Performance of Various Base Isolation Systems for Shear Beam Structure," ASME pressure vessels and piping conference, PVP - VOL. 147, Pittsburgh, 1-7, 1988.

13. Mostaghel, N. and Tanbakuchi, J. "Response of Sliding Structures to Earthquake Support Motion," Earthquake Engineering and Structural Dynamics, 11, 6, 729-748, 1983.

14. Westermo, B. and Udwadia, F. "Periodic Response of a Sliding Oscillator System to Harmonic Excitation," Earthquake Engineering and Structural Dynamics, 11, 1, 135-146, 1983.

15. Constantinou, M. C., Caccese, J. and Harris, H. G., "Frictional Characteristics of Teflon-Steel Interfaces Under Dynamic Conditions," Earthquake Engineering and Structural Dynamics, 15, 6, 751-759, 1987.

16. Younis, C., Tadjbakhsh, I. G., and Saibel, E. A. "Analysis of General Plane Motion with Coulomb Friction," Wear, 91, 319-331, 1983.

17. Newmark, N. M.,"A Method of Computation for Structural Dynamics," ASCE Journal of Engineering Mechanics, 85, EM3, 67-94, 1959.

18. Bhatti, M. A., Pister, K. S., and Polak, E. "Optimal Design of an Earthquake Isolation System," Report UCB/EERC-78/22, University of California, Berkeley, 1978.

19. Dickens, J. M. and Wilson, E. L. "Numerical Method for Dynamic Substructure analysis," Report UCB/EERC-80/20, University of California, Berkeley, 1980.

20. Kan, C. L. and Chopra, A. K. "Coupled Lateral Torsional Response of Buildings to Ground Shaking," Report UCB/EERC-76/13, University of California, Berkeley, 1976.

21. Goodman, T. P. "Analysis of Two Dimensional Motion Resisted by Coulomb Friction," Journal of Engineering for Industry, 85, 17-26, 1963.

22. Park, Y. J., Wen, Y. K. and Ang, A. H. S. "Random Vibration of Hysteretic Systems Under Bidirectional Ground Motion," Earthquake Engineering and Structural Dyanmics, 14, 4, 543-557, 1986.

23. Clough, R. W. and Penzien, J. Dynamics of Structures, McGrawhill, 2 Edition, 1982.

24. Constantinou, M. C. "Random Vibration and Optimization of Design of Aseismic Base Isolation Systems," Ph. D. Thesis, Rensselaer Polytechnic Institute, New York, 1984.

25. Reinhorn, A. M., Rutenberg, A. and Gluck, J. "Dynamic Torsional Coupling in Asymmetric Building Structures," Building and Environment, 12, 251-261, 1977.

26. Derham, C. J., Kelly, J. M. and Thomas, A. G. "Nonlinear Natural Rubber Bearings For Seismic Isolation," Nuclear Engineering and Design, 84, 417-428, 1985.

27. Kelly, J. M. and Hodder, S. B. "Experimental Study of Lead and Elastic Dampers for Base Isolation Systems in Laminated Neoprene Bearings," Bulletin of the New Zealand National Society for Earthquake Engineering, 15, 2, 53-67, 1982.

28. Built, S. M. "Lead Rubber Dissipators for the Base Isolation of Bridge Structures," Report 289,School of Engineering, Dept. of Civil Engineering, University of Auckland, New Zealand, August 1982.

29. Caspe, M. S. and Reinhorn, A. M. "The Earthquake Barrier A Solution for Adding Ductility to otherwise Brittle Buildings," Proc. ATC-17 Seminar on Base Isolation and Passive Energy Dissipation, San Fransisco, CA, 331-342, 1986.

30. Mostaghel, N. and Khodaverdian, M. "Dynamics of Resilient-Friction Base Isolator(R-FBI)," Earthquake Engineering and Structural Dynamics, 15, 3, 379-390, 1987.

31. Ikonomou, A. S. "The Alexsismon: An Application to a Building Structure," Proc. second U.S. National Conference on Earthquake Engineering, Stanford, CA, 1979.

32. Mokha, A., Constantinou, M. C., and Reinhorn, A. M. "Teflon Bearings in Aseismic Base Isolation: Experimental Studies and Mathematical Modeling," Technical Report NCEER-88-038, October, 1988.

33. Gluck, J.,Reinhorn, A. M. and Rutenberg, A. "Dynamic Torsional Coupling in Tall Building Structures," Proc. Institution of Civil Engineers, Part 2, 67, 411-424, June 1979.

34. GTSTRUDL users manual ,GTICES systems labratory,Georgia Institute of Technology, Fourth Edition, April, 1985.

35. Desalvo, G. J. and Swanson, J. A. ANSYS users manual,Swanson analysis systems, Inc.,Houston, Pennsylvania, 1984.

36. Hilmy, S. I. "Adaptive Nonlinear Dynamic Analysis of Three-Dimensional Steel Framed Structures with Interactive Computer Graphics," Ph. D. Thesis, Dept. of Structural Engineering, Cornell University, May, 1984.

37. Kannan, A. M. and Powell, G. H "DRAIN-2D a General Purpose Computer Program for Dynamic Analysis of Inelastic Plane Structures with Users Guide," Reports EERC 73-6 and EERC 73-22, 1973, Revised August 1975.

38. Stricklin, J. A., Martinez, J. E., Tillerson, J. R., Hong. J. H., and Haisler, W. E. "Nonlinear Dynamic Analysis of Shells of Revolution by Matrix Displacement Method," AIAA Journal, 9, 4, 629-636, 1971.

39. Gear, C. W. "The Automatic Integration of Ordinary Differential Equations," Communications of the ACM, 14, 176-190, 1971.

40. Yasaka, A., Mizukoshi, K., Iizuka, M., Takenaka, Y., Maeda, S. and Fujimoto, N. "Biaxial Hysteresis Model for Base Isolation Devices," Internal Report, Kajima Institute of Construction Technology, Kajima Corporation, Tokyo, Japan.

41. Kang-Ning, L.,Shunsuke, Otani,Hiroyuki, A. "Reinforced Concrete Columns Under Varying Axial Load and Bi-directional Horizontal Load Reversals," Proc. Pacific Conference on Earthquake Engineering, New Zealand, 1, 3-9, August 1987.

42. Abel, J. F. and Srivastav, S., DNA-3D Nonlinear Steel Frame Analysis Program, Personal communication, Cornell University, February 15, 1989.

43. Wilson, E. L. and Dovey, H. H. "Three-Dimensional Analysis of Building Systems-TABS," Report UCB/EERC-72/8, University of California, Berkeley, 1972.

44. Wang, Y. P. and Reinhorn, A. M. "Motion Control of Sliding Isolated Structures," 3rd Symposium on Seismic Vibrations and Shock Isolation, ASME/PVP Conference, Hawaii, 1989.

45. Constantinou, M. C., and Mokha, A. " A Model of Friction of Teflon Sliding Bearings," Report to NSF, Dept. of Civil Engineering, SUNY at Buffalo, April, 1989.

46.Kunnath, S. K. and Reinhorn, A. M. "Model for Inelastic Biaxial Bending Interaction of RC Beam-columns," ACI Structural Journal (to be published).

APPENDIX A
3D-BASIS PROGRAM USER'S GUIDE

A.1 Input Format for 3D-BASIS

Free format is used to read all input data, hence conventional delimiters (comma,blank) may be used to separate data items. Dynamic arrays are used. Common block size has been set to 20,000 and should be changed if the need arises.

Note : No blank cards are to be input.

A.2 Problem Title

One card

TITLE	ALPHA-NUMERIC TITLE,upto 80 characters

A.3 Control Information - Structure

One card

SMEV,NF,NP,NE

SMEV =1 For option 1 - Stiffness and mass information to be input.

SMEV =2 For option 2 - Eigenvalues and eigenvectors to be input.

NF =Number of floors excluding base.

Default = 1

NP =Number of pads.

NE =Number of eigenvectors to be retained.

Default = 3

Notes: 1. For explanation of option 1 and option 2 refer to section 1.3.

2. Number of floors refers to the total number of floor levels excluding the base level.

3. Number of pads refers total number of elastomeric bearings and/or sliding bearings.

4. Number of eigenvectors in groups of three to be retained in the analysis, the

minimum being one set of three modes.

A.4 Control Information - Input Motion

One card

MOTIONXY,TSR,LOR,XTH,ULF

MOTIONXY = 1 for single earthquake record at angle of incidence XTH.
= 2 for independent earthquake records along X axis and Y axis.
If MOTIONXY = 1 input WAVEX.DAT
If MOTIONXY = 2 input WAVEX.DAT for X direction. Input WAVEY.DAT for Y direction.
TSR = Time step of earthquake record.
LOR = Length of earthquake record.
XTH = Angle of incidence of earthquake with respect to X axis in anticlockwise direction (for MOTIONXY=1). Default = zero
ULF = Load factor. Default = 1.0

Notes: 1. Two options are available for earthquake record input:

a. MOTIONXY = 1 refers to a single earthquake record input at any angle incidence XTH.In this case input only one earthquake record (read through a single file). See A.19 for wave input information.

b. MOTIONXY = 2 refers to two independent earthquake records input in X and Y direction respectively, eg. El Centro N-S along X direction and El Centro E-W along Y direction. In this case input two independent earthquake records in X and Y directions respectively (read through two files).See A.19 and A.20 wave input information.

2. Time step of earthquake record has to be the same in both X and Y direction for MOTIONXY = 2

3. Length of record has to be the same in both X and Y direction for MOTIONXY = 2.

4. In the case of MOTIONXY = 1 input the value of XTH.

5. Load factor is used to multiply both the earthquake records in X and Y directions.

A.5.1 Parameters for Newmark's Method

One card

GAM,BET

GAM = Parameter which produces numerical damping within a time step.
BET = Parameter which controls the variation of acceleration within a time step.

A.5.2 Integration Parameters

one card

TSI,TOL,FMNORM,MAXMI

TSI= Time step of integration
TOL= Tolerance for hysteretic force computation, at the center of mass of the base.
FMNORM = Reference moment for convergence
MAXMI = Maximum number of iterations within a time step.

Note: 1. Time step of integration for Newmark's method cannot exceed time step of earthquake record. Time step of integration TSI refers to the sliding mode time step, in case sliding bearings are used.

2. Tolerance check for hysteretic force computation at the center mass of the base, done at every time step.

3. If MAXMI is exceeded the program is terminated with an error status.

A.6 Control Information - Hysteretic Model Parameters

A.6.1 Hysteretic Model Parameters

One card

WBET,WGAM

WBET = Parameter which controls the shape of the hysteresis loop, traced by the viscoplasticity model.

WGAM = Parameter which controls the shape of the hysteresis loop, traced by the viscoplasticity model.

Note: 1. WBET = 0.1 and WGAM = 0.9 yields a viscoplasticity model and are preferable values for use.

A.6.2 Force-displacement Loop Parameters

NP cards

ALP(NP,2),YF(NP,2),YD(NP,2)

ALP = Post yielding stiffness to preyielding ratio in X and Y direction.Input zeros if Friction pad information is being input.

YF = Yield force in X and Y direction.Input zeros if friction pad information is being input.

YD = Yield displacement in X and Y direction.

Note: 1. ALP postyielding to preyielding stiffness ratio, when input as 1.0 yields elastic case

2. Yield displacement of 0.005 inches or more is preferable for Teflon-steel interfaces.

3. The order in which bearing information is input has to be maintained the same throughout the input.

A.6.3 Frictional Interface Parameters

FMAX(NP,2),DF(NP,2),PA(NP,2)

FMAX = Coefficient of sliding friction at large velocity in X and Y directions. Input zeros if elastomeric bearing information is being input.

DF = The difference between the Coefficient of sliding friction FMAX and the coefficient coefficient of sliding friction at low velocity in X and Y directions. Input Zeros if elastomeric bearing information is being input.

PA = Constant which controls the transition of coefficient of sliding friction from low to high velocity. Input zeros if elastomeric bearing information is being input.

Note: 1. The order in which bearing information is input has to be maintained the same throughout the input.

A.6.4 Initial Normal Force at Pads

NP card

FN(NP)

FN = Initial normal force for friction interfaces. Input zero for elastomeric bearings.

Note: 1. The order in which bearing information is input has to be maintained the same throughout the input.

A.7.1 Pad Location in X direction

NP Cards

XP(NP)

XP = X Coordinate from reference axis at center of mass of the base to each pad.

Note: 1. The order in which bearing information is input has to be maintained the same throughout the input.

A.7.2 Pad Location in Y Direction

NP Cards

YP(NP) — YP = Y Coordinate from reference axis at center of mass of the base to each pad.

Note: 1. The order in which bearing information is input has to be maintained the same throughout the input.

A.8 Stiffness Information

A.8.1 X Direction (Input only if SMEV = 1)

NF cards

SX(NF) — SX = Stiffness at each floor in X direction.

Note: 1. Stiffness at NF floors in X direction starting from the top floor upto the first floor(excluding the base) to be specified.

A.8.2 Y Direction (Input only if SMEV = 1)

NF cards

SY(NF) — SY = Stiffness at each floor in Y direction.

Note: 1. Stiffness at NF floors in Y direction starting from the top floor upto the first floor(excluding the base) to be specified.

A.8.3 θ Direction (Input only if SMEV = 1)

NF cards

ST(NF) — ST = Stiffness at each floor in θ direction.

Note: 1. Stiffness at NF floors in θ direction starting from the top floor upto the first floor(excluding the base) to be specified.

A.8.4 Eccentricity Information - X Direction (Input only if SMEV = 1)

NF cards

EX(NF) — EX = Eccentricity of center of rigidity from the center of mass of the floor.

A.8.5 Eccentricity Information - Y direction (Input only if SMEV = 1)

NF cards

EY(NF) — EY = Eccentricity of center of rigidity from the center of mass of the floor.

A.8.6 Eigenvalues (Input only if SMEV = 2)

NE cards

W(NE) — W_i = Eigenvalue of i^{th} mode

Note: 1. Input from first mode to the NE mode.

A.8.7 Eigenvectors (Input only if SMEV = 2)

NE cards

E(NF,NE) — E_i = Eigenvector of i^{th} mode

Note: 1. Input from first mode to the NE mode.

A.9 Initial Stiffness of Pads

NP cards

PKIXY(NP,1),PKIXY(NP,2) — PKIXY = Initial stiffness of pads in X and Y direction.

Note: 1. For friction interfaces use initial stiffness = minimum friction force/yield displacement

2. The order in which bearing information is input has to be maintained the same throughout the input.

A.10 Stiffness Information for Linear-elastic Isolation Elements

One card

SXE,SYE,STE,EXE,EYE	SXE = Summation of linear-elastic element stiffnesses in X direction. SYE = Summation of linear-elastic element stiffnesses in Y direction. SXE = Summation of linear-elastic element stiffnesses in θ direction at the center of mass of the base. EXE = Eccentricity of the center of rigidity of linear-elastic isolation element system in X direction from center of mass of the base. EYE = Eccentricity of the center of rigidity of linear-elastic isolation element system in Y direction from center of mass of the base.

A.11 Mass Information - X Direction

NF Cards

CMX(NF)	CMX = Mass at each floor in X direction.

Note: 1. Input from top floor to first floor(excluding base).

A.12 Mass Information - Y Direction

NF Cards

CMY(NF)	CMY = Mass at each floor in Y direction.

Note: 1. Input from top floor to first floor(excluding base).

A.13 Mass Information _θ Direction

NF Cards

CMT(NF)	CMT = Mass moment of inertia of each floor about center of mass of the floor.

Note: 1. Input from top floor to first floor(excluding base).

A.13.1 Distance to the Center of Mass of the Floor

NF cards

XN (NF)	XN = Distance of the center of mass of the floor from the center of mass of the base in X direction. Default = Zero for SMEV = 1.

Note: 1. Input from top floor to first floor (excluding base).

A.13.2 Distance to the Center of Mass of the Floor

NF cards

YN (NF)	YN = Distance of the center of mass of the floor from the center of mass of the base in Y direction. Default = Zero for SMEV = 1.

Note: 1. Input from top floor to first floor (excluding base).

A.13.3 Height of Base and Different Floors

NF + 1 cards

H(NF + 1)	H = Height from ground to the respective floors and base

Note: 1. Input from top floor to base.

A.14 Mass Information of Base

One Card

CMXB,CMYB,CMTB	CMXB = Mass of base in X direction. CMYB = Mass of base in Y direction. CMTB = Mass moment of Inertia of the base about the center of mass of the base.

A.15.1 Damping Information - Structure

NE Cards

DR(NE)	DR = Damping ratio corresponding to each mode.

Note: 1. Input from first mode to the NE mode.

A.15.2 Global Damping Information - At the Center of Mass of the Base

One card

CBX,CBY,CBT	CBX = Global damping coefficient in X dir. CBX = Global damping coefficient in Y dir. CBX = Global damping coefficient in θ dir.

Note: 1. If local damping is used input zeros.

A.15.3 Local Damping Information - At Individual Pads

NP cards

PC(NP)	PC = Damping coefficient at the pad

Note: 1. If global damping is used input zeros.

2. The order in which bearing information is input has to be maintained the same throughout the input.

A.16 Initial Conditions-displacement

NF+1 cards

DI(NF+1,3)	DI = Initial displacement at each floor in X Y and θ directions.

Note: 1. Input from the top floor to the base.

A.17 Initial Conditions-velocity

NF+1 cards

VI(NF+1,3)	VI = Initial velocity at each floor in X Y and θ directions.

Note: 1. Input from the top floor to the base.

A.18 Initial Conditions-acceleration

NF+1 cards

AI(NF+1,3)	AI = Initial acceleration at each floor in X Y and θ directions.

Note: 1. Input from the top floor to the base.

A.19 Earthquake Record in X Direction

File:WAVEX.DAT

X(LOR)	X = acceleration component in the horizontal X direction.

Note:1.If MOTIONXY as specified in A.4 is 1,then input taken to be at an angle XTH specified in A.4 .

A.20 Earthquake Record in Y Direction

File:WAVEY.DAT (Input only if MOTIONXY = 2)

Y(LOR)	Y = acceleration component in the horizontal Y direction.

A.21 Output Parameters

One card

KPF, KPD, IP	KPF = Interval of time before outputing the next force response quantity. KPD = Interval of time before outputing the next displacement response quantity. IP = Pad number at which pad force and displacement information is required.

APPENDIX B
INSTANTANEOUS STIFFNESS FORMULATION

B.1 Algorithm With Instantaneous Stiffness Formulation

In this formulation, instead of nonlinear force or pseudo load, nonlinear instantaneous stiffness is used.

The following assumption is made in addition to those stated in section 1.3:

a.The center of resistance of the isolation system shifts during inelastic action, but its location may be adequately determined from the instantaneous stiffnesses of the isolation devices at discrete time intervals, and used for solution.

Rewriting equation (2.4.3):

$$\mathbf{M}^{*}\Delta\ddot{\mathbf{u}}^{c} + \mathbf{C}^{*}\Delta\dot{\mathbf{u}}^{c} + \mathbf{K}^{*}\Delta\mathbf{u}^{c} + \Delta\mathbf{f} = \mathbf{p}_{\tau} - \mathbf{p}_{t} \qquad (B.1.1)$$

$$\Delta\mathbf{f} = \mathbf{f}_{\tau} - \mathbf{f}_{t}$$

$$= \left\langle \frac{d\mathbf{f}}{d\mathbf{u}} \right\rangle_{t} \Delta\mathbf{u}^{c}$$

$$= \mathbf{K}_{t}^{N}\Delta\mathbf{u}^{c} \qquad (B.1.2)$$

Substituting for $\Delta\mathbf{f}$ in equation (B.1.1):

$$\mathbf{M}^{*}\Delta\ddot{\mathbf{u}}^{c} + \mathbf{C}^{*}\Delta\dot{\mathbf{u}}^{c} + \mathbf{K}^{*}\Delta\mathbf{u}^{c} + \mathbf{K}_{t}^{N}\Delta\mathbf{u}^{c} = \mathbf{p}_{\tau} - \mathbf{p}_{t} \qquad (B.1.3)$$

B.2 Instantaneous Stiffness $\mathbf{K}_{t}^{N}$

Using equation (2.2.3) and (2.2.4), we obtain stiffness of individual hysteretic elements in x and y directions;

$$K_{xi}^{N} = \frac{df_x}{du_x} = K_{xi}\left(1-(1-\alpha)\left(\gamma(Sign\dot{U}_x)Z_x|Z_x| + \beta|Z_x|^2 + \frac{\gamma|\dot{U}_y|Z_x|Z_y|}{\dot{U}_x} + \frac{\beta\dot{U}_y Z_x Z_y}{\dot{U}_x}\right)\right) \qquad (B.2.1)$$

$$K_{yi}^{N} = \frac{df_y}{du_y} = K_{yi}\left(1-(1-\alpha)\left(\gamma(Sign\dot{U}_y)Z_y|Z_y| + \beta|Z_y|^2 + \frac{\gamma|\dot{U}_x|Z_y|Z_x|}{\dot{U}_y} + \frac{\beta\dot{U}_x Z_x Z_y}{\dot{U}_y}\right)\right) \qquad (B.2.2)$$

From these individual hysteretic element stiffnesses, the total stiffness matrix K_t^N is obtained. In a similar manner the stiffness of frictional elements is derived.

B.3 Newmark's Method

Newmark's method is adopted for solution. The procedure is one similar to,the procedure explained in section 2.4.2. Δ f is retained on the left hand side.Rewriting equation (2.4.8):

$$K_t^P \Delta \mathbf{u}^c = \mathbf{q}_t \qquad (B.3.1)$$

B.4 Substructuring to Exploit 'Local' Nonlinearity

Solution to a set of equations is the most time consuming part of a computational algorithm.If nonlinearities are involved, the problem is aggravated. But in this problem, due to the localized nature of the nonlinearity, it is not necessary to form and decompose the whole pseudo-stiffness matrix in equation(B.3.1), at each time step. Substructuring is used effectively to separate the nonlinear part from the linear part of the problem [18]. For this the matrix and vectors in equation (B.3.1) are partitioned to separate linear and nonlinear part, as follows:

$$\begin{pmatrix} K_{EE} & K_{EN} \\ K_{NE} & K_{NN} \end{pmatrix}_t \begin{Bmatrix} \Delta \mathbf{u}^E \\ \Delta \mathbf{u}^N \end{Bmatrix}_t = \begin{Bmatrix} \mathbf{p}^E \\ \mathbf{p}^N \end{Bmatrix}_t \qquad (B.4.2)$$

from which the following expressions are derived:

$$\Delta \mathbf{u}^E = \mathrm{K}_{EE}^{-1}\{\mathbf{p}^E - \mathrm{K}_{EN}\Delta \mathbf{u}^N\} \qquad (B.4.2)$$

where:

$$\Delta \mathbf{u}^N = [-\mathrm{K}_{NE}\mathrm{K}_{EE}^{-1}\mathrm{K}_{EN} + \mathrm{K}_{NN}]^{-1}\{\mathbf{p}^N - \mathrm{K}_{NE}\mathrm{K}_{EE}^{-1}\mathbf{p}^E\} \qquad (B.4.3)$$

K_{EE} is inverted only once and used repeatedly, along with instantaneous nonlinear stiffness K_{NN} ,for solution.

B.5 Computational Algorithm

1. The state of motion is initialized by specifying initial displacement,initial velocity and initial acceleration.

2. Newmark's method is used for integration of equation of motion. The pseudo-stiffness matrix is partitioned, as described in section B.4. Gaussian elimination is used for solution.

3. Using K_t^N from previous time step, the incremental displacement $\Delta \mathbf{u}^c$ at $\tau = t + \Delta t$ is computed.

4. The state of motion at t is updated to the state of motion at $\tau = t + \Delta t$.

5. The forces in the hysteretic elements and the instantaneous stiffnesses of the hysteretic elements is computed, at $\tau = t + \Delta t$,using fourth order Runge-kutta scheme. Also, the instantaneous eccentricities are computed and K_τ^N is assembled. F_τ the resultant force vector at the center of mass of the base is computed.

6. The unbalanced force at time τ is computed.

$$\mathbf{f}_\tau^e = \mathbf{p}_\tau - \{\mathrm{M}^*\ddot{\mathbf{u}}_\tau^c + \mathrm{C}^*\dot{\mathbf{u}}_\tau^c + \mathrm{K}^*\mathbf{u}_\tau^c + \mathrm{F}_\tau\}$$

7. The relative error is computed:

$$\text{Error} = \frac{\|\mathbf{r}^e\|_2}{FMNORM}$$

where, $FMNORM$ = Reference moment for convergence since the storey torque is the dominating element in the vector $\mathbf{f}$, and $\|\mathbf{f}\|_2$ denotes the euclidean norm of vector $\mathbf{f}$; i.e.,

$$\|\mathbf{f}\|_2 = \sqrt{f_x^2 + f_y^2 + f_t^2}$$

If error $\leq$ tolerance, no iteration is needed,computation at the next time step are started from step 3, or else iteration procedure is started as in step 8.

8. Iteration is used within a time step for establishing equilibrium as follows:

(a)

$$\mathrm{K}_\tau^P = \left(\mathrm{M}_t^* \left(\frac{1}{\beta(\Delta t)^2} \right) + \mathrm{C}_t^* \left(\frac{\gamma}{\beta \Delta t} \right) + [\mathrm{K}_t^* + \mathrm{K}_\tau^N] \right)$$

is computed using K_t^N.

(b) δU_t is solved for in:

$$\mathrm{K}_\tau^+ \delta U_\tau = \mathbf{f}_\tau^e$$

(c) The state of motion at $\tau = t + \Delta t$ in step 4, is updated.

(d) Unbalanced force is computed as in step 6, if tolerance is satisfied, computations at the next time step are started from step 3, or else iteration procedure is continued from step 8a, until convergence is reached or maximum number of iterations specified is exceeded, in which case the program is terminated with an error message.

APPENDIX C

COMPARISON OF FORMULATIONS RELATED TO MASS CENTER AND TO APPROXIMATE RIGIDITY CENTER AT BASE

C.1 Introduction

The formulation presented in this report, in option one (see section 1.3), is with reference to the vertical axis of centers of mass at various floor levels including the base. The inelastic behavior of the isolation system is adequately represented by recomputing the eccentricity, as described in Appendix B, i.e.,establishing the instantaneous center of rigidity at the base at discrete time intervals.

In the formulation in reference [4,5], which is briefly described in this report, the reference axis is with respect to approximate center of rigidity (at the initial center of rigidity) of the base. The stiffness at the base is approximately represented by an equivalent diagonal stiffness matrix.

A comparison between the two approaches is considered.

C.2 Assumptions

Comparison with first Option only, is considered

1. Superstructure remains elastic at all times.

2. Floor decks are rigid, walls and columns are inextensible. Each floor has three degrees of freedom, X and Y translations and rotation about a vertical axis. These degrees of freedom are attached to the center of mass of each floor.

3. The center of mass of the floors and the base lie on one vertical axis and the center of resistance of the floors and the base are arbitrarily located.

4. There exists a rigid slab at the base level that connects all isolation elements.

5. Three degrees of freedom at the base are attached to the approximate center of rigidity (Initial location of the center of rigidity).

6. The center of rigidity at the base remains at its initial position. Variation of eccentricity is assumed to be small.

7. The stiffness matrix at the base is represented by an approximate diagonal stiffness matrix assuming off diagonal terms are small, thus not accounting for the change in eccentricity due to nonlinear behavior of the pads.

8. The isolation system is rigid in the vertical direction, and torque resistance of individual pads is neglected.

C.3 Modifications to 3D-BASIS for Approximate Center of Rigidity at the Base as Reference

The program 3D-BASIS is modified in the following manner;

Matrix R in equation (2.3.1) is modified to:

$$\mathrm{R} = \begin{pmatrix} \mathrm{R}_n^* \\ \cdot \\ \mathrm{R}_i^* \\ \cdot \\ \mathrm{R}_1^* \end{pmatrix}$$

where:

$$\mathrm{R}_n^* = \mathrm{R}_i^* = \mathrm{R}_1^* = \begin{pmatrix} 1 & 0 & -Y_o \\ 0 & 1 & X_o \\ 0 & 0 & 1 \end{pmatrix}$$

where X_o and Y_o are coordinates of centers of mass at all the floors and at the base with respect to initial location of center of rigidity of the base.

Mass matrix M_b in equation (2.3.5) is modified to;

$$M_b = \begin{pmatrix} m_{bx} & 0 & -m_{bx}Y_o \\ 0 & m_{by} & m_{by}X_o \\ -m_{bx}Y_o & m_{by}X_o & m_{bt} + m_{bx}Y_o^2 + m_{by}X_o^2 \end{pmatrix}$$

where X_o and Y_o are as defined above.

Stiffness matrix K_t^N as described in, appendix B section B.2, is modified, ignoring the off diagonal terms, to:

$$K_t^N = \begin{pmatrix} K_{bx} & 0 & 0 \\ 0 & K_{by} & 0 \\ 0 & 0 & K_{bt} \end{pmatrix}$$

No instantaneous eccentricities are evaluated.

C.4 Example Comparing the Two Formulations

The base isolated structure described in section 3 and shown in figure 3-6 is considered. Comparison of the response computed using the two formulations, for 15 sec. of the 1940 El Centro earthquake north-south component input in the X direction, is considered. Superstructure damping of 2% of critical is used in all modes. 5% eccentricity in the Y direction is used by offsetting the center of mass of the building at the first floor and the base from the center of rigidity. Figures C-1 and C-2 show the X direction relative base displacement response history and shear force response time history in the bearing at node 8, respectively. In this comparison, inelastic bi-axial interaction effects are not considered.

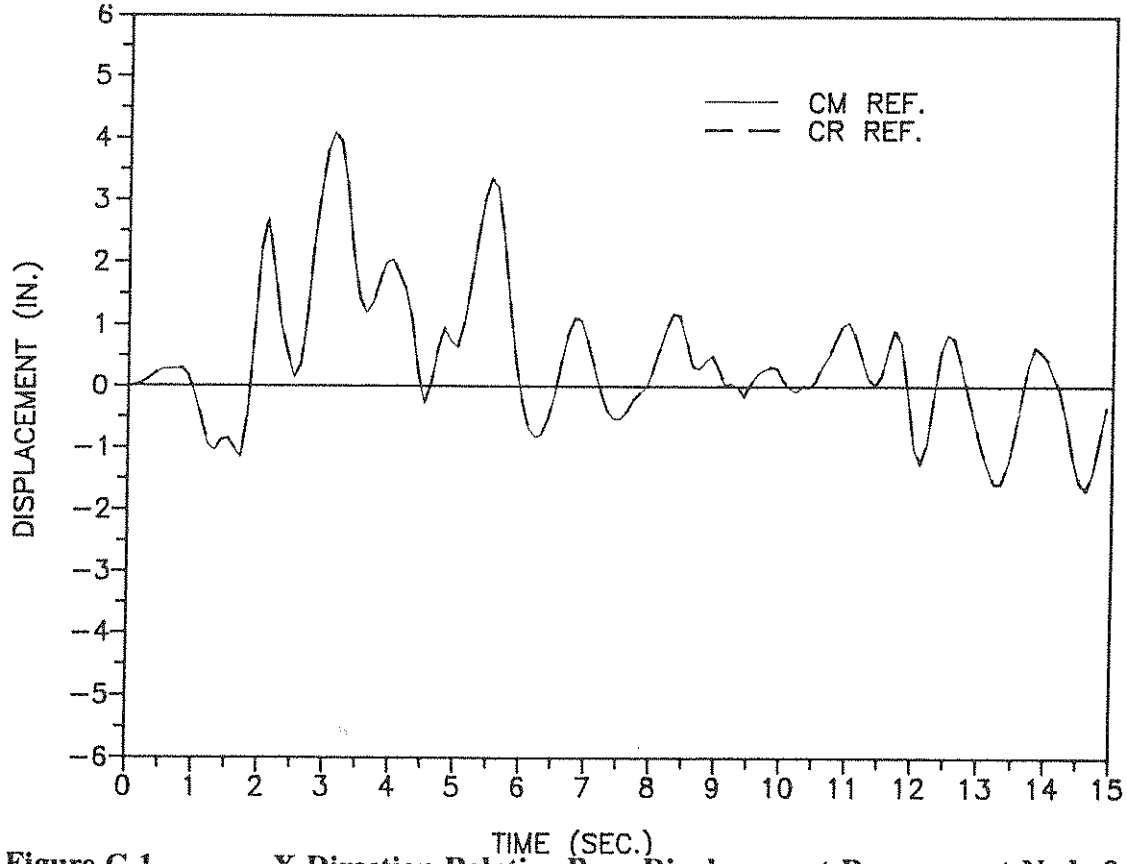

Figure C-1 X Direction Relative Base Displacement Response at Node 8 of the Base Isolated Building Subjected to EL CENTRO Earthquake (S00E component) in X Direction

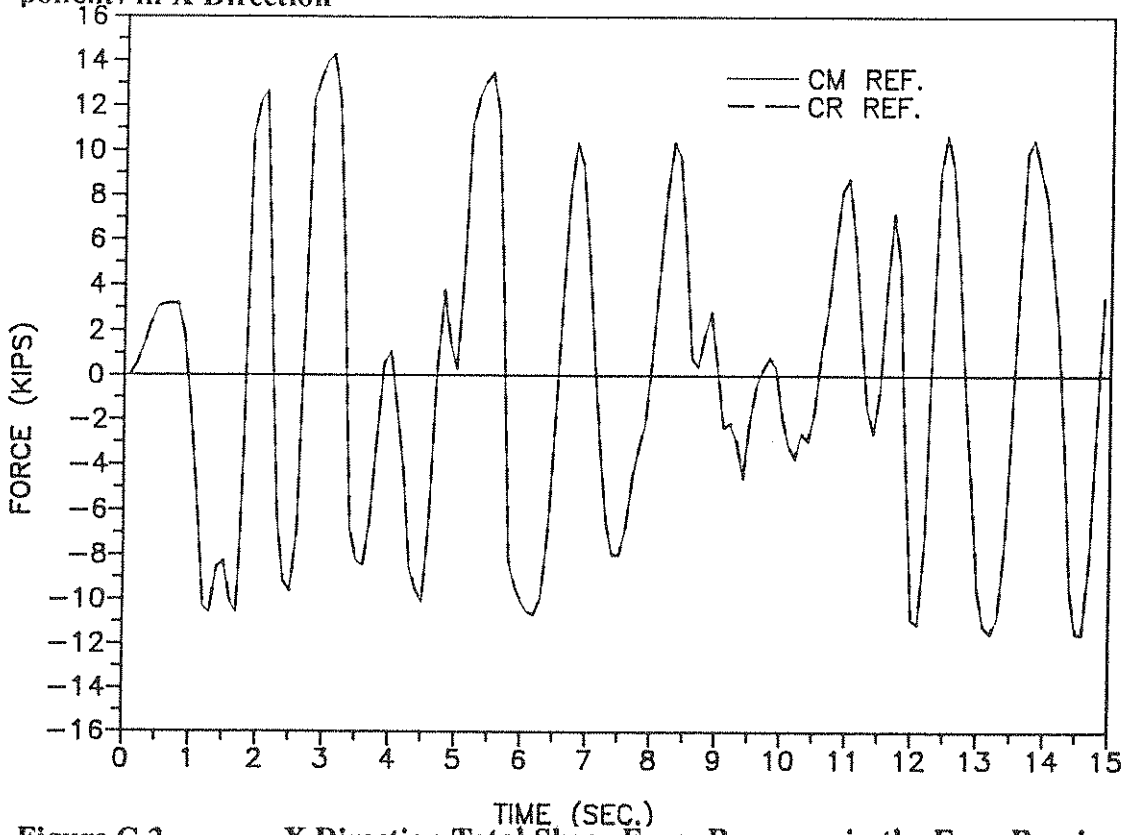

Figure C-2 X Direction Total Shear Force Response in the Four Bearings of the Base Isolated Building Subjected to EL CENTRO Earthquake (S00E component) in X Direction

NATIONAL CENTER FOR EARTHQUAKE ENGINEERING RESEARCH
LIST OF PUBLISHED TECHNICAL REPORTS

The National Center for Earthquake Engineering Research (NCEER) publishes technical reports on a variety of subjects related to earthquake engineering written by authors funded through NCEER. These reports are available from both NCEER's Publications Department and the National Technical Information Service (NTIS). Requests for reports should be directed to the Publications Department, National Center for Earthquake Engineering Research, State University of New York at Buffalo, Red Jacket Quadrangle, Buffalo, New York 14261. Reports can also be requested through NTIS, 5285 Port Royal Road, Springfield, Virginia 22161. NTIS accession numbers are shown in parenthesis, if available.

NCEER-87-0001 "First-Year Program in Research, Education and Technology Transfer," 3/5/87, (PB88-134275/AS).

NCEER-87-0002 "Experimental Evaluation of Instantaneous Optimal Algorithms for Structural Control," by R.C. Lin, T.T. Soong and A.M. Reinhorn, 4/20/87, (PB88-134341/AS).

NCEER-87-0003 "Experimentation Using the Earthquake Simulation Facilities at University at Buffalo," by A.M. Reinhorn and R.L. Ketter, to be published.

NCEER-87-0004 "The System Characteristics and Performance of a Shaking Table," by J.S. Hwang, K.C. Chang and G.C. Lee, 6/1/87, (PB88-134259/AS).

NCEER-87-0005 "A Finite Element Formulation for Nonlinear Viscoplastic Material Using a Q Model," by O. Gyebi and G. Dasgupta, 11/2/87, (PB88-213764/AS).

NCEER-87-0006 "Symbolic Manipulation Program (SMP) - Algebraic Codes for Two and Three Dimensional Finite Element Formulations," by X. Lee and G. Dasgupta, 11/9/87, (PB88-219522/AS).

NCEER-87-0007 "Instantaneous Optimal Control Laws for Tall Buildings Under Seismic Excitations," by J.N. Yang, A. Akbarpour and P. Ghaemmaghami, 6/10/87, (PB88-134333/AS).

NCEER-87-0008 "IDARC: Inelastic Damage Analysis of Reinforced Concrete Frame - Shear-Wall Structures," by Y.J. Park, A.M. Reinhorn and S.K. Kunnath, 7/20/87, (PB88-134325/AS).

NCEER-87-0009 "Liquefaction Potential for New York State: A Preliminary Report on Sites in Manhattan and Buffalo," by M. Budhu, V. Vijayakumar, R.F. Giese and L. Baumgras, 8/31/87, (PB88-163704/AS). This report is available only through NTIS (see address given above).

NCEER-87-0010 "Vertical and Torsional Vibration of Foundations in Inhomogeneous Media," by A.S. Veletsos and K.W. Dotson, 6/1/87, (PB88-134291/AS).

NCEER-87-0011 "Seismic Probabilistic Risk Assessment and Seismic Margins Studies for Nuclear Power Plants," by Howard H.M. Hwang, 6/15/87, (PB88-134267/AS). This report is available only through NTIS (see address given above).

NCEER-87-0012 "Parametric Studies of Frequency Response of Secondary Systems Under Ground-Acceleration Excitations," by Y. Yong and Y.K. Lin, 6/10/87, (PB88-134309/AS).

NCEER-87-0013 "Frequency Response of Secondary Systems Under Seismic Excitation," by J.A. HoLung, J. Cai and Y.K. Lin, 7/31/87, (PB88-134317/AS).

NCEER-87-0014 "Modelling Earthquake Ground Motions in Seismically Active Regions Using Parametric Time Series Methods," by G.W. Ellis and A.S. Cakmak, 8/25/87, (PB88-134283/AS).

NCEER-87-0015 "Detection and Assessment of Seismic Structural Damage," by E. DiPasquale and A.S. Cakmak, 8/25/87, (PB88-163712/AS).

NCEER-87-0016 "Pipeline Experiment at Parkfield, California," by J. Isenberg and E. Richardson, 9/15/87, (PB88-163720/AS).

NCEER-87-0017 "Digital Simulation of Seismic Ground Motion," by M. Shinozuka, G. Deodatis and T. Harada, 8/31/87, (PB88-155197/AS). This report is available only through NTIS (see address given above).

NCEER-87-0018 "Practical Considerations for Structural Control: System Uncertainty, System Time Delay and Truncation of Small Control Forces," J.N. Yang and A. Akbarpour, 8/10/87, (PB88-163738/AS).

NCEER-87-0019 "Modal Analysis of Nonclassically Damped Structural Systems Using Canonical Transformation," by J.N. Yang, S. Sarkani and F.X. Long, 9/27/87, (PB88-187851/AS).

NCEER-87-0020 "A Nonstationary Solution in Random Vibration Theory," by J.R. Red-Horse and P.D. Spanos, 11/3/87, (PB88-163746/AS).

NCEER-87-0021 "Horizontal Impedances for Radially Inhomogeneous Viscoelastic Soil Layers," by A.S. Veletsos and K.W. Dotson, 10/15/87, (PB88-150859/AS).

NCEER-87-0022 "Seismic Damage Assessment of Reinforced Concrete Members," by Y.S. Chung, C. Meyer and M. Shinozuka, 10/9/87, (PB88-150867/AS). This report is available only through NTIS (see address given above).

NCEER-87-0023 "Active Structural Control in Civil Engineering," by T.T. Soong, 11/11/87, (PB88-187778/AS).

NCEER-87-0024 Vertical and Torsional Impedances for Radially Inhomogeneous Viscoelastic Soil Layers," by K.W. Dotson and A.S. Veletsos, 12/87, (PB88-187786/AS).

NCEER-87-0025 "Proceedings from the Symposium on Seismic Hazards, Ground Motions, Soil-Liquefaction and Engineering Practice in Eastern North America," October 20-22, 1987, edited by K.H. Jacob, 12/87, (PB88-188115/AS).

NCEER-87-0026 "Report on the Whittier-Narrows, California, Earthquake of October 1, 1987," by J. Pantelic and A. Reinhorn, 11/87, (PB88-187752/AS). This report is available only through NTIS (see address given above).

NCEER-87-0027 "Design of a Modular Program for Transient Nonlinear Analysis of Large 3-D Building Structures," by S. Srivastav and J.F. Abel, 12/30/87, (PB88-187950/AS).

NCEER-87-0028 "Second-Year Program in Research, Education and Technology Transfer," 3/8/88, (PB88-219480/AS).

NCEER-88-0001 "Workshop on Seismic Computer Analysis and Design of Buildings With Interactive Graphics," by W. McGuire, J.F. Abel and C.H. Conley, 1/18/88, (PB88-187760/AS).

NCEER-88-0002 "Optimal Control of Nonlinear Flexible Structures," by J.N. Yang, F.X. Long and D. Wong, 1/22/88, (PB88-213772/AS).

NCEER-88-0003 "Substructuring Techniques in the Time Domain for Primary-Secondary Structural Systems," by G.D. Manolis and G. Juhn, 2/10/88, (PB88-213780/AS).

NCEER-88-0004 "Iterative Seismic Analysis of Primary-Secondary Systems," by A. Singhal, L.D. Lutes and P.D. Spanos, 2/23/88, (PB88-213798/AS).

NCEER-88-0005 "Stochastic Finite Element Expansion for Random Media," by P.D. Spanos and R. Ghanem, 3/14/88, (PB88-213806/AS).

NCEER-88-0006 "Combining Structural Optimization and Structural Control," by F.Y. Cheng and C.P. Pantelides, 1/10/88, (PB88-213814/AS).

NCEER-88-0007 "Seismic Performance Assessment of Code-Designed Structures," by H.H-M. Hwang, J-W. Jaw and H-J. Shau, 3/20/88, (PB88-219423/AS).

NCEER-88-0008 "Reliability Analysis of Code-Designed Structures Under Natural Hazards," by H.H-M. Hwang, H. Ushiba and M. Shinozuka, 2/29/88, (PB88-229471/AS).

NCEER-88-0009 "Seismic Fragility Analysis of Shear Wall Structures," by J-W Jaw and H.H-M. Hwang, 4/30/88, (PB89-102867/AS).

NCEER-88-0010 "Base Isolation of a Multi-Story Building Under a Harmonic Ground Motion - A Comparison of Performances of Various Systems," by F-G Fan, G. Ahmadi and I.G. Tadjbakhsh, 5/18/88, (PB89-122238/AS).

NCEER-88-0011 "Seismic Floor Response Spectra for a Combined System by Green's Functions," by F.M. Lavelle, L.A. Bergman and P.D. Spanos, 5/1/88, (PB89-102875/AS).

NCEER-88-0012 "A New Solution Technique for Randomly Excited Hysteretic Structures," by G.Q. Cai and Y.K. Lin, 5/16/88, (PB89-102883/AS).

NCEER-88-0013 "A Study of Radiation Damping and Soil-Structure Interaction Effects in the Centrifuge," by K. Weissman, supervised by J.H. Prevost, 5/24/88, (PB89-144703/AS).

NCEER-88-0014 "Parameter Identification and Implementation of a Kinematic Plasticity Model for Frictional Soils," by J.H. Prevost and D.V. Griffiths, to be published.

NCEER-88-0015 "Two- and Three- Dimensional Dynamic Finite Element Analyses of the Long Valley Dam," by D.V. Griffiths and J.H. Prevost, 6/17/88, (PB89-144711/AS).

NCEER-88-0016 "Damage Assessment of Reinforced Concrete Structures in Eastern United States," by A.M. Reinhorn, M.J. Seidel, S.K. Kunnath and Y.J. Park, 6/15/88, (PB89-122220/AS).

NCEER-88-0017 "Dynamic Compliance of Vertically Loaded Strip Foundations in Multilayered Viscoelastic Soils," by S. Ahmad and A.S.M. Israil, 6/17/88, (PB89-102891/AS).

NCEER-88-0018 "An Experimental Study of Seismic Structural Response With Added Viscoelastic Dampers," by R.C. Lin, Z. Liang, T.T. Soong and R.H. Zhang, 6/30/88, (PB89-122212/AS).

NCEER-88-0019 "Experimental Investigation of Primary - Secondary System Interaction," by G.D. Manolis, G. Juhn and A.M. Reinhorn, 5/27/88, (PB89-122204/AS).

NCEER-88-0020 "A Response Spectrum Approach For Analysis of Nonclassically Damped Structures," by J.N. Yang, S. Sarkani and F.X. Long, 4/22/88, (PB89-102909/AS).

NCEER-88-0021 "Seismic Interaction of Structures and Soils: Stochastic Approach," by A.S. Veletsos and A.M. Prasad, 7/21/88, (PB89-122196/AS).

NCEER-88-0022 "Identification of the Serviceability Limit State and Detection of Seismic Structural Damage," by E. DiPasquale and A.S. Cakmak, 6/15/88, (PB89-122188/AS).

NCEER-88-0023 "Multi-Hazard Risk Analysis: Case of a Simple Offshore Structure," by B.K. Bhartia and E.H. Vanmarcke, 7/21/88, (PB89-145213/AS).

NCEER-88-0024 "Automated Seismic Design of Reinforced Concrete Buildings," by Y.S. Chung, C. Meyer and M. Shinozuka, 7/5/88, (PB89-122170/AS).

NCEER-88-0025 "Experimental Study of Active Control of MDOF Structures Under Seismic Excitations," by L.L. Chung, R.C. Lin, T.T. Soong and A.M. Reinhorn, 7/10/88, (PB89-122600/AS).

NCEER-88-0026 "Earthquake Simulation Tests of a Low-Rise Metal Structure," by J.S. Hwang, K.C. Chang, G.C. Lee and R.L. Ketter, 8/1/88, (PB89-102917/AS).

NCEER-88-0027 "Systems Study of Urban Response and Reconstruction Due to Catastrophic Earthquakes," by F. Kozin and H.K. Zhou, 9/22/88, to be published.

NCEER-88-0028 "Seismic Fragility Analysis of Plane Frame Structures," by H.H-M. Hwang and Y.K. Low, 7/31/88, (PB89-131445/AS).

NCEER-88-0029 "Response Analysis of Stochastic Structures," by A. Kardara, C. Bucher and M. Shinozuka, 9/22/88, (PB89-174429/AS).

NCEER-88-0030 "Nonnormal Accelerations Due to Yielding in a Primary Structure," by D.C.K. Chen and L.D. Lutes, 9/19/88, (PB89-131437/AS).

NCEER-88-0031 "Design Approaches for Soil-Structure Interaction," by A.S. Veletsos, A.M. Prasad and Y. Tang, 12/30/88, (PB89-174437/AS).

NCEER-88-0032 "A Re-evaluation of Design Spectra for Seismic Damage Control," by C.J. Turkstra and A.G. Tallin, 11/7/88, (PB89-145221/AS).

NCEER-88-0033 "The Behavior and Design of Noncontact Lap Splices Subjected to Repeated Inelastic Tensile Loading," by V.E. Sagan, P. Gergely and R.N. White, 12/8/88, (PB89-163737/AS).

NCEER-88-0034 "Seismic Response of Pile Foundations," by S.M. Mamoon, P.K. Banerjee and S. Ahmad, 11/1/88, (PB89-145239/AS).

NCEER-88-0035 "Modeling of R/C Building Structures With Flexible Floor Diaphragms (IDARC2)," by A.M. Reinhorn, S.K. Kunnath and N. Panahshahi, 9/7/88, (PB89-207153/AS).

NCEER-88-0036 "Solution of the Dam-Reservoir Interaction Problem Using a Combination of FEM, BEM with Particular Integrals, Modal Analysis, and Substructuring," by C-S. Tsai, G.C. Lee and R.L. Ketter, 12/31/88, (PB89-207146/AS).

NCEER-88-0037 "Optimal Placement of Actuators for Structural Control," by F.Y. Cheng and C.P. Pantelides, 8/15/88, (PB89-162846/AS).

NCEER-88-0038 "Teflon Bearings in Aseismic Base Isolation: Experimental Studies and Mathematical Modeling," by A. Mokha, M.C. Constantinou and A.M. Reinhorn, 12/5/88, (PB89-218457/AS).

NCEER-88-0039 "Seismic Behavior of Flat Slab High-Rise Buildings in the New York City Area," by P. Weidlinger and M. Ettouney, 10/15/88, to be published.

NCEER-88-0040 "Evaluation of the Earthquake Resistance of Existing Buildings in New York City," by P. Weidlinger and M. Ettouney, 10/15/88, to be published.

NCEER-88-0041 "Small-Scale Modeling Techniques for Reinforced Concrete Structures Subjected to Seismic Loads," by W. Kim, A. El-Attar and R.N. White, 11/22/88, (PB89-189625/AS).

NCEER-88-0042 "Modeling Strong Ground Motion from Multiple Event Earthquakes," by G.W. Ellis and A.S. Cakmak, 10/15/88, (PB89-174445/AS).

NCEER-88-0043 "Nonstationary Models of Seismic Ground Acceleration," by M. Grigoriu, S.E. Ruiz and E. Rosenblueth, 7/15/88, (PB89-189617/AS).

NCEER-88-0044 "SARCF User's Guide: Seismic Analysis of Reinforced Concrete Frames," by Y.S. Chung, C. Meyer and M. Shinozuka, 11/9/88, (PB89-174452/AS).

NCEER-88-0045 "First Expert Panel Meeting on Disaster Research and Planning," edited by J. Pantelic and J. Stoyle, 9/15/88, (PB89-174460/AS).

NCEER-88-0046 "Preliminary Studies of the Effect of Degrading Infill Walls on the Nonlinear Seismic Response of Steel Frames," by C.Z. Chrysostomou, P. Gergely and J.F. Abel, 12/19/88, (PB89-208383/AS).

NCEER-88-0047 "Reinforced Concrete Frame Component Testing Facility - Design, Construction, Instrumentation and Operation," by S.P. Pessiki, C. Conley, T. Bond, P. Gergely and R.N. White, 12/16/88, (PB89-174478/AS).

NCEER-89-0001 "Effects of Protective Cushion and Soil Compliancy on the Response of Equipment Within a Seismically Excited Building," by J.A. HoLung, 2/16/89, (PB89-207179/AS).

NCEER-89-0002 "Statistical Evaluation of Response Modification Factors for Reinforced Concrete Structures," by H.H-M. Hwang and J-W. Jaw, 2/17/89, (PB89-207187/AS).

NCEER-89-0003 "Hysteretic Columns Under Random Excitation," by G-Q. Cai and Y.K. Lin, 1/9/89, (PB89-196513/AS).

NCEER-89-0004 "Experimental Study of 'Elephant Foot Bulge' Instability of Thin-Walled Metal Tanks," by Z-H. Jia and R.L. Ketter, 2/22/89, (PB89-207195/AS).

NCEER-89-0005 "Experiment on Performance of Buried Pipelines Across San Andreas Fault," by J. Isenberg, E. Richardson and T.D. O'Rourke, 3/10/89, (PB89-218440/AS).

NCEER-89-0006 "A Knowledge-Based Approach to Structural Design of Earthquake-Resistant Buildings," by M. Subramani, P. Gergely, C.H. Conley, J.F. Abel and A.H. Zaghw, 1/15/89, (PB89-218465/AS).

NCEER-89-0007 "Liquefaction Hazards and Their Effects on Buried Pipelines," by T.D. O'Rourke and P.A. Lane, 2/1/89, (PB89-218481).

NCEER-89-0008 "Fundamentals of System Identification in Structural Dynamics," by H. Imai, C-B. Yun, O. Maruyama and M. Shinozuka, 1/26/89, (PB89-207211/AS).

NCEER-89-0009 "Effects of the 1985 Michoacan Earthquake on Water Systems and Other Buried Lifelines in Mexico," by A.G. Ayala and M.J. O'Rourke, 3/8/89, (PB89-207229/AS).

NCEER-89-0010 "NCEER Bibliography of Earthquake Education Materials," by K.E.K. Ross, 3/10/89, (PB89-218473/AS).

NCEER-89-0011 "Inelastic Three-Dimensional Response Analysis of Reinforced Concrete Building Structures (IDARC-3D), Part I - Modeling," by S.K. Kunnath and A.M. Reinhorn, 4/17/89.

NCEER-89-0012 "Recommended Modifications to ATC-14," by C.D. Poland and J.O. Malley, 4/12/89.

NCEER-89-0013 "Repair and Strengthening of Beam-to-Column Connections Subjected to Earthquake Loading," by M. Corazao and A.J. Durrani, 2/28/89.

NCEER-89-0014 "Program EXKAL2 for Identification of Structural Dynamic Systems," by O. Maruyama, C-B. Yun, M. Hoshiya and M. Shinozuka, 5/19/89.

NCEER-89-0015 "Response of Frames With Bolted Semi-Rigid Connections, Part I - Experimental Study and Analytical Predictions," by P.J. DiCorso, A.M. Reinhorn, J.R. Dickerson, J.B. Radziminski and W.L. Harper, 6/1/89, to be published.

NCEER-89-0016 "ARMA Monte Carlo Simulation in Probabilistic Structural Analysis," by P.D. Spanos and M.P. Mignolet, 7/10/89.

NCEER-89-0017 "Preliminary Proceedings of the Conference on Disaster Preparedness - The Place of Earthquake Education in Our Schools, July 9-11, 1989," 6/23/89.

NCEER-89-0018 "Multidimensional Models of Hysteretic Material Behavior for Vibration Analysis of Shape Memory Energy Absorbing Devices, by E.J. Graesser and F.A. Cozzarelli, 6/7/89.

NCEER-89-0019 "Nonlinear Dynamic Analysis of Three-Dimensional Base Isolated Structures (3D-BASIS)," by S. Nagarajaiah, A.M. Reinhorn and M.C. Constantinou, 8/3/89.